Development of Innovative in-Line Stiffening Element for Out-of-Plane Masonry Walls

by

Joseph Entz

A thesis submitted in partial fulfillment of the requirements for the degree of

Master of Science

in

Structural Engineering

Department of Civil and Environmental Engineering
University of Alberta

ABSTRACT

Tall, slender masonry walls are a competitive solution for resisting both out-of-plane (OOP) and gravity loads in low and high-rise structures. The use of taller and thinner walls is appealing due to the use of less material, need for smaller foundations, faster construction, lower seismic forces, and the ability to create more interior space. However, the design of OOP loaded tall masonry walls, in accordance with CSA S304, has practical limits related to axial load capacity, buckling stability, and reinforcement details. Most conventional masonry wall designs rely on a single reinforcement layer located at the centre of the unit. Designers who seek to enhance wall strength and stiffness by opting for multiple layers of reinforcement or non-conventional units are hindered by empirical limits in the S304 standard. A new type of masonry slender wall, based on a concept similar to seismic boundary elements, is proposed in this study. These elements act as localized regions of strength and stiffness by providing tied reinforcement in two layers close to the surface of the wall.

Results of experimental tests on five course high masonry prisms, containing pre-tied steel reinforcement cages and specially designed masonry units to fit around the cages, indicate that the innovative reinforcing cage has a beneficial effect on both the flexural strength and stiffness of masonry prisms. The response of four 12 course high masonry walls tested under combined axial and OOP load, is also presented. The results indicate that walls with two layers of reinforcement have greater OOP stiffness and flexural strength in comparison to conventionally reinforced walls.

A mechanics-based fibre-section model utilizing plane-section compatibility is used to compare the performance of cage reinforced prisms and walls to conventionally reinforced prisms and walls with various amounts of conventional reinforcing steel.

DEDICATION

The fear of the Lord is the beginning of wisdom,

and the knowledge of the holy is understanding.

Proverbs 9:10

ACKNOWLEDGMENTS

Without the support and continual guidance of Dr. Carlos Cruz-Noguez, this research would not have happened. Thank you.

Financial support for this research was provided by the NSERC Engage Grant program. Technical assistance was provided by Monica Guzman from the Canadian Masonry Design Centre (CMDC) and Dr. Mark Hagel from the Alberta Masonry Council (AMC). The Masonry Contractors Association of Alberta (MCAA) contributed labour, resources, and technical expertise.

Mr. Clayton Pettit and Mr. Odin Guzman Sanchez collaborated in the design of the experiments. The author would like to thank these contributors for their support.

The expertise and contributions of the I.F. Morrison Structures Lab technicians, Cameron West and Greg Miller, were invaluable. Thank you.

TABLE OF CONTENTS

LIST OF TABLES

LIST OF FIGURES

CHAPTER 1: INTRODUCTION

1.1 BACKGROUND

The intent of the design provisions for out-of-plane (OOP) load-bearing slender walls in the masonry code of Canada [1] is that very slender walls (walls with slenderness ratios, height to thickness greater than 30) have ductile behaviour, exhibit no buckling failure, and achieve significant post-yield deformations before masonry crushing in compression. For large moment demands, meeting these code provisions requires the use of thicker and/or stronger blocks to increase the bearing area and stiffness, adding compressive steel reinforcement, or increasing the effective depth of the provided tension reinforcement [1]. Utilizing thicker blocks allows designers to decrease the compression zone depth to effective rebar depth (c/d) ratio and thereby conform to the under-reinforced criterion for slender walls in North American codes [1, 2]. However, this often results in a more expensive and impractical wall to construct given architectural and engineering demands for space, size, and loads.

Therefore, a need exists to develop a type of slender reinforced masonry (RM) wall which conforms to the CSA S304 requirements, while still allowing designers to take full advantage of the benefits offered by this wall type. Meeting flexural strength and stiffness demands with slenderer walls is appealing due to the use of less material, need for smaller foundations, faster construction, lower seismic forces, and the ability to create more interior space.

Conventionally-reinforced tall masonry walls have inherently low OOP stiffness. This characteristic can lead to further undesirable effects when the low OOP stiffness leads to high second-order bending moments. As a result, significant research efforts have been undertaken to understand the behaviour of OOP RM walls.

1.1.1 Research on Slender Reinforced Masonry Walls

Early experimental tests on eccentrically loaded RM walls were conducted by Yokel in 1971. By subjecting a series of walls to concentric and eccentric loads, it was observed that, due to the development of a strain gradient, the eccentrically loaded walls could sustain greater compressive stresses in comparison to concentrically loaded walls [3]. The walls in this study were pin supported and had slenderness ratios ranging from 15.7 to 42.7.

In 1976, Cranston and Roberts investigated the viability of the allowable stress design method as applied to RM walls. They tested a series of 2.6 m high specimens, with slenderness ratios of 18.7, under combined axial and lateral loads. It was demonstrated that the allowable stress method, prominently used up to that point, results in uneconomical designs for RM walls [4].

Further experimental testing was conducted by Hatzinikolas in 1978. A series of RM walls, ranging in height from 2.7 m to 4.7 m, and slenderness ratios from 13.8 to 24, was subjected to eccentric loading. All specimens were tested with pinned-pinned end conditions. A variety of loading scenarios were chosen to cover both single and double flexure. The offset distance of the eccentric load was used to estimate the extent of cracking in the specimen cross-sections, and subsequently, the effective rigidity (EI_{eff}) was calculated. The study concluded by proposing a moment magnifier design method which utilized the effective rigidity of the wall [5].

Initial codification of a slenderness limits for RM walls was provided in Table 24-I of the Uniform Building Code (UBC). The associated clause limited the height to thickness ratio (h/t) of exterior, reinforced, load-bearing masonry walls to 25. Any RM wall with a slenderness ratio greater than this limit was classified as tall and slender [6]. This stipulation was imposed to limit flexural stresses in masonry walls under OOP wind loading in the absence of empirical data. This limit was also intended to safeguard against the possibility of wall buckling under combined axial and lateral loading [6].

The validity of the slenderness limit was investigated in 1979 when the Structural Engineers Association of Southern California (SEAOSC) and the American Concrete Institute - Southern California Chapter (ACI-SC) undertook a research program to demonstrate the safety and structural viability of RM walls with slenderness limits greater than 25. In this study, a series of 7.4 m tall, RM walls with slenderness ratios ranging from 38 to 51.2, were subjected to combined axial and lateral loading using pined-pinned support conditions. The researchers believed that the ability to utilize slender walls in construction would result in less reinforcing steel, smaller footings, reduced construction costs, and reduced construction time [7].

From this experimental study, it was concluded that there was minimal evidence to support a fixed slenderness limit. Several other important conclusions were derived. It was observed that elastic and/or inelastic lateral buckling did not occur in any of the walls for the range of axial load tested (up to 10% of the pure axial capacity). Furthermore, it was noted that second-order effects were more prominent in slender walls; in which case, they accounted for approximately 30% of the yield moment [7].

Although conventional, centrally located rebar was utilized in the slender wall tests by SEAOSC and ACI-SC researchers, rebar is often offset from the middle of the cell, close to the faceshells in alternate sides (staggered pattern). This alternate method of rebar placement has been demonstrated to improve the OOP rigidity and flexural capacity of RM walls by increasing the moment of inertia of the reinforced section relative to conventional reinforcing [6].

1.1.2 Proposed Stiffening Techniques

Various techniques have been investigated to improve the OOP performance of reinforced masonry (RM) walls. The OOP monotonic and cyclic response of a series of 14, 2.4 m high, RM walls was studied by Hamid et al in 1989. It was established that the amount of vertical reinforcement dramatically impacts the OOP capacity of RM walls. Moreover, the tests indicated that staggered, vertical reinforcing bars result in higher energy absorption capacity and displacement ductility in comparison to conventional reinforcing bars placed at the mid-depth [8].

Near-Surface Mounted (NSM) tension reinforcement methods, consisting of placing reinforcement bars (made of stainless steel or FRP) on the tension side of walls, have been demonstrated to improve the OOP strength, ductility, and rigidity of unreinforced masonry walls by as much as 4 to 14 times in specific cases. [9]. The addition of NSM reinforcement on the face of a masonry wall increases both the overall tension reinforcement capacity and the moment arm between the masonry compression block and tension reinforcement force couple. The addition of NSM reinforcing allows for tensile forces to develop in a ductile material on the tension face of the wall. The post-yield strain capacity of the NSM reinforcement allows for greater ultimate curvature, and therefore, enhanced ductility. In unreinforced masonry (URM) walls, the addition of Fibre Reinforced Polymer (FRP) rebar in quantities as low as 0.006% has resulted in a 25% increase in lateral load capacity and a 200-400% increase in lateral energy absorption [10]. Steel bars strategically positioned in groves on the exterior surface of CMU (concrete masonry unit) walls have been shown to provide superior strength, stiffness, and ductility in comparison to other NSM reinforcing techniques such as FRP strip sheets [11]. These methods, however, present challenges in the form of corrosion, fire-resistance, and cost; and generally do not improve the buckling resistance of the wall.

1.1.3 Design of Modern Reinforced Masonry Walls in North America

Clause 9.3.5.4.2 of the U.S. masonry code, TMS 402-16 [2], requires that P-Δ effects in the design of OOP RM walls be accounted for by utilization of a magnified moment, Mu. The magnified design moment may be calculated in one of two ways.

1) Clause 9.3.5.4.2 states that the design moment may be determined using a P-δ (load-displacement) method as follows.

$$M_u = \frac{w_u h^2}{8} + \frac{P_{uf} e_u}{2} + (P_{uf+}P_{uw})\delta_u$$

   The equation above may be utilized if the following conditions are met.

   - The design moment is calculated at the wall mid-height
   - Simple supports are utilized at the top and bottom of the wall
   - The compressive stress due to the strength level axial load must not exceed 20% of the masonry compressive strength (f'm)
   - If the slenderness ratio (kh/t) exceeds 30, the compressive stress due to the strength level axial load must not exceed 0.05f'm

2) Clause 9.3.5.4.3 states that the design moment may be determined by a second-order analysis or by a first-order analysis utilizing a moment magnifier parameter as follows.

$$M_u = M_{u.0}\left(\frac{1}{1 - {P_u}/{P_e}}\right)$$

The treatment of OOP RM walls in the Canadian code is similar to TMS 402. In terms of slenderness, CSA S304-14 utilizes the following three brackets for categorization of RM walls [1].

- $kh/t < 10 - 3.5(e_1/e_2)$ Slenderness ignored
- $kh/t < 30$ Slender
- $kh/t > 30$ Very slender

For walls where slenderness can be ignored, CSA S304 does not require that P-Δ effects be accounted for in determination of the design moment.

For walls with kh/t < 30, P-Δ effects are accounted for in the determination of the total factored moment (M_{ftot}). According to clause 10.7.3.3.2, the total factored moment may be calculated using either a P-δ method or a moment magnifier method.

$$M_{ftot} = M_{fp} + P_f \delta_f \qquad \text{P-Delta method}$$

$$M_{ftot} = M_{fp} C_m / (1 - P_f / P_{cr}) \qquad \text{Moment Magnifier method}$$

For walls with slenderness ratios greater than 30, the P-δ and moment magnifier methods may be used, however; clause 10.7.4.6.1 imposes the following five additional criteria.

- Walls must be constructed with masonry units 140 mm or more in thickness
- Eccentric pin end conditions must be assumed at each end
- The factored axial load can not exceed $0.1\phi_m f'_m A_e$
- Rebar yielding must occur before masonry crushing (i.e., ductile response)
- The total factored moment must be determined at the mid-height of the wall and is calculated as:

$$M_{ftot} = \frac{w_f h^2}{8} + \frac{P_{ft} e}{2} + (P_{fw+} P_{ft})\Delta_f$$

The testing conditions used by the SEAOSC and ACI-SC researches in 1979 may have unintentionally impacted the clauses related to the design of slender masonry walls in CSA S304. In addition to stipulations for minimum block thickness, ductile steel yielding, and a maximum slenderness ratio of 30, clause 10.7.4.6 also limits the axial load to 10% of the wall's pure axial capacity and requires a pin-support assumption [1]. Both are conditions used by the SEAOSC and ACI-SC researchers.

1.1.4 Effective Flexural Rigidity, EI*eff*

RM walls are often required to resist combinations of axial and OOP loads. However, the strength of a RM wall is compromised by the introduction of secondary moments acting on the defected shape. The OOP response of a RM wall is influenced by external factors such as applied lateral load, applied axial load, and the degree of axial load eccentricity. Other effects, such as, material and geometric non-linearities are equally influential. Adding further complexity, is the fact that sectional properties vary along the length of the wall due to the tensile cracks developed as a result of masonry's inherently low tensile strength. All these factors impact the effective flexural rigidity (EI_{eff}) of the wall which dictates the OOP response.

In 1976, Drysdale conducted tests on a series of eccentrically loaded masonry walls. He demonstrated that the design provisions in CSA S304 at the time were conservative [12]. Further research published in 1986, demonstrated that the negative effects of slenderness, as dealt with by CSA S304, are over-estimated for most slenderness ratios while the effects of load eccentricity appear to be under-estimated. This analytical and experimental study concluded that reassessment of current design provisions would result in increased ultimate capacity in most scenarios [13].

In 2001, a series of 36 empirical tests [14] on 150 mm x 400 mm x 1200 mm, pin-supported, RM walls under simultaneously axial and OOP loads, produced several important findings related to modes of failure, and effective flexural rigidity as explained by the interaction between applied axial load and internal moment.

- For a given RM section there is a singular level of axial load which will produce the maximum moment capacity. It was observed that the flexural capacity of a RM specimen increases as the axial load converges to this unique point from below. On the increasing branch of the P-M interaction curve, the mode of failure tends to be tension dominant. Upon reaching the maximum moment value, higher axial load levels tend to result in compression dominant failure and decreasing moment capacity.

- On the ascending portion of the P-M interaction diagram for a RM wall, the effects of axial load on the flexural capacity outweigh the effects of the axial load acting on the deformed shape. Furthermore, OOP ductility tends to decrease as the axial load increases. Within the range of 0.3PMax to 0.5PMax, the failure mechanism shifts from ductile to brittle. When the axial load exceeds approximately 0.6PMax, the failure mode is entirely brittle and become more explosive.

- There is a marked difference in the way in which doubly-reinforced and singly-reinforced specimens respond to increasing levels of axial load. At lower levels of axial load, doubly-reinforced specimens benefit more, in terms of flexural capacity, due to the larger moment arm between the reinforcing layers. However, the reverse is true at higher axial loads where compression failure is dominant. This observation may be rationalized by the fact that rebar buckling causes faceshell spalling and premature collapse in the doubly-reinforced sections at higher axial load levels.

The effective flexural rigidity, $EI_{eff,}$ at any section in a RM wall may be regarded as a single parameter defined as the ratio of internal moment to curvature. Since there exists a unique combination of curvature and bending moment at each section in a RM wall, there must also exist a unique value of EI_{eff} at each section. CSA S304-16 provides the following equation for calculation of EI_{eff} in an attempt to account for slenderness effects when using the moment magnifier or P-Delta method. This equation assumes a single value of EI_{eff} for the entire member regardless of the moment/curvature ratios at different sections.

$$EI_{eff} = E_m \left[0.25I_o - (0.25I_o - I_{cr}) \left(\frac{e - e_k}{2e_k} \right) \right]$$

Further complexity is added by the CSA S304 assumption that a linear relationship exists between the masonry compressive strength, f'm, and the masonry modulus of elasticity, E_m, calculated as 850f'm. There is warranted uncertainty regarding this assumed linear relationship since E_m changes as the stress level increases due to changes in applied load and crack propagation further into the RM section [15].

When the ratio of effective flexural rigidity to uncracked flexural rigidly (EI_{eff}/EI_0) is determined empirically and compared to the same ratio as calculated using the S304 equation for EI_{eff}, several differences become apparent [14]. The empirically calculated ratio is generally larger than the theoretical ratio, which indicates that test values of EI_{eff} are generally larger than the corresponding code values. This difference becomes more pronounced with increasing axial load. Moreover, the difference is generally larger for specimens with a single layer of reinforcement due to the depth of tensile crack propagation. In regions where the ratio of load eccentricity to section thickness (e/t) is greater than 0.4, the divergence between the empirical and the S304 values of EI_{eff} is greatest. The empirical values may be up to three times higher.

EI_{eff} deteriorates as tensile cracks propagate further into the RM section due to increasing moments. When this phenomenon is analyzed in the context of applied axial load, it may be observed that the deterioration is most drastic for specimens with low levels of axial load. For specimens loaded at 0.01Pmax, EI_{eff} deteriorates by almost 100% percent at ultimate. For specimens loaded to 0.9Pmax, the deterioration is only 15% at ultimate [14].

When empirically established flexural capacities of RM specimens are compared to corresponding code predicted capacities, it has been noted that there is significant underestimation by CSA S304 in regions where compression failure dominates, generally between 0.3PMax and 0.8PMax. In calculation of the code predicted capacities, slenderness effects were accounted for by incorporation of the EI_{eff} parameter from S304. Therefore, it appears that the low estimation of flexural capacity by S304 is due to the underestimation of EI_{eff} [14].

An analytical modeling technique, accounting for both geometric and material nonlinearities was developed to study the OOP behaviour of RM walls under various loading conditions [16]. The effects of masonry crushing, longitudinal reinforcing steel, and tensile cracking were included in the development of moment-curvature (M-C) relationships of various RM sections. Using iterative and convergence techniques the validity of the analytical model was established based on data collected from several series of empirical tests conducted on similar RM walls. The results of this analytical study provide the following key insights.

- For a given eccentricity ratio (e/t), the axial capacity of a RM wall decreases with increasing slenderness. This is due to the development of higher second-order moments in more slender specimens. Additionally, for a given slenderness ratio, the axial capacity of a RM wall increases as the deflected shape changes from symmetric single curvature to double curvature.

- When all other parameters are constant, the effect of increasing slenderness was observed to decrease the axial capacity but increase the OOP ductility. The increase in ductility was noted to be most prominent for walls bent in single curvature due to the critical combination of moment magnifier effects and material nonlinearity.

- Increasing load eccentricity has a diminishing effect on axial capacity and a magnifying effect on OOP ductility. Specimens tested with smaller eccentricities were observed to fail due to masonry crushing, resulting in reduced ductility in comparison to specimen tested at larger eccentricities.

- For walls tested with simultaneous axial and lateral loads, slenderness has a dramatic effect on the reduction of lateral load capacity and flexural stiffness. In comparison to a wall with a slenderness ratio of 6, a typical wall with a slenderness ratio of 36 was shown to experience a 44% reduction in lateral load capacity, solely due to increased second-order effects.

As found in previous research [14], it was concluded that at fixed values of h/t, the extent to which CSA S304 underestimates EI_{eff} at ultimate load is dependent on loading eccentricity. The underestimation was observed to increase in significance as the loading eccentricity decreased and the failure mode progressed from pure tension, to combined tension and compression, and then to mainly compression [16].

The analytical model showed that for eccentricity ratios (e/t) up to 0.6, the deterioration of EI_{eff} is more rapid for walls bent in symmetric single curvature than for walls in double curvature [16]. Moreover, for walls bent in single curvature, the masonry stress level and depth of compression at the section of maximum moment are lower than for walls bent in double curvature. Considering both observations, it appears that the reduction in EI_{eff} is primarily due to tensile cracking in walls bent in single curvature. For walls bent in double curvature, the reduction in EI_{eff} is primarily due to the variation in E_m which is influenced by the non-linear stress/strain relationship of the masonry material at higher strain levels. This result is a reduction in both the extent of tensile crack propagation and OOP deflection, which leads to reduced second-order effects and higher effective flexural rigidity.

Due to the complex and highly interactive effects of the various parameters involved, it is difficult to generate a single equation to calculate EI_{eff}. The following two equations have been proposed as a lower bound approximation for EI_{eff} for two ranges of eccentricity ratios [16].

$$EI_{eff}/EI_0 = 0.80 - 1.95(1.00 - 0.01h/t)(e/t) \quad for \quad 0.0 \leq e/t \leq 0.04$$

$$EI_{eff}/EI_0 = 0.022(1.00 + 0.35h/t) \quad for \quad e/t > 0.04$$

A 2007 study [17] in which 12, 2.4 m high, RM walls were subjected to combined axial and lateral load, has corroborated some of the aforementioned findings. By inducing compression dominant failure, it was demonstrated that when using the EI_{eff} value proposed by S304, the calculated ultimate capacity is approximately 51-63% of the actual capacity.

It was found in 2017 that CSA S304 underestimates the load bearing capacity of RM walls subjected to simultaneous axial and OOP loading [18]. By comparing the actual capacities of masonry specimens from nearly four decades of empirical tests to their predicted capacities from CSA S304, it was demonstrated that the design moment, as calculated by the moment magnifier approach, is conservative. Overestimation of the design moment stems from underestimation of the Effective Rigidity (EI_{eff}) of cracked masonry sections. It was shown that for walls subjected to pure axial load, the overestimation becomes more prevalent with increasing wall height and decreasing load eccentricity. For walls subjected to simultaneous axial and OOP load, CSA S304 is especially conservative for high axial load levels. Data selected for this study encompassed a wide variety of design parameters, including: various end fixity conditions, specimen heights ranging from 2.4 m to 7.4 m, and slenderness ratios ranging from 2.9 to 51.

In 2018, a study [19] of three, 1.2 m high masonry walls, with slenderness ratios of 12.6 and 10.2, tested with pined-pined and fixed-pinned support conditions, demonstrated that the pined-pinned condition imposed by CSA S304 for walls with slenderness ratios greater than 30, is not realistic in certain case. It was found that when the base of an OOP loaded masonry wall is detailed in accordance with standard construction practices, the deformed profile is more closely predicted by that of an ideally fixed-pinned element than by a pinned-pinned element. It was concluded that a significant increase in lateral deflection occurs when the base of the wall is forced to behave as pinned [20].

1.1.5 Stiffening Elements

An innovative masonry element known as an "inline boundary element" or "stiffening element" has been used to enhance the in-plane performance of RM shear walls. It is anticipated that these "stiffening elements" can be adapted for use in slender walls to enhance the OOP stiffness and flexural strength.

Confined, in-line stiffening elements are an effective method for improving the in-plane seismic response of in-plane walls by enhancing the structural integrity of the regions of the wall under compression. Tied rebar "cages" are provided at the ends of the walls for three distinct purposes.

Firstly, the confining effect of the rebar cage increases the ultimate compressive strain capacity of the grout inside the ties and delays crushing. Secondly, the transverse ties prevent buckling of the longitudinal reinforcement in compression. Finally, the rebar cages enhance the overall structural ductility of the system by increasing the compressive strain capacity of the confined grout on the compression side of the wall and thereby facilitates yielding of the tension steel on the tension side of the wall [21]. The layer of steel in compression facilitates the development of higher tensile strain in the tension side rebar. This allows for development of greater curvature at the section level, and therefore, enhanced ductility.

A 2012 publication demonstrated that shear walls which employ confined concrete boundary elements can achieve ultimate drift values nearly twice those of similar masonry walls without boundary elements [22]. By testing four shear walls with aspect ratios of 2.0, it was shown that in-line boundary elements in masonry walls increase in-plane ductility by up to 48% and the total energy dissipation capacity by up to 260% in comparison to similar masonry walls without in-line boundary elements. The initial in-plane stiffness and ultimate in-plane capacity were also increased due to the presence of axial compressive stress in the boundary elements.

The promising results from these experimental tests have led to the proposal of a new category of Seismic Force Resisting System (SFRS) for CSA S304 known as Special Ductile Masonry Shear Walls [23]. This clause would contain prescriptive design requirements for masonry shear walls which utilize integral confined elements at the boundaries.

1.2 PROBLEM STATEMENT

Most conventional, loadbearing masonry walls designed to resist OOP loads rely on a single reinforcement layer, placed at the centre of a block, for flexural reinforcement. For slender walls, OOP stiffness is one of the primary considerations in the design of flexural reinforcement. A stiffer wall will result in reduction of OOP deflection, and therefore, second-order moment. Code constraints and practical limitations hinder designers who opt for multiple layers of reinforcement or non-conventional units seeking to enhance wall strength and/or stiffness. For instance, North American masonry codes limit the amount of reinforcement that can be placed on a tall wall to ensure it yields. Non-conventional units are difficult or expensive to acquire or produce for typical projects.

Relaxation of the slenderness limits and the associated constraints placed on the design and construction of tall masonry walls in CSA S304 would undoubtedly allow for more economical wall designs and better utilization of available space and materials. However, a general acceptance of empirically established design practices, and a posture of resistance toward revising long-established code clauses, creates uncertainty about whether such changes are possible. For such changes to occur, the results of any research program would have to unequivocally establish that the current methods and prescriptions are outdated. This is a complex, expensive, and time-consuming task, especially given the inherent complexity involved in testing masonry walls and assemblages.

Instead of modifying the existing criteria in CSA S304, a more fruitful approach is to develop an entirely new wall type not governed by the stipulations which currently apply to the design and construction of tall masonry walls. There exists a need to develop an innovative wall design which will allow for tall, slender masonry walls to be used as a viable option for resisting axial and OOP loads in low-rise and high-rise buildings

1.3 SCOPE

The specimens selected for testing in this research program were limited to five course high masonry prisms (slenderness ratio kh/t = 5.26) and 12 course high masonry walls (kh/t = 12.63). This decision was made since it was desired to understand the behaviour of the stiffening element at the assemblage level first, before attempting to implement it in a tall wall (kh/t > 30). As such, it is acknowledged that the results obtained in this study will not yet be directly applicable to the design of very slender walls (kh/t > 30) as per S304-14. However, it is expected that the experimental tests in this study provide insights on the structural performance of the stiffening elements, effectiveness range, constructability, and significant design parameters. The pilot study of five course high prisms in chapter one will be used to explore the feasibility of the cage-reinforcing concept and to investigate the basic performance of in-line stiffening elements under concentric and eccentric loads. Furthermore, the results of chapter one and two are intended to explore the uncertainty surrounding the potential of compressive rebar buckling and the viability of the proposed sliding block units in typical masonry.

It was understood prior to commencement of the research that load-deflection (P-Delta) effects for prisms and short walls are not as prominent as they are for tall walls. However, it was anticipated that this effect would nonetheless be observable and quantifiable in the chosen specimens. The P - Delta phenomenon was indeed observed, allowing for conclusions and recommendations to be drawn from the test results.

The study included walls and assemblages in which flexural strength governed the performance at failure. Out-of-plane shear failure and sliding are not mechanisms that control the behaviour except in cases with low axial load and low reinforcement ratios. This mode of failure sometimes occurs in in unreinforced masonry parapets and it rarely controls on loadbearing walls of common heights, thickness, and loads.

1.4 OBJECTIVES

The objectives of this research program are as follows.

1. Assessment of OOP design methods for flexure in the Canadian code

   The validity and/or veracity of the CSA S304 prescriptions for flexural strength of masonry prisms and walls will be investigated. Comparisons will be made between empirical test results and code predicted capacities for both prisms and walls.

2. Development of an innovative stiffening element

   Development of the stiffening element will comprise a comprehensive investigation of parameters such as; feasibility of the sliding masonry units, determination of the optimal vertical reinforcing ratio, and determination of an efficient transverse tie spacing. Additionally, aspects related to construction, such as, grout and mortal type, grout workability, and rebar cage clearances will also be assessed.

3. Assessment of stiffening element structural performance at the prism level

   Stiffening elements will first be explored in the context of five course high masonry prisms. Its effect on prism stiffness, flexural strength, and core integrity will be investigated. Comparisons will then be made with conventionally-reinforced prisms in terms of flexural strength and stiffness.

4. Assessment of stiffening element structural performance at the wall level

   Findings from the prism tests will be utilized in the adaptation of stiffening elements to full-scale wall applications. The performance of walls with stiffening elements will be compared to the performance of other wall types. The effects of the stiffening element on the walls' OOP stiffness and flexural strength will be quantified and discussed.

5. Recommendations for future research

   Insights gained from this research program will be presented in order to assist future research on this topic. Suggestions will be given for specimen parameter alterations, testing configuration changes, and modeling techniques.

CHAPTER 2: PRISMS WITH IN-LINE STIFFENING ELEMENTS

2.1 SUMMARY

Flexural reinforcement of loadbearing, out-of-plane (OOP) walls is usually achieved via reinforcing bars placed in the middle of grouted cells. Although this method of reinforcing is usually effective for non-slender walls with low levels of OOP moment, it is not efficient for slender walls with large OOP moments. Low flexural stiffness in slender walls leads to increased OOP deflection and subsequent second-order moments. Providing additional reinforcement to meet the flexural strength demands can produce over-reinforced sections and result in code non-compliance. Therefore, the need exists to develop an innovative masonry assemblage with increased flexural stiffness to allow for efficient design of slender masonry walls.

An innovative reinforcing scheme, relying on pre-tied cages consisting of four 10M bars to provide flexural reinforcement for masonry bending members, is presented in this paper. The moment capacity and flexural stiffness of several masonry assemblages is explored by testing five course high prisms under concentric and eccentric loading. The behaviour of the innovative prisms under eccentric loading is compared to that observed in conventionally reinforced prims (i.e., reinforced with a single layer of steel at mid-cell). The results indicate that the innovative reinforcing cage has a beneficial effect on both the flexural strength and stiffness of masonry prisms. A mechanics-based fibre-section model utilizing plane-section compatibility is used to compare the performance of the cage reinforced prisms to conventionally reinforced prisms with various amounts of centrally located reinforcing steel.

Insight collected from the research on masonry prisms will be utilized in the construction and testing of four walls in chapter three. The innovative masonry assemblage and reinforcing scheme will be adapted for wall tests to investigate its performance in designs that are representative of modern industry practices.

2.2 INTRODUCTION

This chapter presents a pilot study on the use of stiffening elements in masonry prisms. The system consists of a pre-tied reinforcement cage that fits in one masonry unit, effectively becoming a "concealed column". The system is used in combination with specially designed units able to slide around the cage. The stiffening elements act as regions of localized strength and stiffness, increasing the buckling strength and reducing second order effects. It is noted that under significant axial loads, the reinforcement layer in compression will likely also increase ductility in OOP walls by enhancing the crushing strength of the confined grouted core and by facilitating the development of higher tensile strain in the tension (convex) side rebar. This chapter focuses on concentric and eccentric tests conducted on five course high prisms reinforced with either conventional central rebar or a reinforcing cage. The results are discussed in terms of feasibility of construction, strength, stiffness, structural performance, and failure modes.

2.3 EXPERIMENTAL SETUP

2.3.1 Materials

2.3.1.1 Concrete Blocks

Two types of bocks were used for construction of all prisms in this study: 190 mm x 390 mm full-lintel blocks with 35 mm faceshells and 190 mm x 390 mm half-lintel blocks with 35 mm faceshells. The nominal block compressive strength was 15 MPa.

2.3.1.2 Mortar

Type S mortar was used for all joints. The mortar was prepared by experienced masons using standard industry procedures. A total of six - 2" cubes were tested to establish the mortar compressive strength. The cubes had an average compressive strength of 13.75 MPa with a standard deviation of 0.48 MPa. Data for the mortar cube tests is presented in Table 2.1

Table 2.1 – Mortar Cube Data

Cube #	Peak Axial Load (kN)	Compressive Strength (MPa)
1	37.6	14.6
2	33.7	13.1
3	36.4	14.1
4	34.6	13.4
5	35.4	13.7
6	35.2	13.6

2.3.1.3 Grout

Course grout was used to fill all the prisms. The grout was mixed to achieve adequate workability to ensure flow between the rebar cages and the prism faceshells. A total of four - 4" diameter cylinders were tested to establish the grout compressive strength. The cylinders had an average strength of 35.93 MPa with a standard deviation of 5.81 MPa. Data for the grout cylinder tests is presented in Table 2.2.

Table 2.2 – Grout Cylinder Data

Cylinder #	Peak Axial Load (kN)	Compressive Strength (MPa)
1	210.4	26.0
2	320.1	39.5
3	326.0	40.2
4	308.6	38.1

2.3.1.4 Rebar

All prisms were reinforced with either 10M or 15M reinforcing bars with a nominal yield strength (f_y) of 400 MPa. Tensile tests established the actual yield strength as 440 MPa and the yield strain as 0.0024 mm/mm. Using Hooke's Law with the recorded stress and strain readings in the elastic region, the modulus of elasticity (E) was calculated to be 184 000 MPa. Figure 2.1 shows the stress/strain response for the 10M bars. The response is virtually identical up to the yield plateau with only slight divergence in the stain-hardening stage.

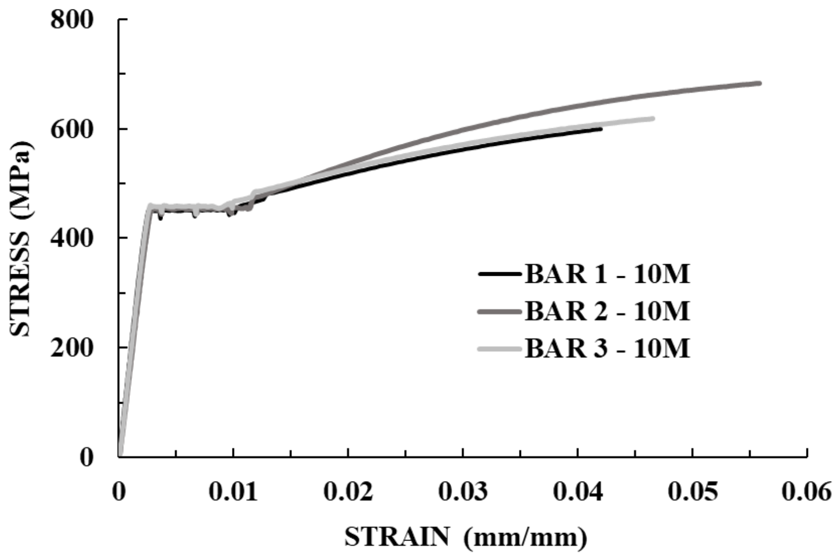

Figure 2.1 – Rebar Stress vs. Strain

2.3.2 Test Specimens

A total of 40 fully-grouted masonry prisms were constructed in the I.F. Morrison Structures Laboratory at the University of Alberta (Table 2.3). All prisms were five courses high and constructed with full-lintel and half-lintel blocks (Fig. 2.2). Five prisms were unreinforced, and 35 prisms were constructed with either conventional or cage reinforcing. Five course prisms were selected for testing to reduce the effects of end confinement and to capture overall member response rather than predominantly material response as is typical for two or three course prisms. The mortar joints were 10 mm thick, resulting in an overall prism height of 990 mm. Alternate courses of full lintel and half-lintel blocks were used to produce a running bond pattern. The end webs were removed from all blocks which resulted in open ends on the three courses with full lintels blocks. These openings were staggered and fully blocked to allow grouting (Fig. 2.3). Experienced masons constructed the prisms using typical industry procedures.

Table 2.3 – Prism Specimen Summary

Prism ID	Reinforcing Type	Test Type
1, 2, 3, 4, 5	4-10M Cage w/ ties @ 150 mm c/c	Concentric Load
21, 22, 23, 24, 25	4-10M Cage w/ ties @ 112 mm c/c	Concentric Load
26, 27, 28, 29, 30	4-10M Cage w/ ties @ 64 mm c/c	Concentric Load
36, 37, 38, 39, 40	Unreinforced	Concentric Load
6, 7, 8, 9, 10	4-10M Cage w/ ties @ 150 mm c/c	Eccentric Load, e = t/6 (31.7 mm)
11, 12, 13, 14, 15	4-10M Cage w/ ties @ 150 mm c/c	Eccentric Load, e = t/3 (63.3 mm)
16, 17, 18, 19, 20	4-10M Cage w/ ties @ 150 mm c/c	Eccentric Load, e = 5t/12 (79.2 mm)
32, 33	2-15M Conventional	Eccentric Load, e = t/3 (63.3 mm)
34, 35	2-15M Conventional	Eccentric Load, e = 5t/12 (79.2 mm)

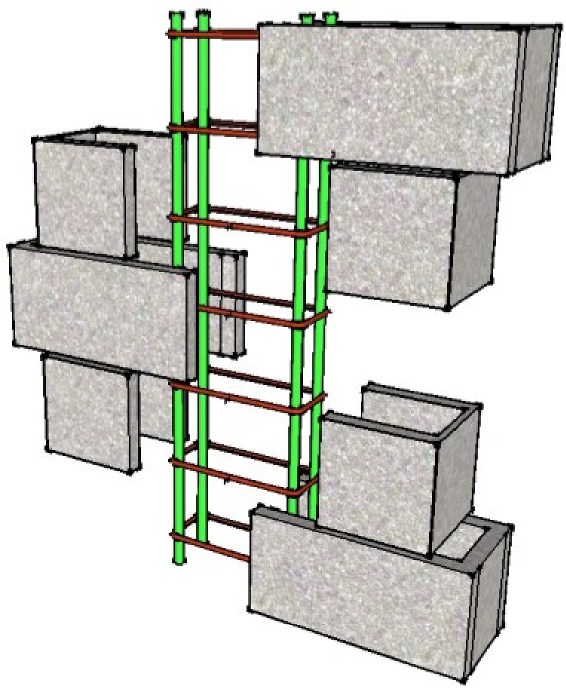

Figure 2.2 – Typical Prism Construction

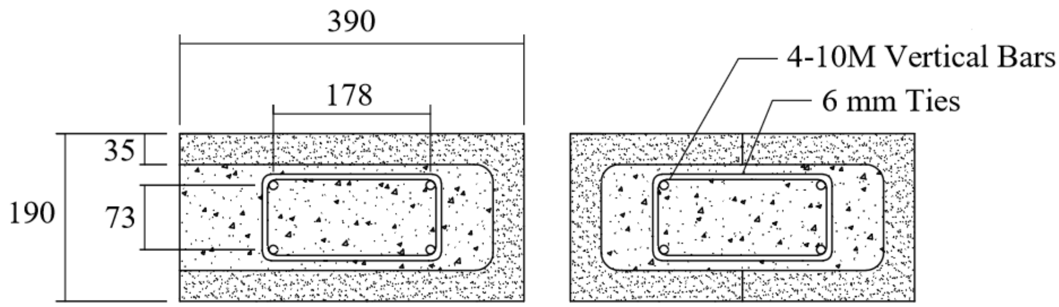

A) Cage-Reinforced Prism

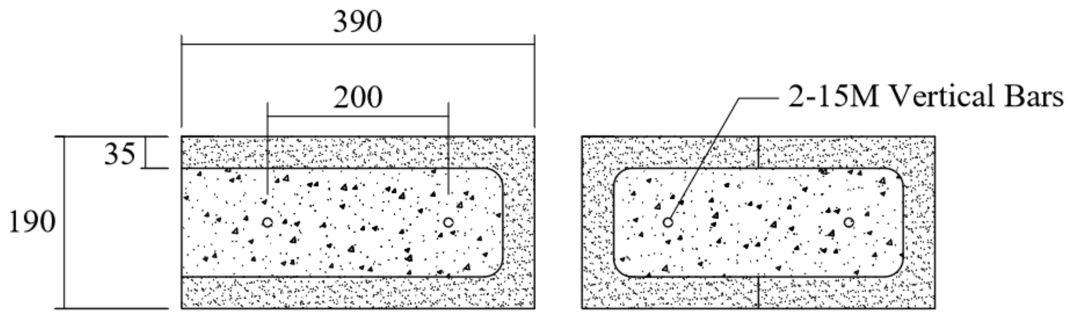

B) Conventionally-Reinforced Prism

Figure 2.3 – Prism Sections

Cage reinforcing was provided for 30 prisms. The pre-tied reinforcing cages were fabricated with four 10M (11.3 mm dia.) bars as longitudinal reinforcement and 6.34 mm smooth wire ties for transverse reinforcement (Fig. 2.4). Three specific tie spacings were selected to assess their efficiency in preventing rebar buckling. According to S304-14, transverse tie spacing for reinforcing bars in compression should be the lesser of 16 times the diameter of the longitudinal bars (181mm), 48 times the diameter of the ties (304 mm), or the least dimension of the member (190 mm). Therefore, the spacing that controls, according with this criterion, is 181 mm.

It must be noted that these requirements are similar to those found in reinforced concrete codes. For the rebar cage inside the masonry prism, however, it could be argued that the least dimension of the member could also be the width of the "confined" core, which is significantly smaller than 190 mm. This revised width can be calculated approximately as the width of the unit less the thickness of the faceshells, equal to 190 mm – 2 (32mm) = 126 mm.

To investigate the influence of the tie spacing in preventing rebar buckling, a range of tie spacings were provided. These were chosen as 150 mm, 112 mm, and 64 mm translating into 7, 9, and 15 ties per prism, respectively. Five prisms were reinforced as per conventional masonry construction practices, with bars at the middle of the cell (2-15M), providing the same reinforcement ratio as that of the prisms with cages. The remaining five prisms were fully grouted and unreinforced.

Figure 2.4 – Reinforcing Cages

Figure 2.5 – Finished Prisms

2.3.3 Test Procedure

Compressive tests were conducted using an MTS hydraulic press with a maximum axial capacity of 6200 kN. A displacement-controlled loading rate of 2 mm/minute was utilized for all axial loads. Prior to testing, the top and bottom of each prism was capped with a 10 mm thick layer of plaster. A 7/16" thick fiber board layer was used on top and bottom in addition to the plaster cap.

2.3.3.1 Concentric Testing

To investigate the response of the prisms under pure axial load, quantify the grouted masonry strength (f'm), and to determine the impact of tie spacing on reinforcement buckling and grouted core integrity, 20 grouted, unreinforced prisms were tested under purely concentric load. Five prisms were unreinforced, five prisms had the maximum tie spacing of 150 mmc/c, five prisms had the intermediate tie spacing of 112 mm c/c, and the remaining five prisms had a tie spacing of 64 mm c/c.

2.3.3.2 Eccentric Testing

Eccentric loading was utilized to investigate the response of the prisms to a combination of axial load and bending moment. Three eccentricities were selected for investigation: t/6 (31.7 mm), t/3 (63.3 mm), and 5t/12 (79.2 mm), as in similar studies [24]. The eccentric axial load was applied via two machined steel channel caps at the top and bottom of the prisms (Fig. 2.6). At the top and bottom, roller assemblies were provided to allow for uninhibited OOP rotation (Fig. 2.7). Three sets of holes were machined in the channel caps to allow for attachment of the roller assemblies at the three required eccentricities.

Figure 2.6 – Machined Channels

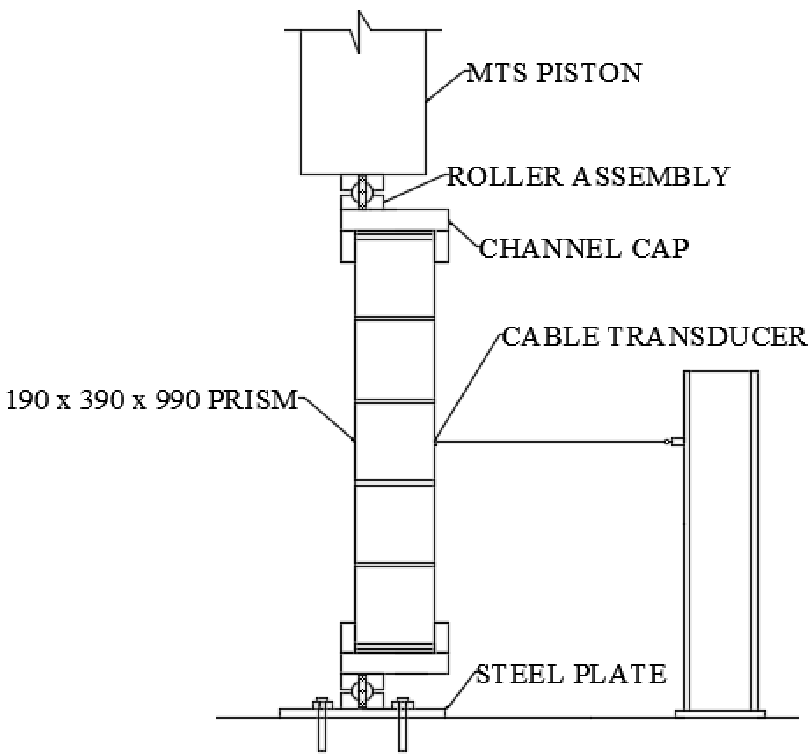

Figure 2.7 – Eccentric Testing Setup

2.4 INSTRUMENTATION

Each of the prisms with cage reinforcing was instrumented with four strain gauges, one on each bar at mid-height (Fig. 2.4). For each conventional prism, only two strain gauges were used. Axial load was applied via a 6 200 kN capacity MTS hydraulic press. The axial displacement was recorded directly by the MTS module. Mid-height prism deflection was recorded via a cable transducer mounted on a stub column several meters from the MTS press (Fig, 2.8).

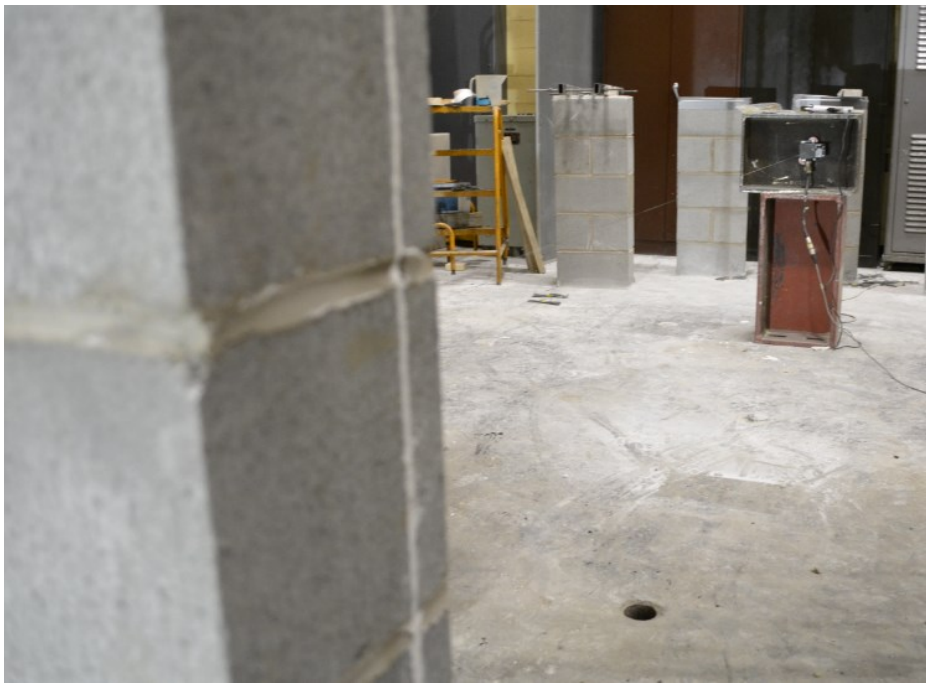

Figure 2.8 – Cable Transducer on Column in Background (Prism in Foreground)

Figure 2.9 – Cable Transducer to Prism Attachment

2.5 TEST RESULTS

Data collected from the 20 concentric and 19 eccentric tests is presented in this section. One of the conventional prisms was not tested due to a construction defect.

In all the subsequent graphs, charts, figures and discussions, the following sign convention has been utilized: axial compression and compressive strains are positive while axial tension and tensile strains are negative.

2.5.1 Concentrically Loaded Prisms

2.5.1.1 Failure Modes – Unreinforced Prisms

Failure of the grouted, unreinforced prisms was characterised by significant multidirectional cracking on all four sides. The faceshells and core both cracked, and the prims separated into two or more pieces at ultimate load. Figure 2.10 contains photos representative of the state of damage of the unreinforced prisms upon removal from the testing apparatus.

Prism 36 **Prism 40**

Figure 2.10 – Unreinforced Prism Damage

2.5.1.2 Grouted Compressive Strength (f'm) – Unreinforced Prisms

From the five unreinforced prism specimens, the grouted masonry compressive strength (f'm) was established to be 21.0 MPa. Table 2.4 contains the peak axial capacity of each prism. The average axial capacity is 1559 kN with a standard deviation of 238 kN.

Table 2.4 – Unreinforced Prism Data

Prism #	Peak Axial Load (kN)	Compressive Strength (MPa)
36	1663	22.4
37	1543	20.8
38	1785	24.1
39	1162	15.7
40	1642	22.2

2.5.1.3 Failure Modes – Cage Reinforced Prisms

Under pure axial load, the failure mechanism of the three prism types was observed to be consistent. Each prism was loaded at a uniform rate until its ultimate axial capacity was reached. Further vertical displacement of the MTS head was applied until the load decreased to approximately 100 kN. Prior to reaching peak load, vertical cracks developed in the exterior of the concrete blocks at arbitrary locations. Ultimate load was reached when portions of the concrete faceshell abruptly separated from the prism core and the axial load dropped sharply. Upon imposing further MTS displacement, the axial resistance of the prisms continued to decline while further spalling occurred. Figure 2.11, 2.12, 2.13 contain photos representative of the state of damage of each of the three prism types upon removal from the testing apparatus. As noted previously, there is no significant difference in the damage pattern between the three prism types

Prism 21 **Prism 24**

Figure 2.11 – Prism Damage (64 mm Tie Spacing)

Prism 28 **Prism 26**

Figure 2.12 – Prism Damage (112 mm Tie Spacing)

Prism 5 **Prism 4**

Figure 2.13 – Prism Damage (150 mm Tie Spacing)

Assessment of the damage photos warrants the conclusion that the confined core appears to be well-preserved in all cases. This correlates directly with one of the objectives of this study; namely, to assess the effects of the reinforcing cage on the integrity of the grouted core. Subsequent discussion will focus on the increased rigidity provided by an un-damaged core.

Longitudinal rebar buckling was not observed in any of the concentrically tested prisms even though the strain readings in Table 2.5 indicate that several of the bars exceeded the compressive yield strain (0.0024 mm/mm) at ultimate load. Since none of the bars were observed to buckle, and since there was no significant difference in axial capacity across the three prism types, it may be concluded that the tie spacing requirement from CSA S304-14 for compressive members is sufficient to prevent buckling of longitudinal reinforcement.

2.5.1.4 Force-Displacement Response and Strain Data – Cage Reinforced Prisms

Table 2.5 provides a summary of the data collected from each of the concentrically tested prisms. In addition to the peak axial load, the corresponding compressive strain at peak load in each bar is also provided. The last column in Table 2.5 contains the total rebar force developed in each prism at ultimate load as calculated by Hooke's Law using the rebar strain and modulus of elasticity.

Table 2.5 – Concentric Prism Test Results

Prism ID	Tie spacing (mm)	Peak Axial Load (kN)	Axial Deformation (mm)	Peak Rebar Strain (10^{-6} mm/mm)				Peak Rebar Force (kN)
				Bar 1	**Bar 2**	**Bar 3**	**Bar 4**	
1	150	2254*	4.55	1976	7092	1815	2046	151
2	150	1884	3.96	1336	1788	1871	1472	119
3	150	1885	4.03	1824	1289	1519	2024	122
4	150	1670	3.69	1311	1094	1777	1974	113
5	150	1777	4.10	2043	1310	1475	1851	123
		Avg. = 1804	**Avg. = 4.07**	**Avg. = 1622**				**Avg. = 119**
21	112	1585	3.70	1756	1040	1004	1487	97
22	112	1812	3.82	1354	1685	1756	1542	116
23	112	1536	3.60	1503	2319	1309	2001	131
24	112	1611	3.63	1532	2407	1047	1769	124
25	112	1675	3.68	1591	1963	1908	1968	137
		Avg. = 1644	**Avg. = 3.69**	**Avg. = 1647**				**Avg. = 121**
26	64	1744	4.02	1905	1361	1782	2170	133
27	64	1784	3.97	1815	1751	2843	2274	151
28	64	1777	3.95	1597	2061	1961	6883*	147
29	64	1960	3.99	1805	1921	2010	1963	142
30	64	1839	3.92	1559	2059	1879	2406	145
		Avg. = 1821	**Avg. = 3.97**	**Avg. = 2200**				**Avg. = 144**

In the preceding table, all data from prism 1 was omitted from all calculations. The peak axial capacity of this prism was approximately 300 kN higher than that of any other prism. Exclusion of this prism from the data set is justified by the fact that the MTS axial loading rate was set too high in the initial test, about 2 times higher than that used in the rest of the tests. It is possible that the faster loading rate artificially increased the axial capacity of this prism. Additionally, the peak rebar strain value for bar 4 of prism 28 was omitted from all calculations since it is approximately three times as high as the other strain values for prism 28. It is possible that the prism was not completely centered in the loading apparatus, causing a loading eccentricity and an inordinate axial load in bar 4.

Table 2.5 shows that the peak compressive strength was consistent for all prisms regardless of tie spacing, and that only the rebar strains are influenced by this parameter. Bars in prisms with closer tie spacings develop higher compressive strains (and forces) at peak load. None of the bars in prisms with the largest tie spacing (150 mm) showed yielding at peak load. Of the intermediate spacing (112 mm), one prism (24) reached rebar yielding at peak load, and of the minimum tie spacing (64 mm), two prisms (27 and 30) reached rebar yielding at peak load. Figure 2.14 contains graphs of the data collected for each of the concentrically tested prisms, organized by transverse tie spacing. In each figure, graph I shows the axial load vs. axial deformation response under pure compression and graph II shows the average compressive strain in the four bars over the entire range of applied axial load.

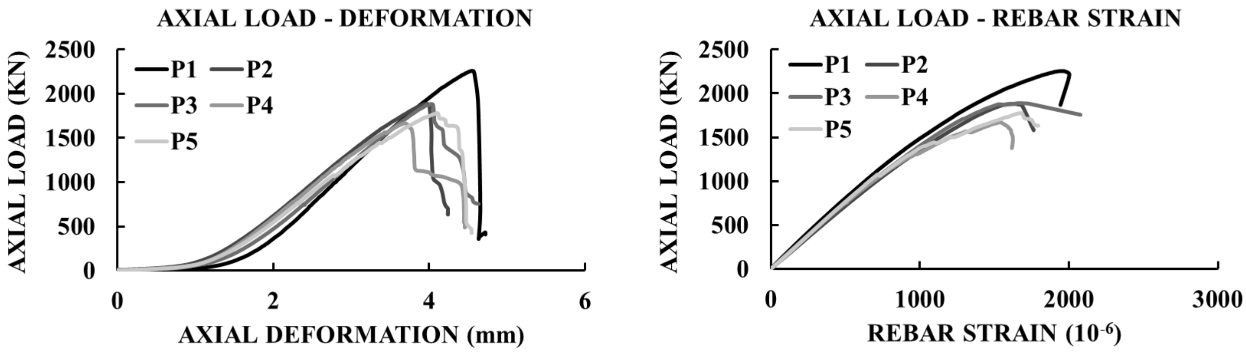

I) (A) – 64 mm Tie Spacing II)

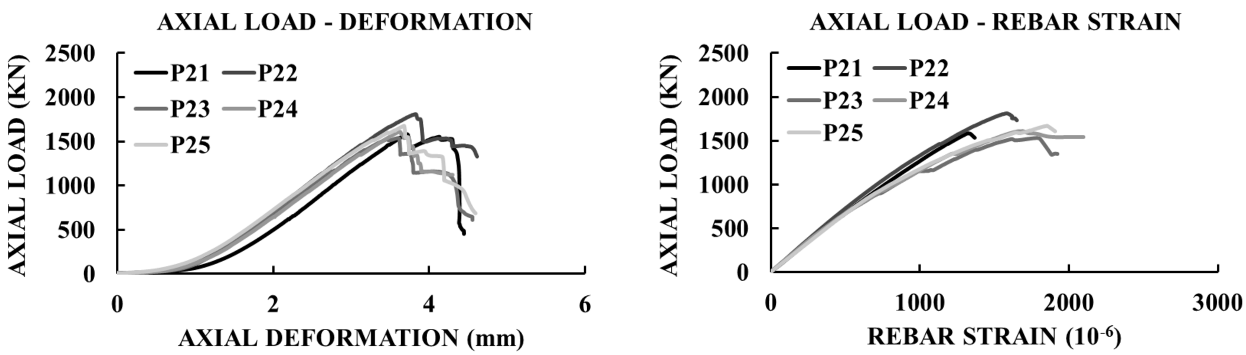

I) (B) – 112 mm Tie Spacing II)

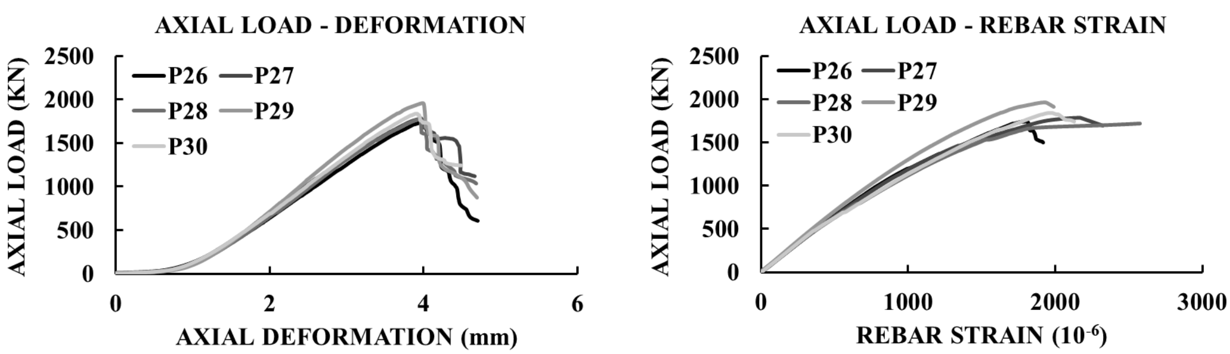

I) (C) – 180 mm Tie Spacing II)

Figure 2.14 – Test Data (Concentric Load)

In Figure 2.14, the compressive response shows an initial portion in which the MTS6000 settled on the fibreboard ply that was used as capping. After that portion, the load rises steadily, in a nearly elastic manner up to the peak load, after which there is a sudden drop in strength. Similarly, the bar strains show a consistent increase in compression up to failure.

2.5.2 Eccentrically Loaded Prisms

A total of 19 prisms were tested under eccentric load (Table 2.3); 15 prisms were cage-reinforced and 4 were conventionally-reinforced. Of the cage reinforced prisms, five were tested at an eccentricity of t/6 (31.7 mm), five were tested at an eccentricity of t/3 (63.3 mm), and five were tested at an eccentricity of 5t/12 (79.2 mm). Two of the conventional prisms were tested at t/3 (63.3 mm) and the remaining two were tested at 5t/12 (79.2 mm).

2.5.2.1 Failure Modes – Cage Reinforced Prisms

Under eccentric axial load, the extent of damage for each prism appears to be dependent on the degree of loading eccentricity. Each prism was loaded at a uniform rate until its ultimate axial capacity was exceeded. As in the concentric tests, further vertical displacement of the MTS head was applied until the load dropped to approximately 100 kN. Prior to reaching peak load, horizontal cracks began to develop in the bed joints on the tension face of the prisms. Peak load was reached when the concrete masonry crushed on the compression face and the axial load dropped sharply. Further vertical MTS displacement resulted in rapid lateral deflection and decline in axial resistance.

Characteristic observations made at each test eccentricity are described next. Prisms tested at an eccentricity of t/6 (31.7 mm) all displayed a similar failure mechanism (Fig. 2.15). Cracks developed initially in the face shell on the compression side prior to reaching the ultimate load. When successive load was applied, the face shells spalled. The cores of all the prisms tested at this eccentricity remained mostly intact.

Prism 6 **Prism 9**

Figure 2.15 – Prism Damage (31.7 mm Ecc.)

At peak load, prisms tested at an eccentricity of t/3 (63.3 mm) exhibited a crack in the compression face shell. Upon development of a crack, a part of the face shell on the compression side of the prism became detached (Fig. 2.16).

Prism 15 **Prism 12**

Figure 2.16 – Prism Damage (63.3 mm Ecc.)

Prisms tested at an eccentricity of 5t/12 (79.2 mm) exhibited little damage at ultimate load (Fig. 2.17). At peak load, the faceshell broke away from the core, initiating collapse.

Prism 20 **Prism 18**

Figure 2.17 – Prism Damage (79.2 mm Ecc.)

2.5.2.2 Force-Displacement Response and Strain Data – Cage Reinforced Prisms

Table 2.6 provides a summary of the data collected from each of the eccentrically tested, cage-reinforced prisms. In addition to the peak axial load, the corresponding mid-span deflection, peak convex side rebar strain, and peak concave side rebar strain is given for each prism. In Table 2.6, axial compression and compressive strain are positive while tensile strain is negative.

Table 2.6 – Eccentric Prism Test Results (Cage Reinforcing)

Prism ID	Eccentricity (mm)	Peak Load (kN)	Peak Mid-Span Deflection (mm)	Peak Convex Side Rebar Strain (10^{-6} mm/mm)		Peak Concave Side Rebar Strain (10^{-6} mm/mm)	
				Bar 1	**Bar 2**	**Bar 1**	**Bar 2**
6	31.7 (t/6)	1082	4.0	230	N/A	1361	1138
7	31.7 (t/6)	1029	2.6	243	302	1247	1080
8	31.7 (t/6)	986	3.2	248	459	1241	774
9	31.7 (t/6)	1007	4.6	355	355	1255	1104
10	31.7 (t/6)	1157	4.0	462	381	1390	1410
		Avg. = 1052	**Avg. = 3.7**	**Avg. = 337**		**Avg. = 1200**	
11	63.3 (t/3)	682	7.8	-866	-883	667	N/A
12	63.3 (t/3)	518	6.8	-842	-787	N/A	681
13	63.3 (t/3)	646	6.7	-636	-951	1022	808
14	63.3 (t/3)	598	7.1	-1500	-929	990	557
15	63.3 (t/3)	679	6.9	-1006	-812	953	720
		Avg. = 625	**Avg. = 7.0**	**Avg. = -921**		**Avg. = 800**	
16	79.2 (5t/12)	456	11.7	-2757	N/A	315	259
17	79.2 (5t/12)	422	10.8	-2500	-2349	629	81
18	79.2 (5t/12)	399	9.7	-1599	-1739	332	457
19	79.2 (5t/12)	416	11.3	-1850	-2176	295	452
20	79.2 (5t/12)	416	10.5	-2537	-2510	400	468
		Avg. = 422	**Avg. = 10.8**	**Avg. = -2224**		**Avg. = 369**	

Table 2.6 shows that the prism peak axial load capacity decreases with increasing loading eccentricity, while the mid-span deflection increases. In relation to prisms tested at t/6 (31.7 mm), the average peak axial capacity of prisms tested at t/3 (63.3 mm), is 41% lower, and the average peak mid-span deflection is 89% higher. The average peak axial capacity of prisms tested at 5t/12 (79.2 mm), is 60% lower, and the average peak mid-span deflection is 192% higher.

The data in Table 2.6 clearly indicates that the concave side rebar strain tends to decrease (become less compressive) with increasing eccentricity, while the convex side rebar absolute strain tends to increase (become more tensile).

Figure 2.18 contains graphs of the data collected for each of the eccentrically loaded, cage-reinforced prisms. In each figure, graph I shows the axial load vs. lateral deflection response, and graph II) shows the average of the compressive and tensile strain in the four bars over the entire range of applied axial load. In each of the strain diagrams there are two distinct families of curves. As indicated on the figures, one family represents the convex side rebar, and the other represents the concave side rebar. Axial compression and compressive strain are positive while tensile strain is negative.

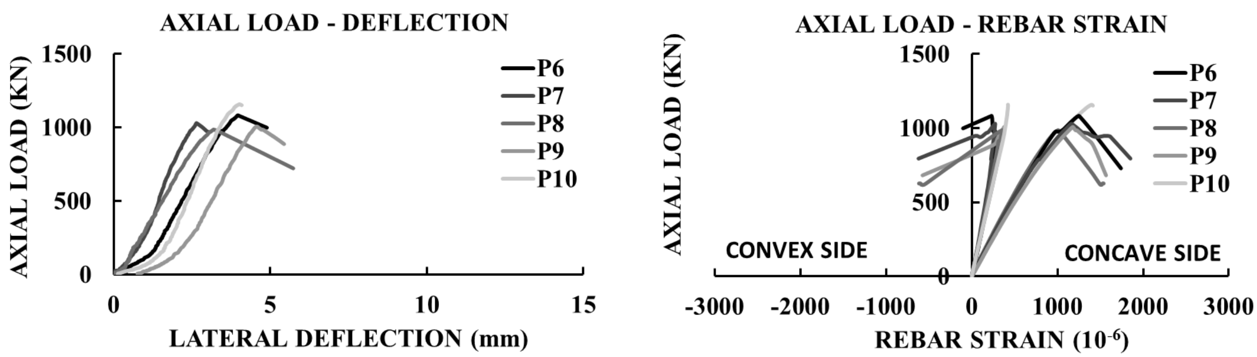

I) (A) – Ecc. = t/6 (31.7 mm) II)

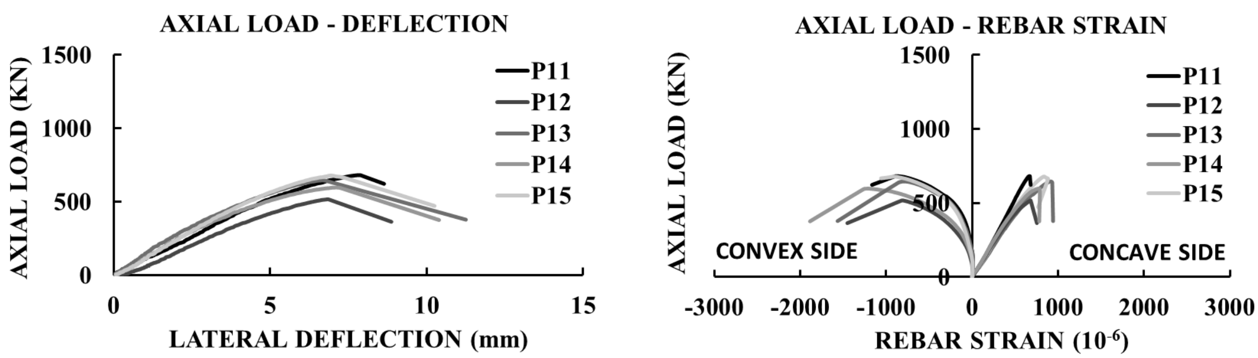

I) (B) – Ecc. = t/3 (63.3 mm) II)

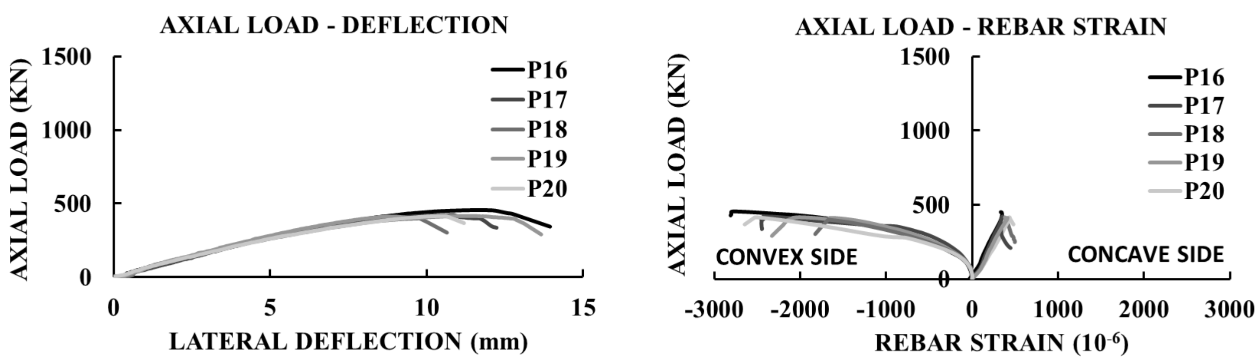

I) (C) – Ecc. = 5t/12 (79.2 mm) II)

Figure 2.18 – Eccentric Test Data (Cage Reinforcing)

Figure 2.18A shows that for prisms tested at an eccentricity of t/6 (31.7 mm), all four bars stayed in compression (positive strain) up to the peak axial load. Peak load was reached when the masonry crushed on the concave face. Further vertical displacement of the MTS head resulted in rapid lateral deflection and a necessary shift in the neutral axis towards the prism concave face. As a result, the bars on the convex side cross from compressive strain into tensile strain shortly after peak load.

For prisms tested at t/3 (63.3 mm), the bars on the convex side crossed from compressive strain into tensile strain at approximately 25% of peak axial load. Peak load was reached when the masonry crushed on the concave prism face.

For prisms tested with an eccentricity of 5t/12 (79.2 mm), the bars on the convex side were in tension, and the bars on the concave side were in compression from commencement of the test until peak axial load. Tensile rebar yielding was observed in three of the five prisms. Peak load was reached when the masonry crushed on the concave prism face.

2.5.2.3 Failure Modes – Conventionally Reinforced Prisms

Figure 2.19 and Figure 2.20 contain representative photos of the damage and deformation experienced by conventionally reinforced prisms subjected to eccentric loading. Similar to the cage reinforced prisms, the extent of damage appears to be dependent on the degree of loading eccentricity. The damage appears to be higher at lower eccentricities, as noted previously with cage reinforced prisms. It should be noted that the conventionally-reinforced prism intended for testing at t/6 (31.7 mm) had a significant construction defect and was discarded.

Prism 32 **Prism 33**

Figure 2.19 – Prism Damage (63.3 mm Ecc.)

Prism 34 **Prism 35**

Figure 2.20 – Prism Damage (79.2 mm Ecc.)

2.5.2.4 Force-Displacement Response and Strain Data – Conventionally Reinforced Prisms

Table 2.7 provides a summary of the data collected from each of the eccentrically tested, conventionally-reinforced prisms. In addition to the peak axial load, the corresponding mid-span deflection, and peak tensile strain values are given for each prism.

Table 2.7 – Eccentric Prism Test Results (Conventional Reinforcing)

Prism ID	**Testing Eccentricity (mm)**	**Peak Load (kN)**	**Peak Mid-Span Deflection (mm)**	**Peak Rebar Strain (10^{-6} mm/mm)**	
				Bar 1	**Bar 2**
32	63.3 (t/3)	593	8.7	-345	-487
33	63.3 (t/3)	602	8.3	-72	-562
		Avg. = 598	**Avg. = 8.5**	**Avg. = -366**	
34	79.2 (5t/12)	333	12.4	-2249	-1051
35	79.2 (5t/12)	426	11.8	-1689	-1816
		Avg. = 379	**Avg. = 12.8**	**Avg. = -1701**	

Table 2.7 shows that the prism peak axial load capacity decreases with increasing loading eccentricity, while the mid-span deflection increases. In relation to prisms tested at t/3 (63.3 mm), the average peak axial capacity of prisms tested at 5t/12 (79.2 mm), is 37% lower, and the average peak mid-span deflection is 51% higher. The data in Table 2.7 clearly indicates that the peak absolute rebar strain tends to increase (become more tensile) with increasing eccentricity.

Figure 2.21 contains graphs of the data collected from each of the four eccentrically loaded, conventionally-reinforced prisms. In each figure, graph I shows the axial load vs. lateral deflection response and graph II shows the average strain in the 2-15M central reinforcing bars over the entire range of applied axial load.

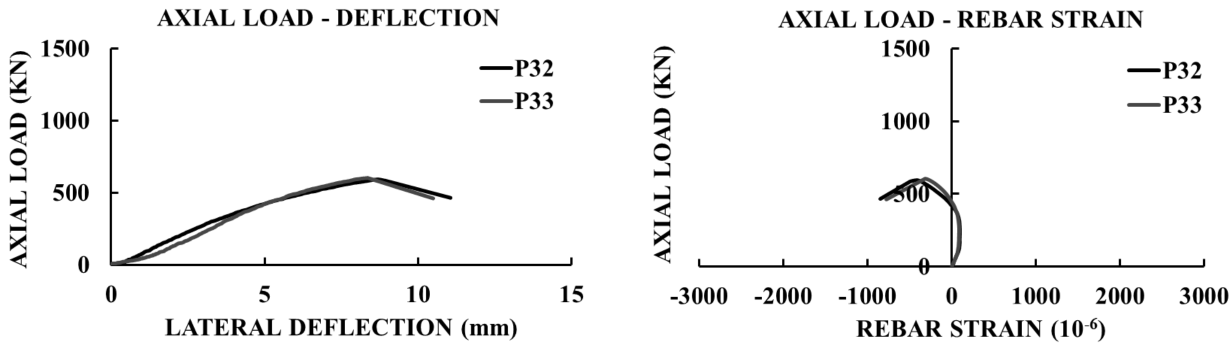

I) (A) – Ecc. = t/3 (63.3 mm) II)

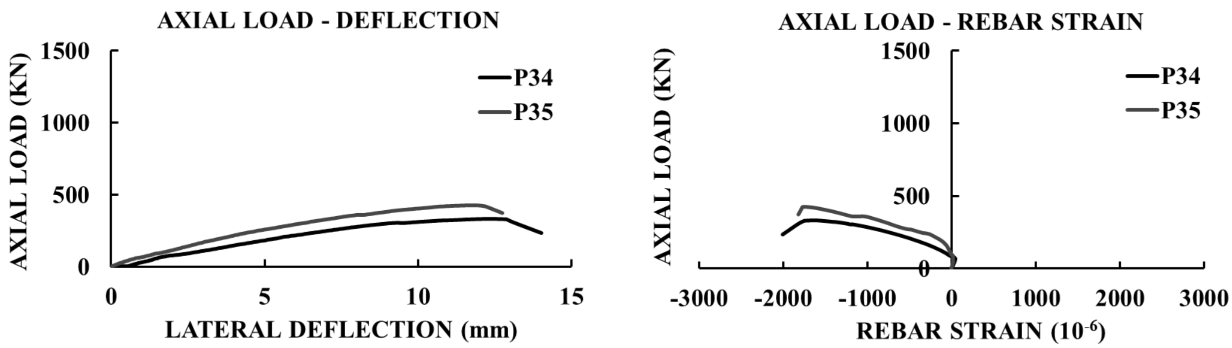

I) (B) – Ecc. = 5t/12 (79.2 mm) II)

Figure 2.21 – Test Data (Eccentric Load) - Conventional Prisms

Figure 2.21 shows that for prisms tested at an eccentricity of t/3 (63.3 mm), the two central 15M bars were in compression up to approximately 2/3 peak load. At this point, the bars crossed into tension and reached a maximum tensile strain of -0.000366 mm/mm at peak load. Rebar yielding was not observed in either prism.

For prisms tested at an eccentricity of 5t/12 (79.2 mm), the two central 15M bars were in tensile strain for nearly the entire duration of the test. At peak load, the average tensile strain was -0.001701 mm/mm. Brittle failure was observed in both prisms.

2.6 LOAD-DISPLACEMENT RESPONSE ANALYSIS

The difference in lateral stiffness between the cage-reinforced and conventionally-reinforced prisms is of great interest since it correlates with one of the objectives of this study. Recall that the stiffness of a masonry wall directly impacts the design moments due to additional second-order moments caused by deflection. A stiffer element will result in reduced mid-span deflection, and subsequently, lower second-order moments. Although second-order moments represent only a small portion of the total moment for five-course high prisms, contribution to the total moment is much greater for tall, slender walls. Chapter 3 will focus in part on the importance of lateral stiffness in tall masonry walls.

Table 2.8 provides a summary of the peak average axial capacity and peak average mid-span deflection for each family of eccentrically tested prisms.

Table 2.8 – Axial Load-Deflection Data

Eccentricity (mm)	Reinforcing Type	Peak Average Axial Load (KN)	Peak Average Mid-Span Deflection (mm)
31.7 (t/6)	4-10M Cage	1052	3.7
63.3 (t/3)	4-10M Cage	625	7.0
63.3 (t/3)	2-15M Conventional	598	8.5
79.2 (5t/12)	4-10M Cage	422	10.8
79.2 (5t/12)	2-15M Conventional	379	12.8

Figure 2.22 shows the average load-displacement response for each of the five families of eccentrically tested prisms. Each curve represents the average response of all the prisms in that particular family with the curve truncated at the failure point of the weakest prism within each grouping.

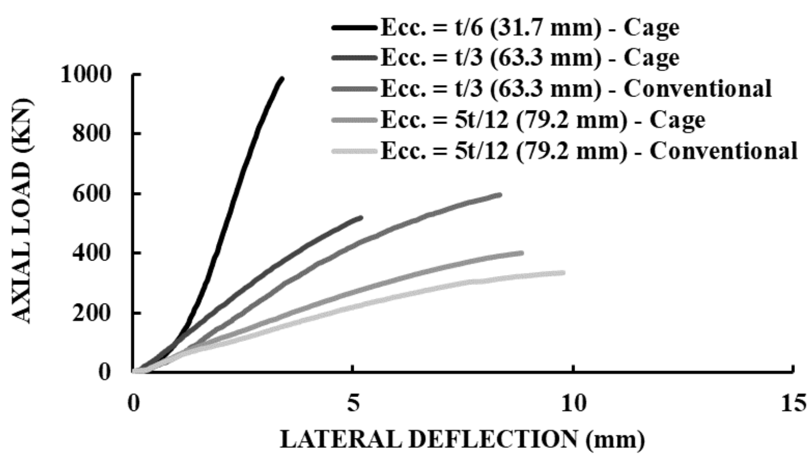

Figure 2.22 – Load-Displacement Response Comparison

The average lateral mid-span deflection for cage reinforced and conventionally reinforced prisms with a loading eccentricity of t/3 (63.3 mm) is 7.0 mm and 8.5 mm, respectively. Since there are no other design or testing variables, it appears that the cage reinforcing is exclusively responsible for providing a 21.4% stiffness enhancement in comparison to conventional reinforcement with equal steel area. Furthermore, the average OOP mid-span deflection for cage-reinforced and conventionally reinforced prisms with a loading eccentricity of 5t/12 (79.2 mm) is 10.8 mm and 12.1 mm, respectively. It appears that the cage reinforcing provides a 12.1% stiffness enhancement when compared to conventional reinforcement with equal steel area when all other parameters are equal.

The discrepancy in prism stiffness enhancement, 21.4% vs 12.1%, at two different load eccentricities can best be explained by an analysis of the rebar strains at failure. Figure 2.23(A) and Figure 2.23(B) show the peak convex side and concave side rebar strain for each of the eccentrically tested, cage reinforced prisms.

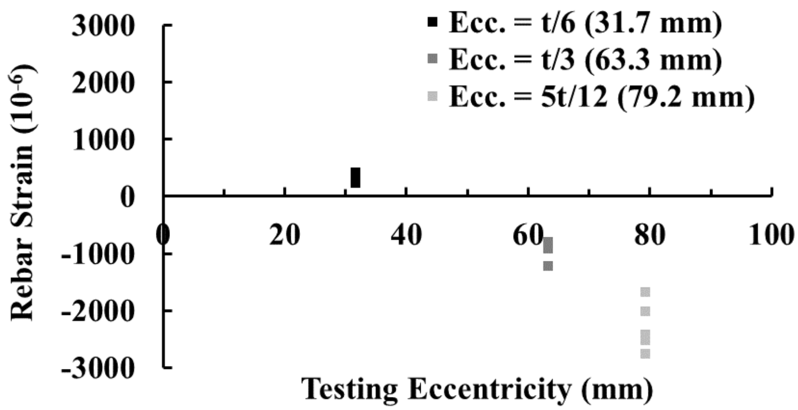

A) Convex Side Rebar Strain

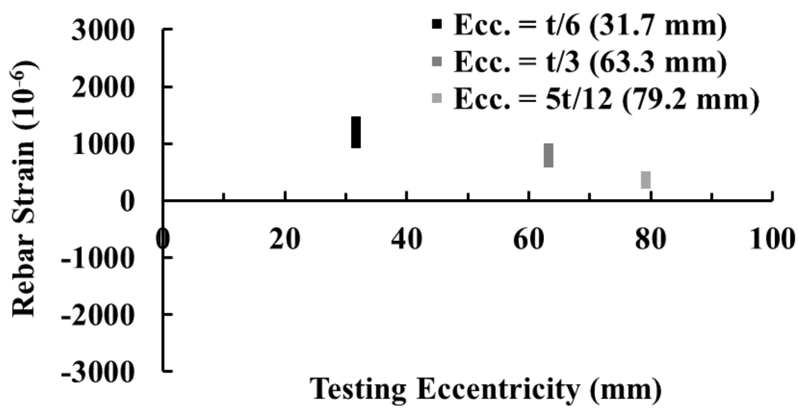

B) Concave Side Rebar Strain

Figure 2.23 – Peak Rebar Strain - Cage Reinforcing

At peak load, the average absolute convex side rebar strain in prisms tested at t/3 (31.7 mm) is 380% higher than the average absolute convex side rebar strain in the prisms tested at t/6 (63.3 mm); the average absolute convex side rebar strain in the prisms tested at 5t/12 (79.2 mm) is 800% higher.

At peak load, the average concave side rebar strain in prisms tested at t/3 is 35% lower than the average concave side rebar strain in the prisms tested at t/6; the average concave side rebar strain in prisms tested at 5t/12 is 70% lower.

Table 2.9 provides a summary of the data plotted in Figure 2.23.

Table 2.9 – Rebar Strain Summary

Eccentricity (mm)	**Reinforcing Type**	**Peak Average Convex Side Rebar Strain (10^{-6} mm/mm)**	**Peak Average Concave Side Rebar Strain (10^{-6} mm/mm)**
31.7 (t/6)	4-10M Cage	337	1200
63.3 (t/3)	4-10M Cage	-921	800
79.2 (5t/12)	4-10M Cage	-2224	369

To explain the stiffness enhancement, the data in Figure 2.23 and Table 2.9 must be interpreted as follows. Larger load eccentricities cause higher moments, which result in reduced axial capacity. The reduced axial load, combined with a higher bending moment, results in a shift of the neutral axis toward the concave prism face. The proximity of the neutral axis to the concave side rebar layer is directly proportional to the amount of compressive strain it develops. Figure 2.23(B) clearly shows that the compressive strain in the concave side rebar layer increases as the loading eccentricity decreases.

Therefore, it can be concluded that the level of axial load is directly correlated with the degree of expected stiffness enhancement. Higher axial load allows for engagement of the concave side rebar layer in compression for a wider range of moment. This will necessarily result in an increase in stiffness due to the relative difference in the steel and masonry compressive strength and modulus of elasticity. The modulus of elasticity of the compression reinforcing is approximately 10 times greater than the modulus of elasticity of the masonry it displaces. At peak axial load, the average concave side rebar strain in the prisms tested at t/3 (63.3 mm), and at 5t/12 (79.2 mm) is 0.000369 mm/mm and 0.0008 mm/mm, respectively. Assuming 2-10M compression bars and using a modulus of elasticity of 184 000 MPa, these strains translate to approximately 13.6 kN and 29.4 kN of compressive rebar force. Although these rebar forces are small relative to the overall axial loads in the specimens, they provide a significant contribution to the stiffness.

2.7 P-M RESPONSE

Table 2.10 provides the first order moment, caused by eccentric loading, and the second-order moment, caused by axial loading in combination with lateral deflection, for each eccentrically tested prism. The first-order moment is calculated as the product of the axial load and the loading eccentricity, and the second-order moment is calculated as the product of the axial load and the mid-span deflection. The total moment given in the last column of Table 2.10 is the summation of the first-order and second-order moments. The P-M interaction diagrams in subsequent discussions will utilize data from Table 2.10.

Table 2.10 – Eccentric Test Moments

Prism ID	Peak Load (kN)	Eccentricity (mm)	Peak First-Order Moment (kN-m)	Peak Mid-Span Deflection (mm)	Peak Second-Order Moment (kN-m)	Peak Total Moment (kN-m)
6	1082	31.7 (t/6)	34.3	4.0	4.3	38.6
7	1029	31.7 (t/6)	32.6	2.6	2.7	35.4
8	986	31.7 (t/6)	31.2	3.2	3.1	34.4
9	1007	31.7 (t/6)	31.9	4.6	4.6	36.5
10	1157	31.7 (t/6)	36.7	4.0	4.7	41.3
	Avg. = 1052				**Avg. = 3.9**	**Avg. = 37**
11	682	63.3 (t/3)	43.2	7.8	5.3	48.5
12	518	63.3 (t/3)	32.8	6.8	3.5	36.3
13	646	63.3 (t/3)	40.9	6.7	4.3	45.2
14	598	63.3 (t/3)	37.8	7.1	4.3	42.1
15	679	63.3 (t/3)	43.0	6.9	4.7	47.7
	Avg. = 625				**Avg. = 4.4**	**Avg. = 44**
16	456	79.2 (5t/12)	36.1	11.7	5.3	41.4
17	422	79.2 (5t/12)	33.4	10.8	4.6	38.0
18	399	79.2 (5t/12)	31.6	9.7	3.9	35.5
19	416	79.2 (5t/12)	33.0	11.3	4.7	37.7
20	416	79.2 (5t/12)	32.9	10.5	4.4	37.3
	Avg. = 422				**Avg. = 4.6**	**Avg. = 38**
31						
32	593	63.3 (t/3)	37.5	8.7	5.2	42.7
33	602	63.3 (t/3)	38.1	8.3	5.0	43.1
	Avg. = 598				**Avg. = 5.1**	**Avg. = 43**
34	333	79.2 (5t/12)	26.3	12.4	4.1	30.5
35	426	79.2 (5t/12)	33.7	11.8	5.0	38.8
	Avg. = 379				**Avg. = 4.6**	**Avg. = 35**

As expected, the peak axial resistance of the prisms in Table 2.10 is influenced directly by the testing eccentricity. The contribution of the second-order moment to the total moment is approximately 10.9% for the cage-reinforced prisms, and 12.5% for the conventionally reinforced prisms. Based on the discussion in the previous section, this finding appears to be reasonable since the second-order moment is directly related to lateral stiffness.

2.8 PLANE SECTION COMPATIBILITY ANALYSIS

Data points obtained from masonry prisms tested at three different eccentricities (e=t/6, e=t/3, and e=5t/12) are superimposed on a theoretical P-M interaction diagram calculated for the prism in Figure 2.3. The interaction diagram was developed using $f'_{m,\,gr}$ = 21.0 MPa as obtained from the average of the concentric prism compressive strength in Table 2.4.

The P-M interaction diagrams were obtained as follows. A mechanics-based fibre-section analysis model was implemented to produce the P-M interaction diagrams for Figure 2.25, 2.26, 2.27, and 2.28. The discretization of a typical prism section is shown in Figure 2.24. For these theoretical models, the prism section was divided into 100 masonry fibers in the out-of-plane direction. Each layer of reinforcing steel was modeled as a single fibre of equivalent area with the same width as the masonry section. Incremental values of strain were enforced on the masonry compression face for a desired level of axial load. For each strain increment, equilibrium of forces was employed to determine the location of the neutral axis by utilizing strain compatibility and established stress-strain constitutive relationships for steel and masonry. The corresponding moment was then calculated from the unbalanced forces and the curvature from the ratio of the masonry compressive strain to the compression zone depth. Due to the inherent restrictions present in this type of this analysis, the model does not account for the possibility of other failure mechanisms, such as compression buckling and member instability. It is assumed that failure occurs at the section level due to material failure such as steel yielding or masonry crushing. Based on the empirical observations of the failure mechanism presented in the previous sections, this assumption appears to be correct.

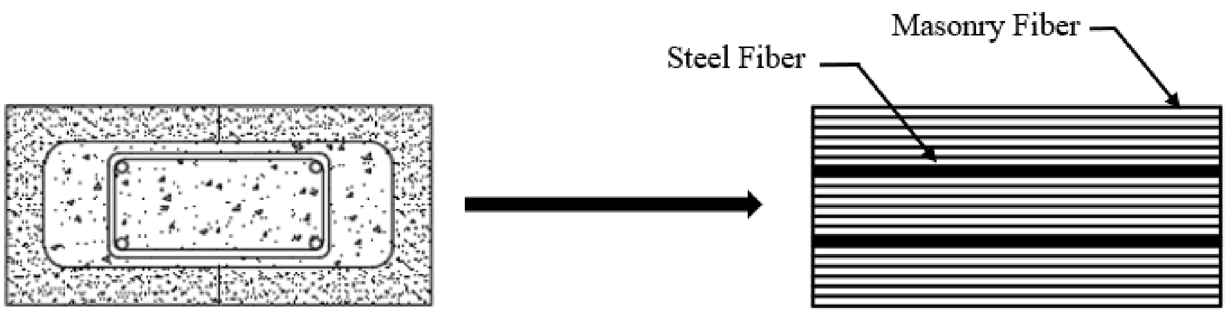

Figure 2.24 – Fiber Section Model

To validate the previous assumptions regarding the prism failure mechanism, and to investigate the ability of the plane-section model to accurately predict prism capacity, several theoretical P-M interaction diagrams are presented next. Figure 2.25 shows a reasonable correlation between the experimental data and the predicted P-M response for the cage reinforced prisms. For comparison, code-based P-M interaction diagrams were also developed using resistance factors equal to 1.0.

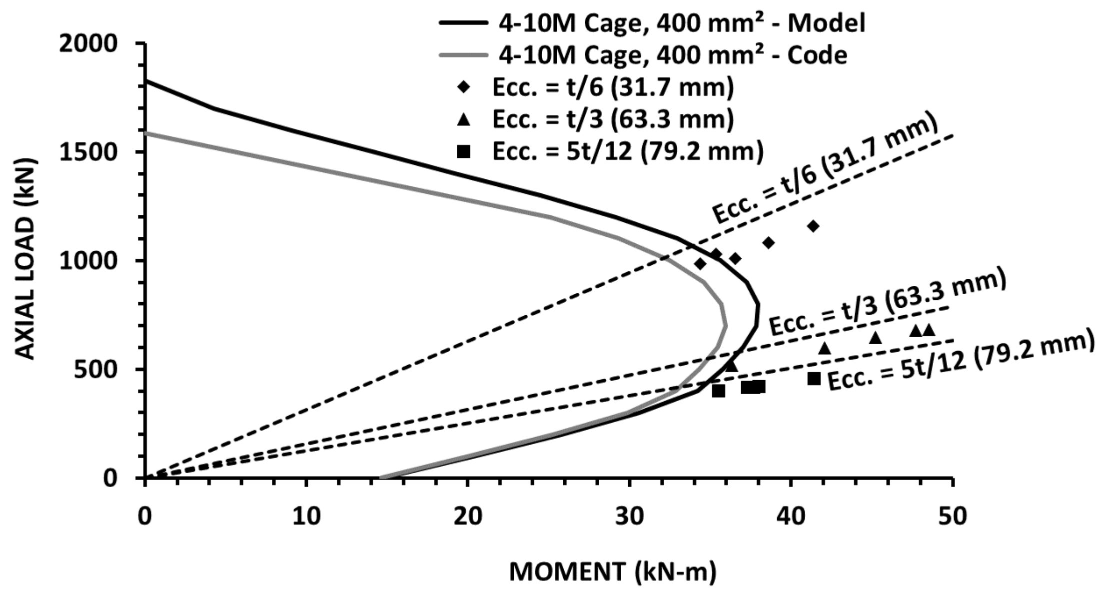

Figure 2.25 – P-M Interaction (Cage Reinforcing)

Another theoretical P-M interaction diagram was developed for a conventionally reinforced prism with two central 15M reinforcing bars. Figure 2.26 contains a plot of the P-M interaction diagram and the data points collected from prisms tested at two different eccentricities (e=t/3 and e=5t/12). The model does not predict the conventional prism capacities as well as it does the cage reinforced prism capacities.

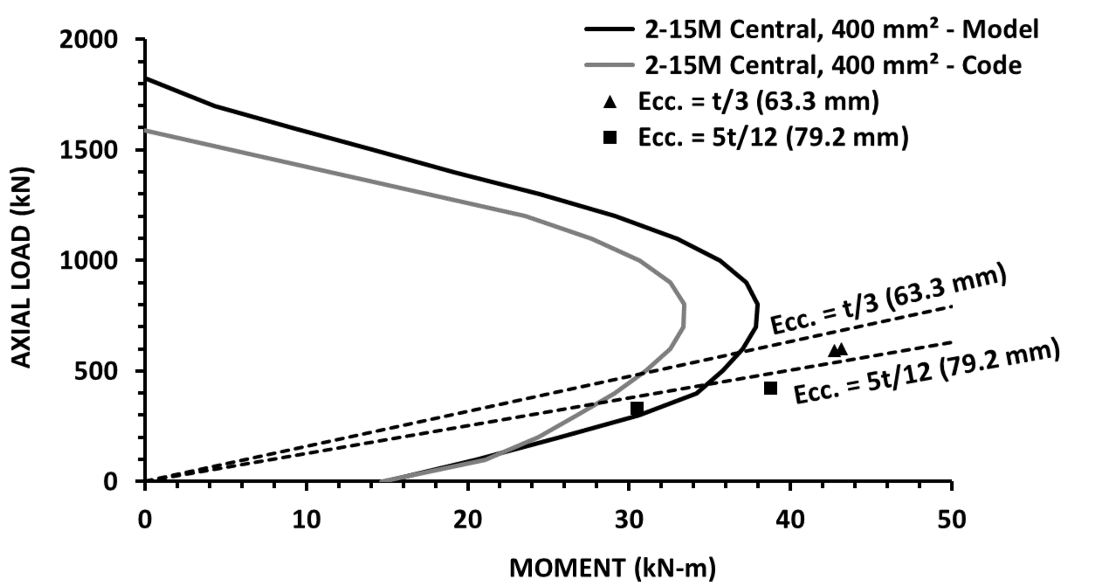

Figure 2.26 – P-M Interaction (Conventional Reinforcing)

2.8.1 P-M Response Comparison

To investigate the performance of a cage-reinforced prism in contrast to an array of conventional prism designs, the P-M interaction response of a 190mm x 390 mm cage reinforced prism section is compared with that of five conventional prisms each reinforced with one or two central bars, providing steel areas ranging between 100 mm^2 and 600 mm^2.

Figure 2.27 demonstrates that the cage-reinforced prism has a higher moment capacity than conventional prisms reinforced with a single 10M, 15M, or 20M bar over the entire range of axial load. In each of these three cases, the cage reinforced prism has a higher reinforcing ratio, therefore; it is intuitive that the innovative prism will have a higher axial capacity in pure compression due to the relative difference in the compressive strength of steel and masonry. In each case, the moment capacity is also greater over the entire range of axial load. The combination of a steel layer in compression, and an increase in the distance of the tension steel layer from the neutral axis, both characteristics of cage reinforcing, results in higher moment capacity. The effects of the compression steel will be discussed further in the following section

Figure 2.28 shows that the cage-reinforced prism has a higher moment capacity than conventional prisms reinforced with (2)-15M or (2)-20M bars for a range of axial load from approximately 25% to 70% of the peak load. In each scenario, it is expected that the cage reinforced prism will have a lower pure axial capacity due to the lower reinforcing ratio and the relative difference in the compressive strength of steel and masonry. However, similar to the previous three design scenarios, the innovative prism has a higher moment capacity due to a layer of steel in compression and greater distance of the tension steel layer from the neutral axis

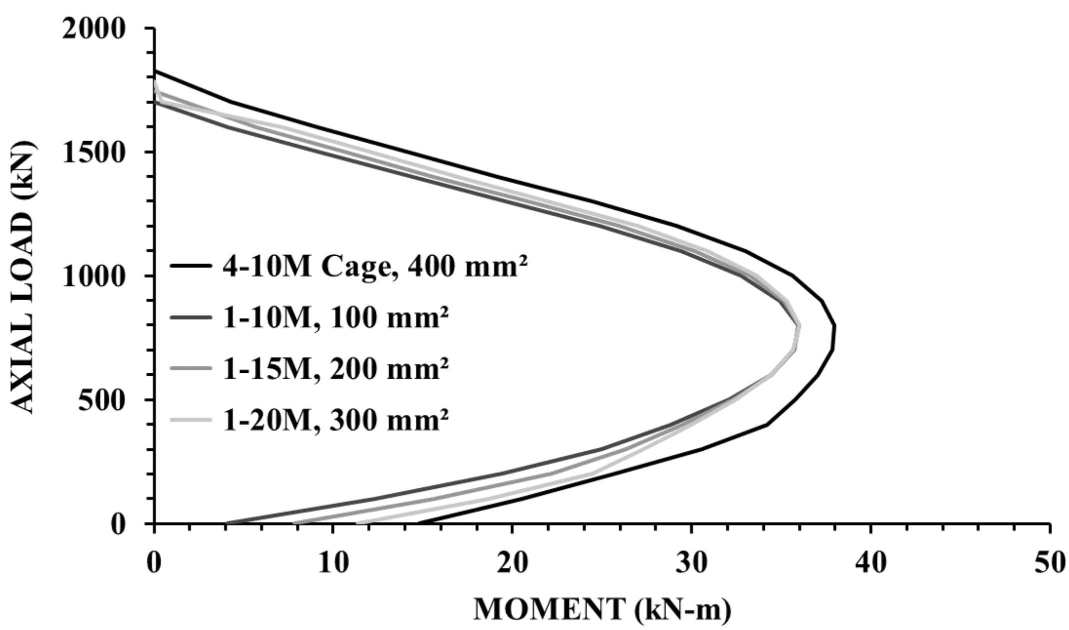

Figure 2.27 – P-M Interaction Diagrams (A_s < 400 mm^2)

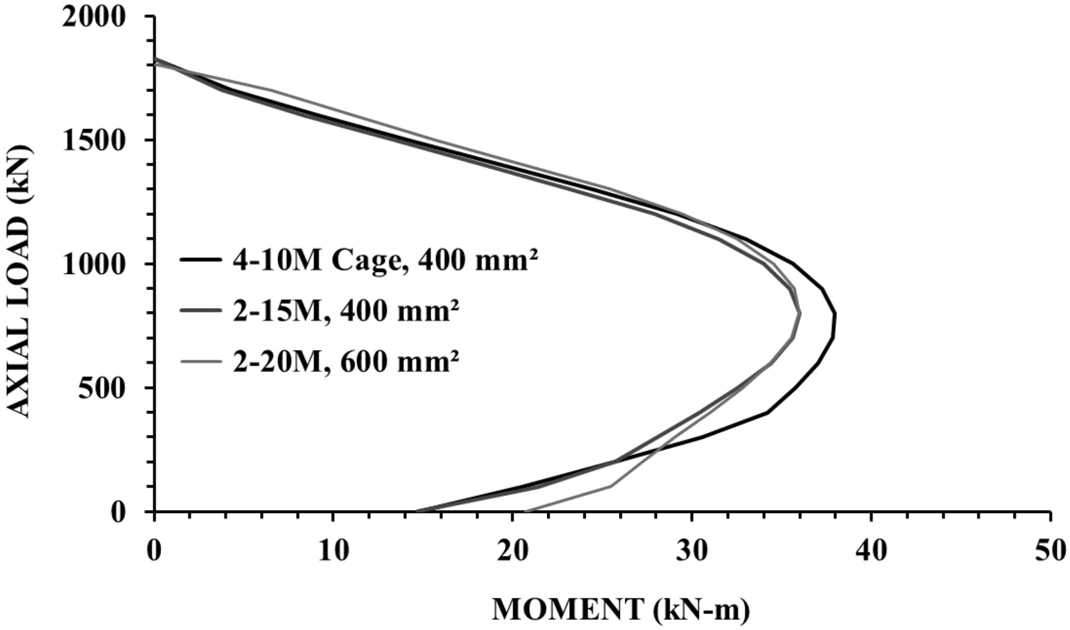

Figure 2.28 – P-M Interaction Diagrams ($A_s \geq 400\ mm^2$)

Based on the empirical test results in Figure 2.25 and Figure 2.26, the fiber-section model appears to predict the eccentrically tested prism capacities with reasonably good accuracy. It is noted that the model predicts the capacity of the cage-reinforced prisms is with better accuracy than it does the conventionally-reinforced prisms. For each reinforcing configuration, the model underestimates the prism capacity, providing conservative results. The model prediction is significantly more accurate than the code-based capacity for both the cage-reinforced and conventionally-reinforced prisms.

CHAPTER 3: WALLS WITH IN-LINE STIFFENING ELEMENTS

3.1 SUMMARY

A single layer of centrally located rebar is typically used as flexural reinforcing for load-bearing masonry walls. In specific cases, such as in tall, slender walls in which the out-of-plane (OOP) moment is large, this conventional method of reinforcement results in large amounts of steel that need to be placed in the wall. This is because slender masonry walls have inherently low flexural stiffness, which leads to large OOP deflections and therefore, higher second-order moments that require more reinforcement. Under these circumstances, the wall design requires over-reinforced sections that are not permitted by the code, which requires the flexural steel reinforcement to yield.

Previous empirical research has tentatively established that in-line stiffening elements increase the flexural strength, stiffness, and core integrity of concentrically and eccentrically loaded masonry prisms. This innovative reinforcing scheme consists of pre-tied rebar cages, provided as flexural reinforcement. In this study, the novel masonry assemblage and reinforcing scheme are adapted for full-scale tests in anticipation that the promising results obtained during prism testing can be realized in a slender wall designs representative of industry practices.

The response of four full-scale masonry walls tested under combined axial and OOP load is presented in this chapter. Two of the walls were constructed with pre-tied reinforcing cages, one wall had conventional central rebar, and the remaining wall had two layers of un-tied rebar. When comparing the three walls tested at 350 kN axial load, the results indicate that the walls with two layers of rebar have greater OOP stiffness and flexural strength in comparison to the conventionally reinforced wall, despite having significantly lower rebar strength. There was little difference in the flexural capacity and OOP stiffness of the cage reinforced wall and the wall with two layers of un-tied rebar. The cage-reinforced wall had slightly greater elastic OOP stiffness for lateral loads up to 40 kN, but not beyond. The remaining cage-reinforced wall, which was tested at 680 kN axial load had the greatest OOP stiffness and strength of the four walls due to the significantly higher level of axial load.

A mechanics-based fibre-section model utilizing plane-section compatibility was also used to compare the performance of the cage reinforced walls to conventionally reinforced walls with various amounts of centrally located reinforcing steel.

3.2 INTRODUCTION

This chapter presents a study on the use of in-line stiffening elements in full scale masonry walls. Four full-scale walls were subjected to simultaneous axial and OOP loading via a load-controlled vertical hydraulic press and a displacement controlled lateral jack. All four walls were 190 mm thick, 1190 mm long, and 2390 mm high; corresponding to a slenderness (kh/t) ratio of 12.58. One wall was reinforced with conventional, centrally-located rebar; another wall was reinforced with un-tied rebar in two separate layers; and two walls were reinforced with "stiffening elements" consisting of two layers of rebar in a pre-tied cage. The stiffening elements fit inside a masonry wall, effectively becoming a “concealed column”. It is utilized in combination with specially designed units able to slide around the pre-tied cage. The stiffening elements act as regions of localized strength and stiffness, increasing the buckling strength and reducing second-order effects. The focus of this section is on combined axial and flexural tests conducted on four masonry walls reinforced with three different reinforcing schemes. The results are discussed in terms of strength, stiffness, ductility, failure modes, and structural integrity.

The findings of this study will be used in a future research program which will include walls with higher slenderness ratios subjected to various end fixity conditions, different from pinned-pinned. The purpose of this study is to serve as an exploratory study to determine the feasibility of use of the system in a wall system and determine any design limitations based on its structural performance.

3.3 EXPERIMENTAL SETUP

3.3.1. Materials

3.3.1.1 Concrete Blocks

Three types of bocks were used for construction of the four walls in this study: 190 mm x 390 mm standard blocks with 35 mm faceshell, 190 mm x 390 mm full-lintel blocks with 35 mm faceshell, and 190 mm x 190 mm half-lintel blocks with 35 mm faceshell. The nominal block compressive strength was 15 MPa as provided by the manufacturer.

3.3.1.2 Mortar

Type S mortar was used for all joints in the walls. The mortar was prepared by experienced masons using standard industry procedures. A total of four 2” cubes were tested to establish the mortar compressive strength. The mortar cubes had an average compressive strength of 10.3 MPa with a standard deviation of 0.3 MPa.

3.3.1.3 Grout

Course grout was used for all core fills. The grout was mixed to achieve adequate workability to ensure flow between the rebar cages and the block faceshells. A total of four 4” diameter cylinders were tested to establish the grout compressive strength. The grout cylinders had an average strength of 29.7 MPa with a standard deviation of 2.9 MPa.

3.3.1.4 Ungrouted Masonry Strength

From a series of three, five course high, hollow prisms tests, the ungrouted masonry compressive strength was established to be 19.69 MPa with a standard deviation of 0.75 MPa. Using a weighted area method in combination with the grout and mortar compressive strength values, the grouted masonry compressive strength (f’m) was determined to be 26.3 MPa.

3.3.1.5 Rebar

All walls were reinforced with either 10M or 15M weldable reinforcing bars with a nominal yield strength (f_y) of 400 MPa. Tensile tests established the average yield strength and modulus of elasticity of the 10M bars to 635 MPa and 188,880 MPa, respectively. The yield strength and modulus of elasticity of the 15M bars were determined to be 475 MPa and 193,790 MPa, respectively. The yield strain for the 10M bars and 15M bars was calculated to be 0.00336 μm and 0.0025 μm, respectively. Figure 3.1 shows the stress/strain response for each of the bars tested. Note that the yield strength of the 10M bar is significantly higher than that of the 15M (by 33.7%), which is not typical of Gr. 400 steel. This has an influence on the strength of the walls, which will be discussed in Section 3.5.2.

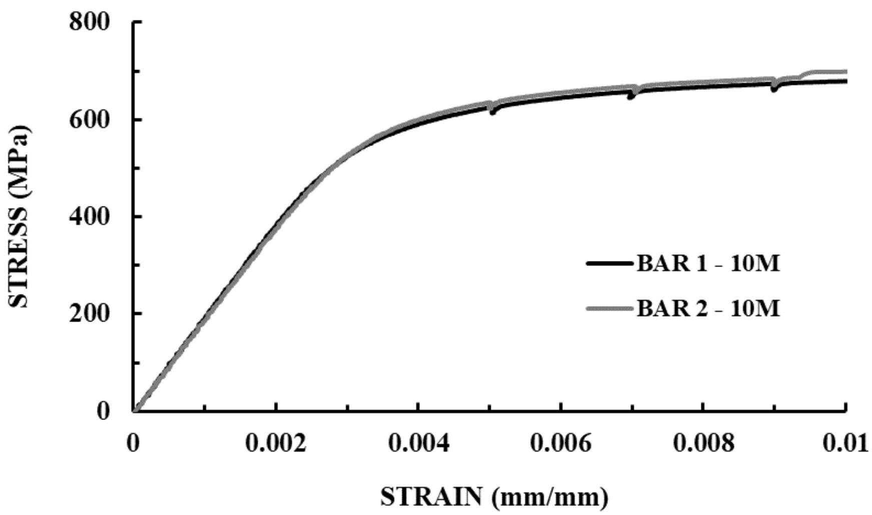

A) - 10M Rebar

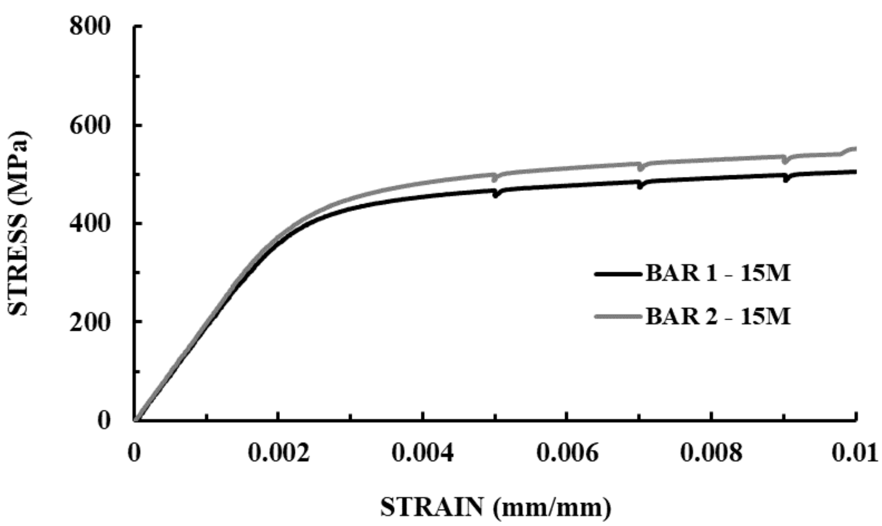

B) – 15M Rebar

Figure 3.1 – Rebar Stress-Strain Diagrams

3.3.2 Test Specimens

Four reinforced masonry walls were constructed in the I.F. Morrison Structures Laboratory at the University of Alberta. All four walls were 12 courses high, three courses wide, partially-grouted, and constructed with standard blocks, full-lintel blocks, and half-lintel blocks in a running bond pattern. (Fig. 3.2, 3.3, and 3.4). All mortar joints were 10 mm thick, resulting in an overall wall height of 2 390 mm. Experienced masons constructed the walls using typical industry procedures.

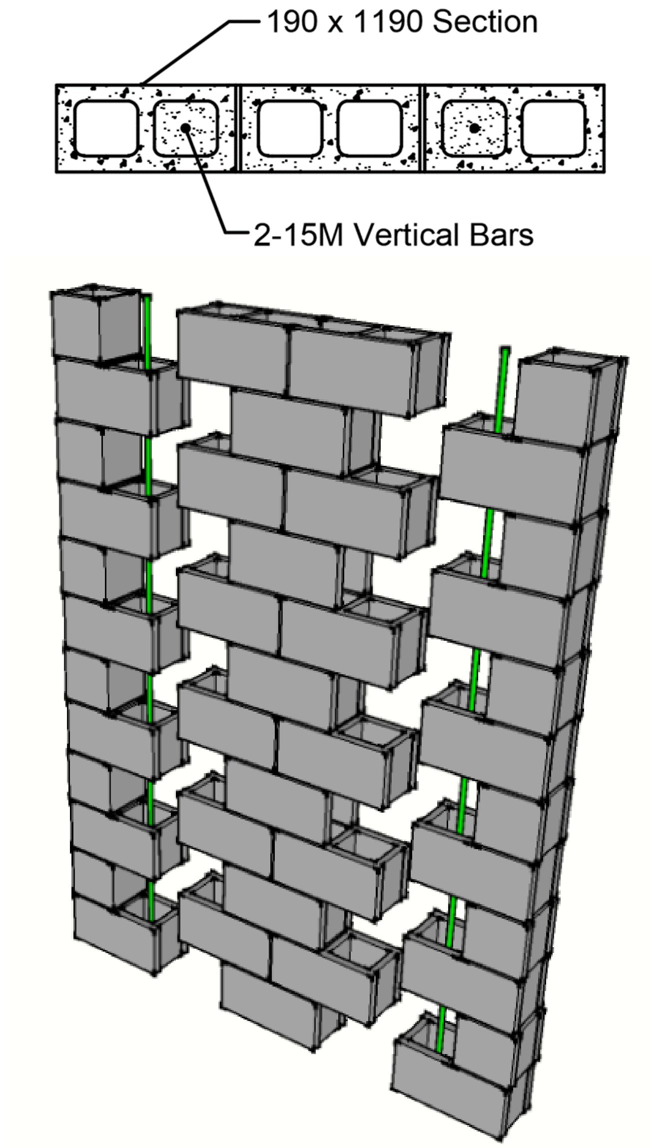

Figure 3.2 – Wall 1 (*Conventional*) Construction

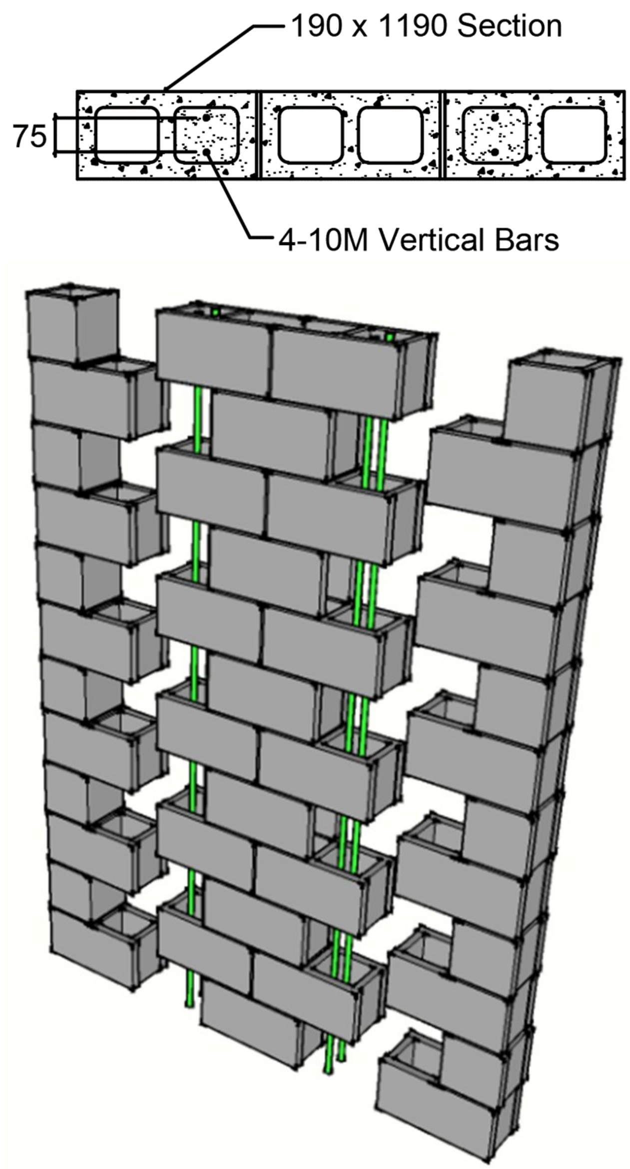

Figure 3.3 – Wall 2 (*Boundary Rebar*) Construction

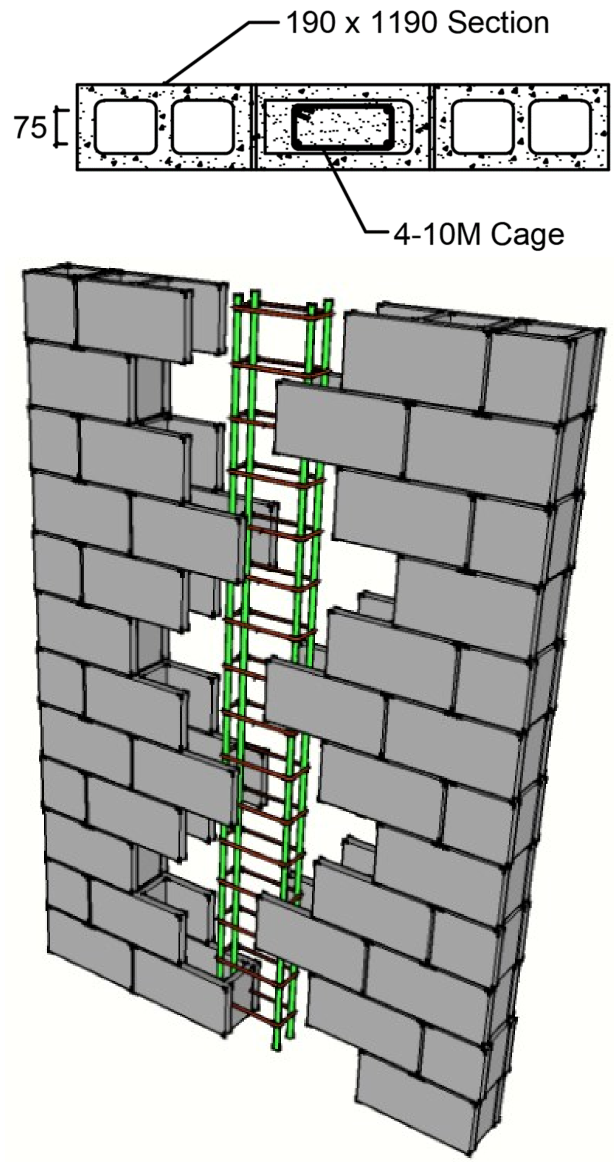

Figure 3.4 – Wall 3/Wall 4 (*Cage*) Construction

Three different reinforcing schemes were used for the walls, each with 400 mm^2 of vertical reinforcing steel. Wall 1 was reinforced with two 15M bars located in the centre of the section, wall 2 was reinforced with four un-tied 10M bars in two-layer, and wall 3 and 4 were reinforced with a cage consisting of four tied 10M bars. For walls 2, 3 and 4, the two layers of 10M rebar were spaced at 75mm in the OOP direction. The pre-tied reinforcing cages used in wall 3 and 4 were fabricated with four 10M (11.3 mm dia.) bars for longitudinal reinforcement and 6.34 mm smooth wire ties for transverse reinforcement (Fig. 3.5). The available space was divided evenly, resulting in 15 transverse ties spaced at 150 mm c/c. Previous research from the prism testing program in Chapter 2 established that a tie spacing of 181 mm (for this specific design) was sufficient to prevent buckling.

The bases of all the reinforcing bars were welded to 1" thick steel plates prior to construction of the walls (Fig. 3.5). The steel plates were utilized to facilitate transportation of the wall specimens to the testing apparatus, and to provide a means of mechanically securing the walls to the rotating base.

Figure 3.5 – Reinforcing

Throughout the construction process, efforts were made to ensure that the reinforcing bars stayed aligned in their proper position within the grouted cores (Fig. 3.6). Minimal construction deviation was desired in order to guarantee the accuracy of the empirical results and promote reproducibility in the wall models.

Figure 3.6 – Typical Wall Construction

Cast-in-place threaded rod anchors were installed at the top of each wall to secure a steel channel cap prior to loaded (Fig. 3.7). The threaded anchors were inserted into templates and then positioned on top of the wall in designated locations (Fig. 3.8).

Figure 3.7 – Threaded Anchors

Figure 3.8 – Completed Walls

3.3.3 Test Procedure

The four walls were tested using an MTS hydraulic press with a maximum axial capacity of 6200 kN (Table 3.1). A force-controlled, concentric vertical load was applied first, and held constant while the lateral load was applied at 1 mm/minute. An axial load of 350 kN, 6% of Aef'm, was used for wall 1, 2 and 3. This axial load was selected to ensure that the walls experienced a significant level of axial compression while still allowing for rebar yielding due to flexure prior to collapse. To simplify calculations, it was decided that the depth of the masonry compression block should not exceed the depth of the faceshell at failure. The fourth wall was tested at an axial load of 680 kN, 11% of Aef'm, in order to study the performance of the cage reinforcing at compression levels higher than it would reasonably experience in service conditions. The precise level of axial load for wall 4 was dictated by a compressive strain/zero-strain constraint for the inner rebar layer at ultimate.

Table 3.1 – Wall Test Summary

Wall	**Reinforcing**	**Axial Load (kN)**
1 – *Conventional*	2-15M – Central	350
2 - *Boundary Rebar*	4-10M – Untied	350
3 - *Cage - 350 kN Axial*	4-10M – Cage	350
4 - *Cage - 680 kN Axial*	4-10M – Cage	680

Axial load was applied to the top of the walls via a stub column and a spreader beam (Fig. 3.9 and 3.10). The spreader beam transferred the vertical load to the wall through a roller assembly at each end. The roller assemblies were mounted on a thick steel channel cap which spanned the length of the wall and applied a uniformly distributed load.

Lateral load was applied at 1/3 points of the wall by a spreader truss. The truss was mounted on a horizontal jack pushing from a column nearby. The lateral load at the top of the wall was directed back to the column by a pair of tension bracing members equipped with a threading mechanism. The nuts on the threaded rods were adjusted periodically throughout the testing procedure to safeguard against lateral drift at the top of the wall as horizontal load was applied.

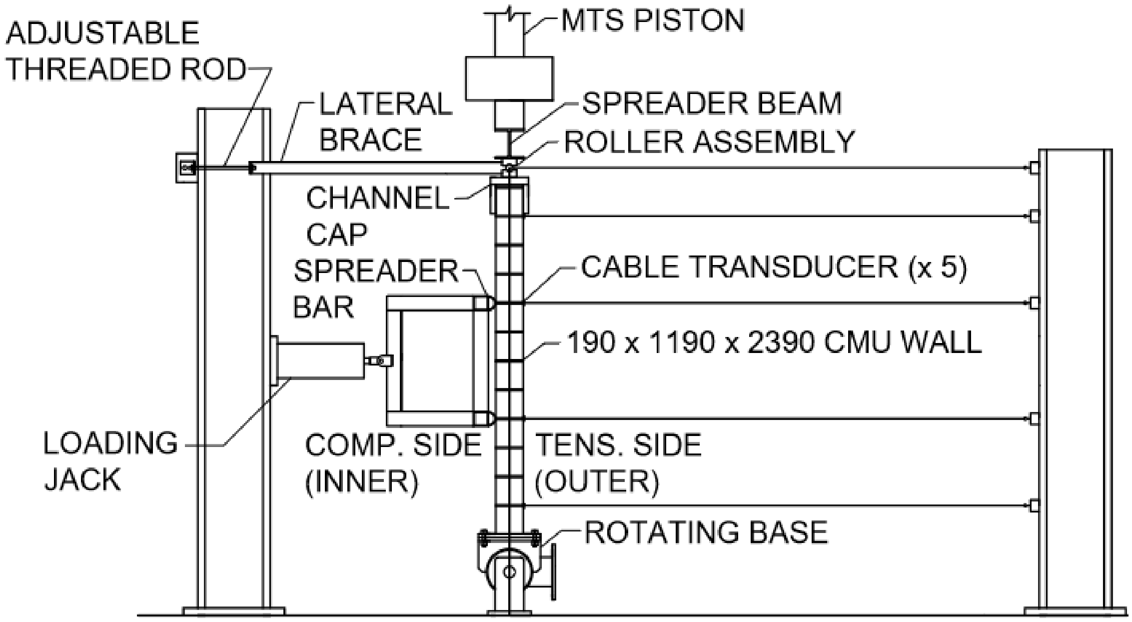

Figure 3.9 – Testing Assembly

Figure 3.10 – Wall Prior to Testing

A rotating base was designed to allow for simulation of a true pin connection at the wall base (Fig. 3.11). The large bearings on each end were virtually frictionless in relation to the applied load. A thick steel plate was welded to the top of the rotating assembly to receive the wall base plates.

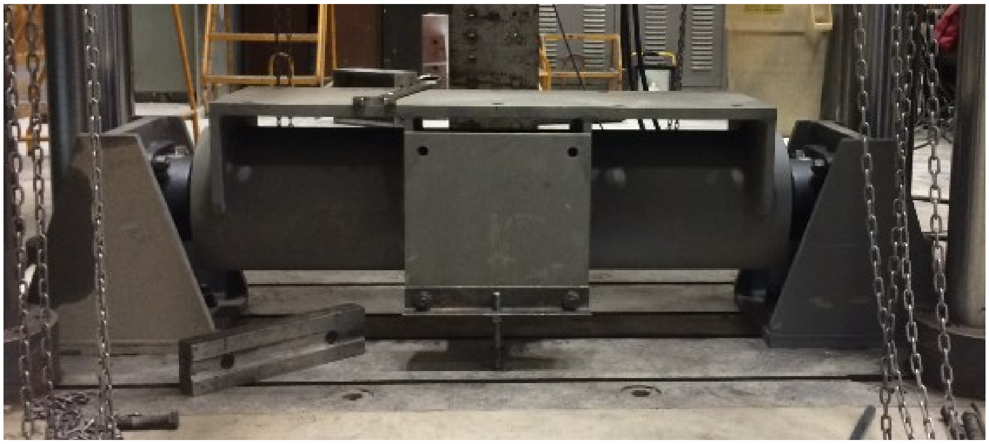

Figure 3.11 – Rotating Base

A machined steel channel cap was positioned on top of each wall and secured via cast-in-place threaded anchors. The channel legs were significantly long to ensure that rotation was prevented at the steel/masonry interface, but not too long to prevent the wall from deforming freely due to end clamping. Two steel tabs were welded to the channel for attachment of the lateral braces (Fig. 3.12 and Fig. 3.13).

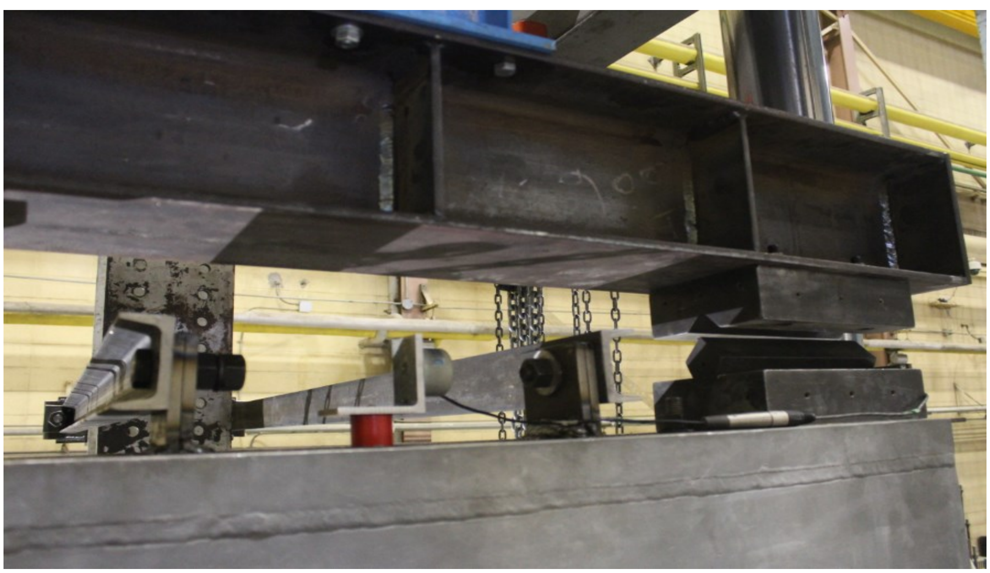

Figure 3.12 – Wall Cap with Lateral Bracing

Figure 3.13 – Bracing to Column Connection

3.4 INSTRUMENTATION

Instrumentation for the wall tests consisted of a series of cable transducers, strain gauges, clinometers, and load cells. To record the rebar strain at various locations in the wall throughout the duration of the test, each reinforcing bar was instrumented with 3 strain gauges located at 1/3 points (Fig. 3.14 and Fig. 3.15) For three of the walls, strain gauges were also mounted on both wall faces at 1/3 points to record the masonry compressive/tensile strains. These strain readings will be utilized to construct strain profiles in subsequent discussions.

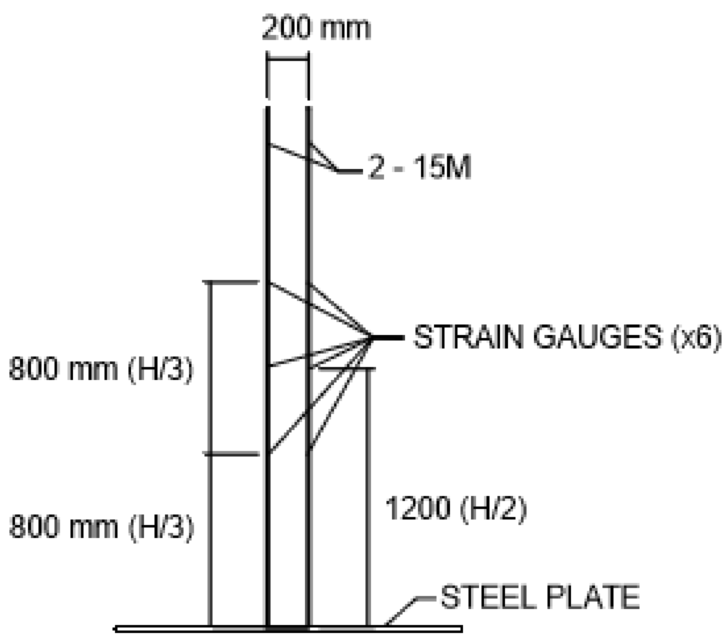

Figure 3.14 – Wall 1 Strain Gauge Placement (In-Plane)

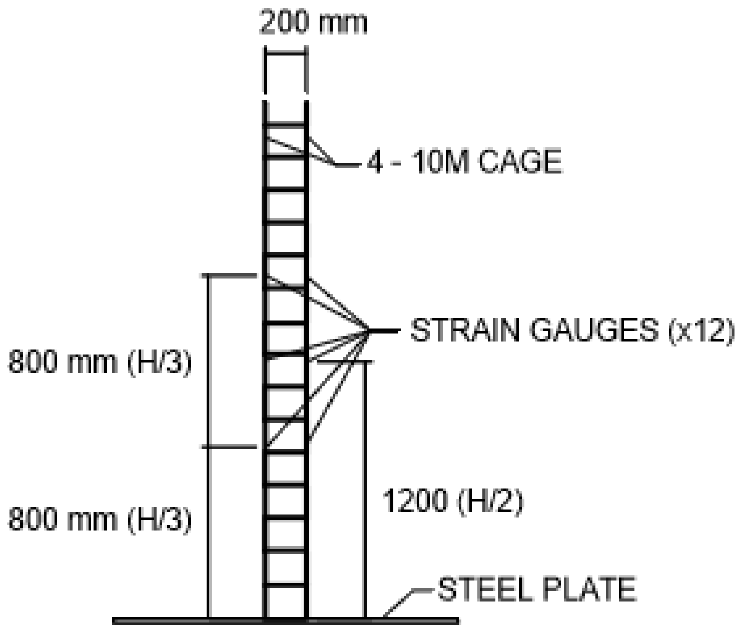

Figure 3.15 – Wall 2/3/4 Strain Gauge Placement (In-Plane)

Cable transducers were used to measure the OOP deflection for each wall (Fig. 3.16). The number of cable transducers used to record the OOP deflection varied between two and six; therefore, the deformed shape of each wall will be reproduced with varying degrees of accuracy. Clinometers were mounted on the top and bottom of the wall assembly to compare the relative rotation between the ends and thereby verify the symmetry of the bending moment. The axial compression and lateral load were recorded by the MTS module directly from the load cells.

Figure 3.16 – Cable Transducers

3.5 TEST RESULTS

Data collected from the wall tests is presented in this section. For all the subsequent graphs, charts, figures and discussions, the following sign convention has been utilized: axial compression is positive, tension strain is positive, and compressive strain is negative.

The load-displacement response of the four walls is presented in Figure 3.17. Quantifying OOP stiffness is one of the main objectives this study since it directly impacts the design moments due to additional second-order moments caused by deflection.

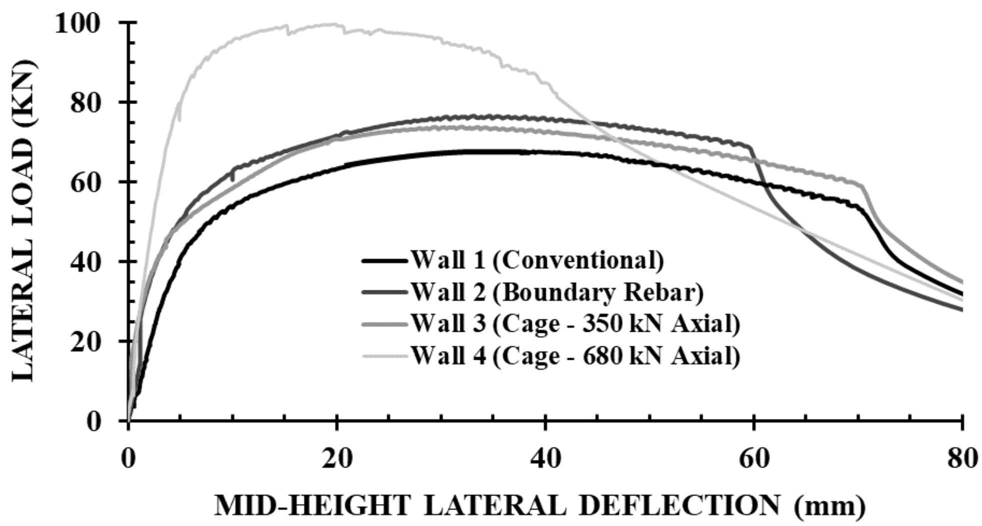

Figure 3.17 – Load-Displacement Response

From Figure 3.17, it is evident that the response of wall 2 and wall 3 is similar in terms of peak lateral load capacity and OOP deflection. Wall 1 has both lower peak lateral capacity and stiffness in comparison to wall 2 and 3. Wall 4 has much higher lateral load capacity and OOP stiffness than the other three walls due to the significantly higher applied axial load. In-depth analysis of the load-displacement response of each wall is presented in Section 3.5.2.

3.5.1 Failure Modes

For the three walls tested at 350 kN axial load, the mode of failure was generally consistent. All three walls remained nearly elastic up to 40 kN lateral load. At this load, the OOP elastic stiffness was calculated as 8.2 kN/mm, 14.3 kN/mm, and 14.8 kN/mm for wall 1, 2, and 3, respectively (Table 3.3). At this point a slight curve could be seen in all three walls when viewed from the side (Fig. 3.18).

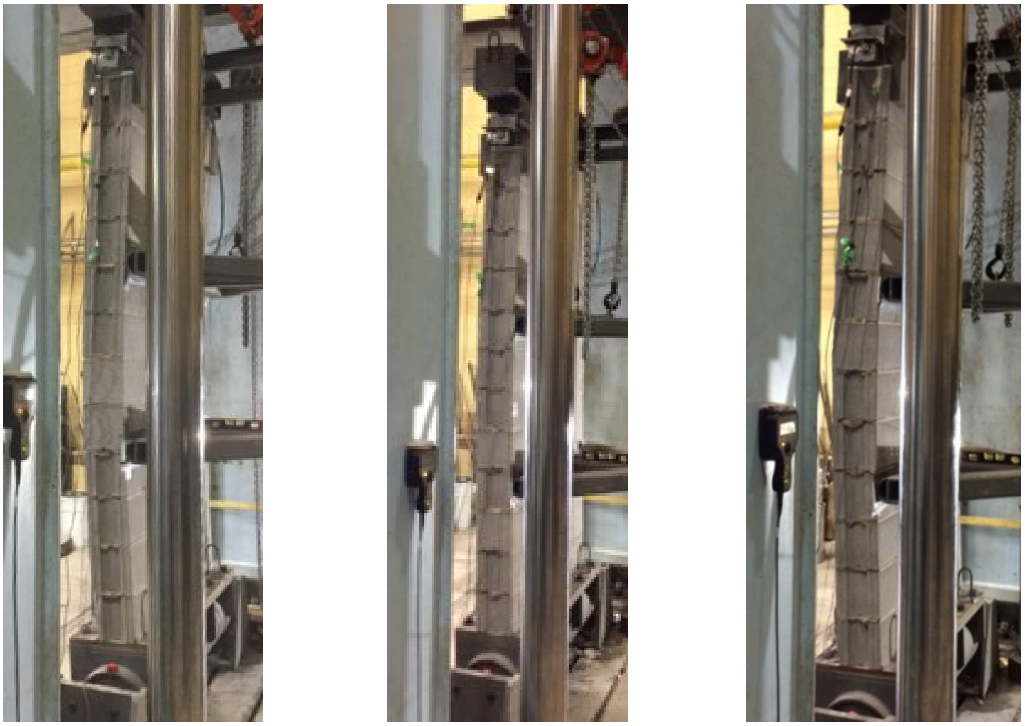

Figure 3.18 – OOP Deformation (Wall 1, Wall 2, Wall 3)

Further application of lateral load lead to extensive horizontal cracking in the mortar joints on the tension face of the walls between the load application points (Fig. 3.19). Since the walls were tested using a four-point bending setup, the first-order moment is constant and at a maximum between the load application points. These cracks widened up to a maximum of approximately 10 mm just prior to collapse.

Figure 3.19 – Tension Face Cracking

Upon reaching a lateral load of approximately 65 kN, the loading rate began to decrease for all three walls. At this point the rebar in all three walls was beginning to yield and the OOP stiffness was declining. Once yielding occurred, the deformation profile began to change. Since the bending moment at mid-height is largest due to the contribution of second order effects, the rebar at mid-height yielded first. Upon reaching yield at mid-height, a region of reduced stiffness was created, and a hinge developed. As the wall began to hinge, the resulting deflection profile progressed from parabolic to a triangular pattern, characteristic of rigid body motion (Fig. 3.20). The masonry strain at mid-height on the compression face of the wall increased rapidly until eventual masonry crushing in the compression side and subsequent collapse.

Figure 3.20 – Deformed Shape at Collapse

Wall 4 was tested with an axial load of 680 kN and the progression to failure was similar to that of the other three walls. A noticeable difference, however, was a reduction in OOP deformation both prior to, and after yielding. At lateral loads up to 65 kN, the OOP elastic stiffness was calculated as 19.1 kN/mm (Table 3.2). Prior to collapse, horizontal cracks developed in the mortar joints between the load application points on the tension face, similar to the other three walls. However, these cracks were significantly smaller due the reduced section curvature and OOP deflection. Additionally, at collapse, vertical cracks immediately propagated down the entire wall due to shear stress caused by the relative difference in the compressive strength of the grouted and ungrouted cores.

Figure 3.21, 3.22, 3.23, and 3.24 contain photos of the damage in each wall after collapse. In each case the damage is extensive, particularly at mid-height. In all four specimens, the grouted core was completely disintegrated at places, leaving the rebar exposed

Figure 3.21 – Wall 1 (*Conventional*) Damage

Figure 3.22 – Wall 2 (*Boundary Rebar*) Damage

Figure 3.23 – Wall 3 (*Cage – 350 kN Axial*) Damage

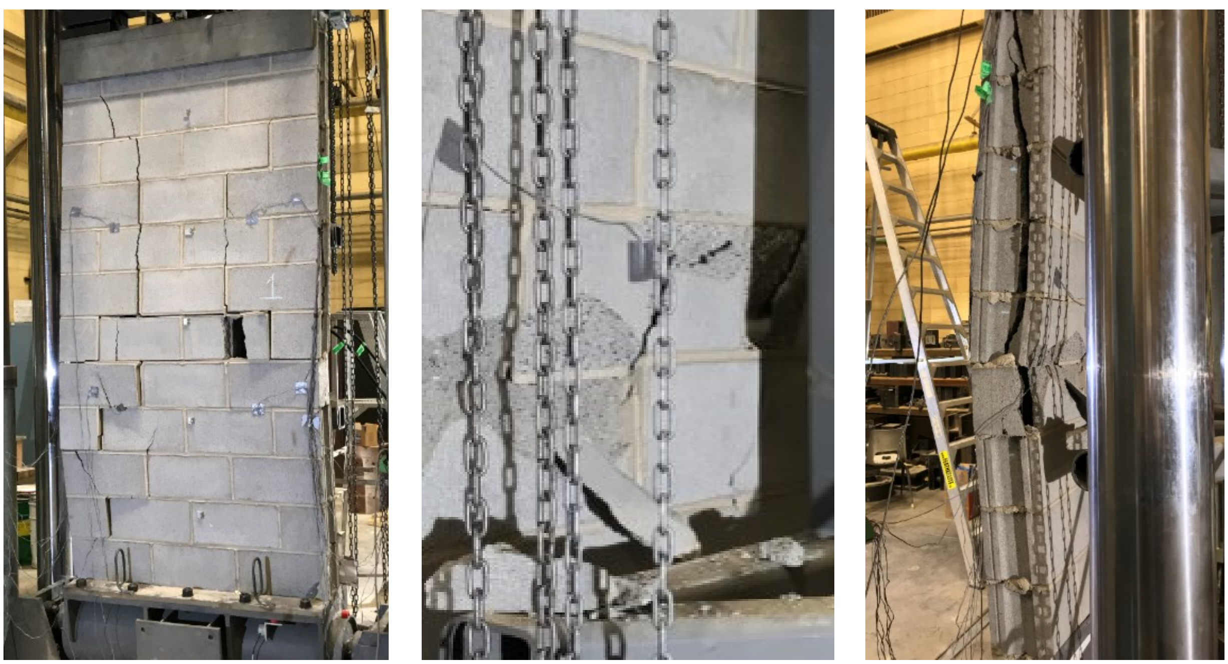

Figure 3.24 – Wall 4 (*Cage – 680 kN Axial*) Damage

3.5.2 Load Displacement Response

Analysis of the load-displacement response of the four wall specimens is critical since quantifying OOP stiffness is one of the main objectives this study. Recall that the stiffness of a masonry wall directly impacts the design moments due to additional second-order moments caused by deflection. A stiffer wall will result in reduced mid-span deflection, and subsequently, lower second-order moments. Table 3.2 provides a summary of the wall OOP deflections at peak lateral load and at collapse.

Table 3.2 – Peak OOP Deflection

Wall	**Peak Lateral Load (kN)**	**OOP Deflection at Peak Load (mm)**	**Lateral Load at Collapse (kN)**	**OOP Deflection at Collapse (mm)**
1 - *Conventional*	67.7	38.9	51.5	70.8
2 - *Boundary Rebar*	76.6	34.7	64.8	60.3
3 - *Cage - 350 kN Axial*	73.9	32.1	57.4	70.7
4 - *Cage - 680 kN Axial*	99.6	19.8	82.2	41.1

From Table 3.2 it is evident that wall 2 and wall 3 have a similar response in terms of peak lateral load capacity and OOP deflection. The peak lateral load capacity of walls 2 and 3, both reinforced with two layers of rebars, varies by only 3.5%; the OOP deflection at peak load varies by 7.5%. Wall 1, with a single layer of rebar at mid-cell has both lower lateral capacity and stiffness in comparison to wall 2 and 3. The peak lateral load capacity of wall 1 is approximately 9.5% lower than that wall 2, and the OOP deflection at peak load is 10.7% higher. Wall 4 has much higher lateral load capacity and OOP stiffness than the other three walls due to the significantly higher applied axial load.

When comparing the load-displacement response of wall 1 to the response of wall 2, 3, or 4, care must be taken to consider the significant difference in rebar yield strength (wall 1 had bars which were 34% stronger than those in walls 2-4). However, it can be readily seen in Figure 3.17 that the strength and initial stiffness of wall 1 are significantly lower than those of walls 2 and 3, due to the placement of reinforcing bars closer to the faceshells (which increases the moment arm and increases the moment of inertia), in comparison to rebar placed in the center of the wall. Since the elastic modulus of the bars in all the walls is comparable, the stronger rebar does not play a role in increasing the initial stiffness.

The difference in the OOP stiffness of wall 2 and wall 3 at higher levels of lateral load is most likely explained by the positioning of the reinforcing bars within the grouted cells. Since the four bars in wall 3 were tied in a cage, there was little room for movement within the cell when the grout was poured. There was no more than 6 mm of possible movement in any direction. However, the bars in wall 2 were not tied, and were therefore free to move up to approximately 25 mm. Although attempts were made to ensure that the un-tied bars remained in the proper position, it is possible that the lateral pressure of the wet grout, poured in the centre of the cell, forced the bars toward the perimeter of the cell. This would result in an increased moment arm, and moment of inertia, and explain the higher OOP stiffness of wall 2. Figure 3.25 shows a top-down view of a reinforced cell in wall 3 where the tendency of the vertical bars to deviate for the design position can be readily seen.

Figure 3.25 – Rebar Positioning

On the other hand, a comparison of the response of wall 4 with respect to walls 2 and 3 is not particularly useful due to the much higher axial load using for testing Wall 4. Wall 4 was tested with 680 kN of axial load, instead of 350 kN as used for the other three walls. The higher axial load was selected to ensure compressive strains in the inner layer of rebar throughout the duration of the test, with the purpose of increasing the flexural stiffness. The higher axial load increased the OOP stiffness as seen in Figure 3.17. Additional insights gained from wall 4 will be further discussed in Section 3.5.3.

Table 3.3 provides a summary of the midspan OOP deflection of the four walls at six levels of lateral load. OOP loads of 30 kN and 40 kN were selected to provide insight into the response of the four walls in the elastic range. The remaining four lateral loads correspond to the yield load of the four walls. Empty cells in Table 3.3 indicate that failure had already occurred for that particular wall, and no data was available.

Table 3.3 – Mid-Height OOP Deflection

Wall	**MID-HEIGHT OOP DEFLECTION (mm)**					
	30 kN	**40 kN**	**59.9 kN (Wall 1 Yield)**	**68.6 kN (Wall 3 Yield)**	**74.5 kN (Wall 2 Yield)**	**97.2 kN (Wall 4 Yield)**
1 - *Conventional*	3.3	4.9	22.9	-	-	-
2 - *Boundary Rebar*	1.6	2.8	8.6	16.1	25.2	-
3 - *Cage - 350 kN Axial*	1.4	2.7	10.9	17.4	-	-
4 - *Cage - 680 kN Axial*	1.2	1.8	3.0	3.6	4.2	11.8

From Table 3.3 it is apparent that the OOP stiffness of wall 1 is significantly lower than that of wall 2 and 3 over the entire range of lateral load; however, as mentioned previously, due to the difference in rebar yield strength, a meaningful comparison cannot be made.

The difference in OOP deflection between wall 2 and wall 3 is extremely small (< 5%) at lateral loads below 45 kN. Until approximately 40 kN OOP load, wall 3 displays slightly higher stiffness. At OOP loads greater that 40 KN, wall 3 is stiffer than wall 2.

The OOP stiffness of wall 4 diminishes by over 50% in the second half of the elastic range. For lateral loads up to 60 kN, the stiffness is 20 kN/mm. At 97 kN lateral load, the stiffness is 8.2kN/mm.

Figures 3.26 to 3.29 contain plots of the deformed shapes of the four walls at the yield lateral loads presented in Table 3.3. Deformed profiles, for walls which collapsed prior to attaining the OOP load indicated in each figure, are not presented.

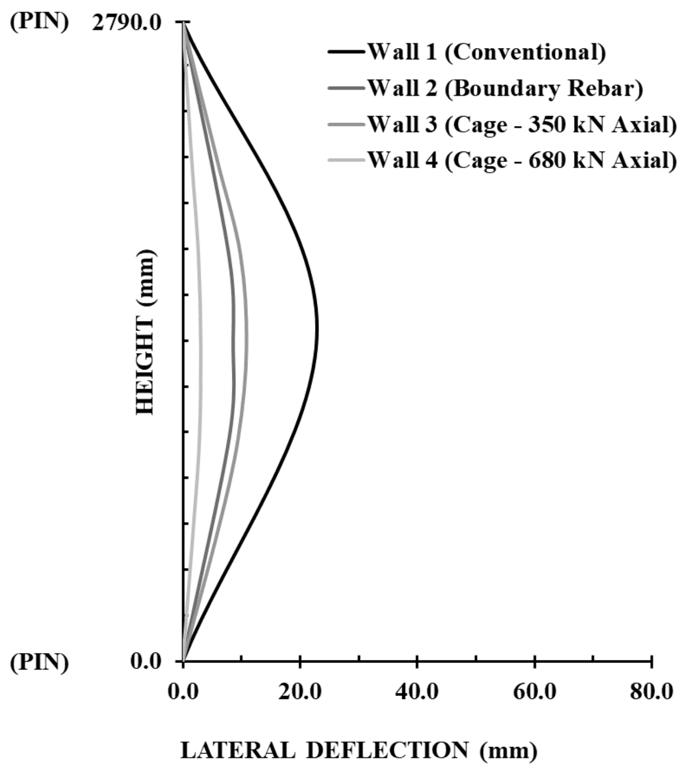

Figure 3.26 – Deflection Profiles (59.9 kN OOP Load)

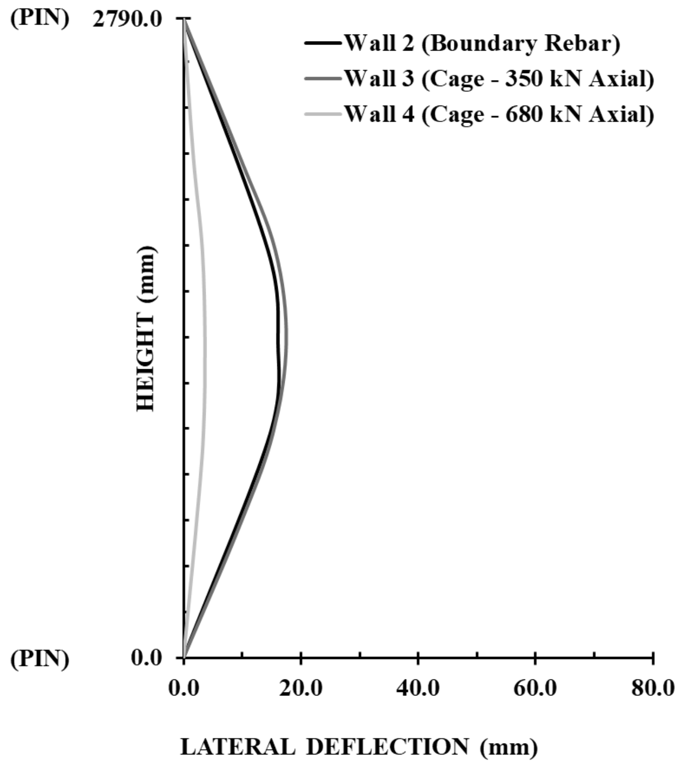

Figure 3.27 – Deflection Profiles (68.6 kN OOP Load)

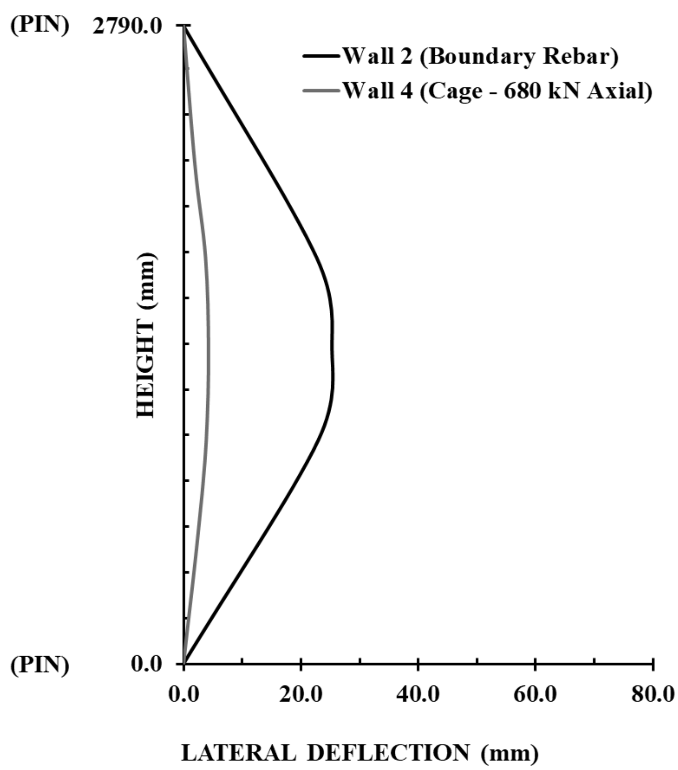

Figure 3.28 – Deflection Profiles (74.5 kN OOP Load)

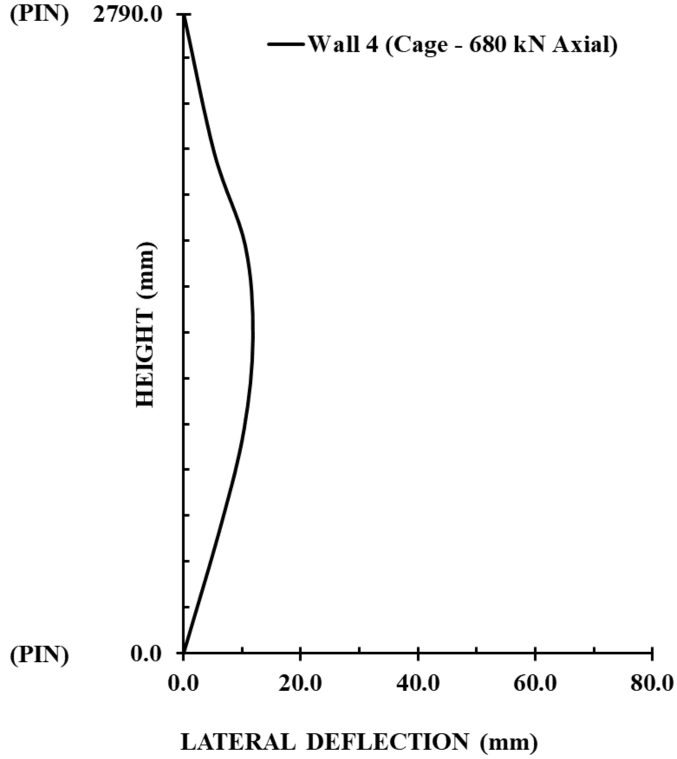

Figure 3.29 – Deflection Profiles (97.2 kN OOP Load)

From Figure 3.26 it is evident that the OOP deflection of wall 1 is significantly higher than that of wall 2 and 3 at yield, despite having stronger rebar. This indicates that cage reinforcing provides superior stiffness with an identical reinforcing ratio. The deformed profiles of wall 2 and wall 3 are virtually identical in Figure 3.26 and Figure 3.27, indicating that they have similar OOP stiffness up until yield. The OOP deflection of wall 4, at yield, is approximately half of the wall 2 and wall 3 OOP deflection at yield.

3.5.3 Strain Data

Table 3.4 summarizes the strain in the inner and outer rebar layers for all four walls at various levels of OOP load. All the strain readings were taken at mid-height (maximum moment), and therefore, represent the maximum rebar strains.

Table 3.4 – Wall Rebar Strain Data

Lateral Load (KN)	**Wall 1** ***Conventional***	**Wall 2** ***Boundary Rebar***		**Wall 3** ***Cage - 350 kN Axial***		**Wall 4** ***Cage - 680 kN Axial***	
	Center	**Inner**	**Outer**	**Inner**	**Outer**	**Inner**	**Outer**
10	-216	-183	-179	-220	-163	-261	-245
20	-215	-196	-158	-237	-139	-282	-225
30	-203	-205	-121	-252	-85	-304	-207
40	-152	-205	-33	-258	101	-327	-186
50	78	-141	277	-165	746	-350	-163
60	895	163	912	117	1963	-372	-133
65	1513	428	1390	288	2680	-384	-106
70		810	2173	505	3771	-396	-77
75		1358	3667			-409	-40
80						-424	43
90						-423	405
95						-357	901
100						-8	2428

The data in Table 3.4 clearly demonstrates that the section neutral axis in all four walls progresses toward the inner side as the lateral load increases. Under pure axial load, prior to application of any lateral load, all reinforcing bars are in compression. At this stage, there was no strain gradient across the wall sections and the neutral axis was not defined. As OOP load is applied, the neutral axis approaches the outer layer of rebar (central layer in wall 1) and progresses toward the middle of the section. Successive load progresses the neutral axis even further, causing the strain in the outer layer of rebar (central layer in wall 1) to cross the x-axis into tension. Further application of OOP load forces the neutral axis to progress past the inner layer of rebar and at this stage all the bars are in tension.

Figure 3.30, 3.31, 3.32, and 3.33 show the lateral load vs. rebar strain at three locations for each wall specimen. In each diagram, “top” represents the upper load application point, “middle” represents mid-height of the wall, and “bottom” represents the lower load application point.

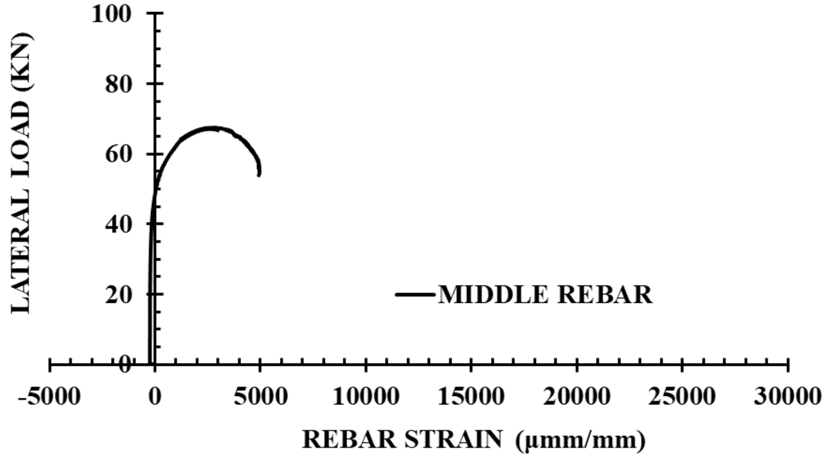

A) - Top

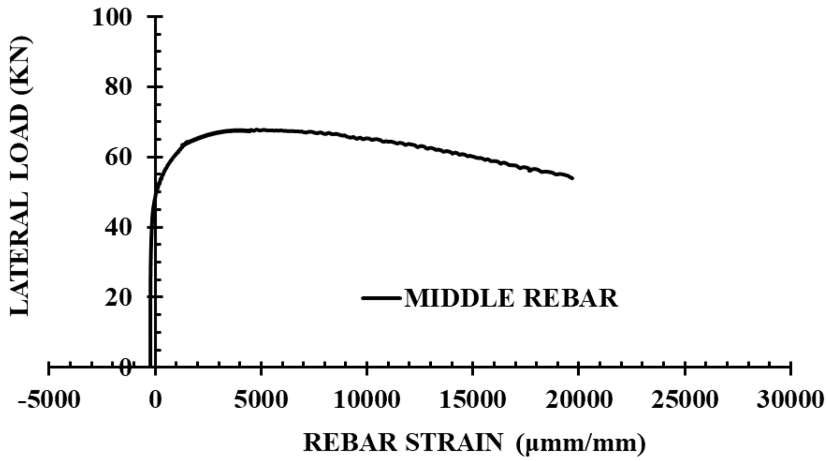

B) - Middle

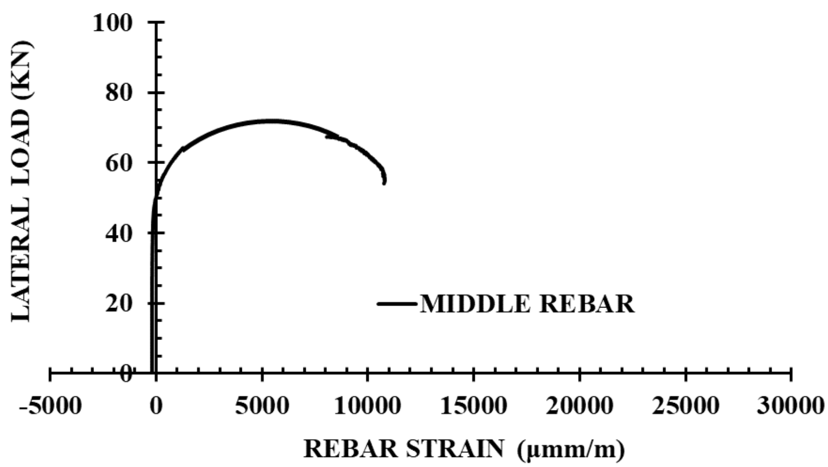

C) - Bottom

Figure 3.30 – Wall 1 (*Conventional*) Strain Plots

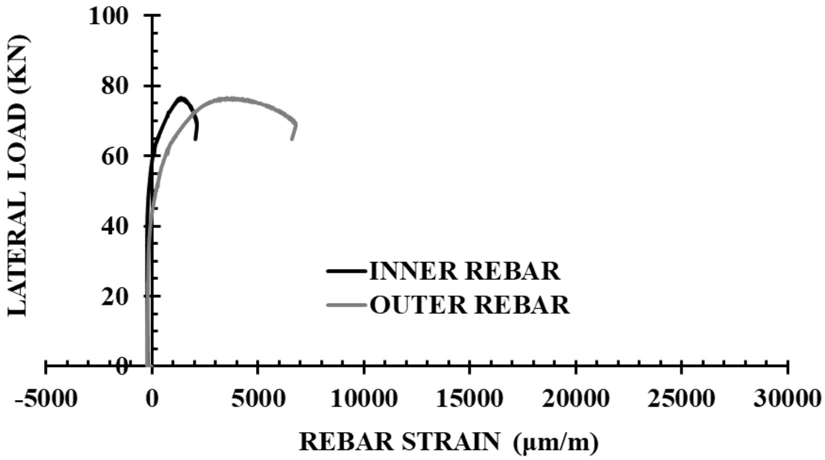

A) - Top

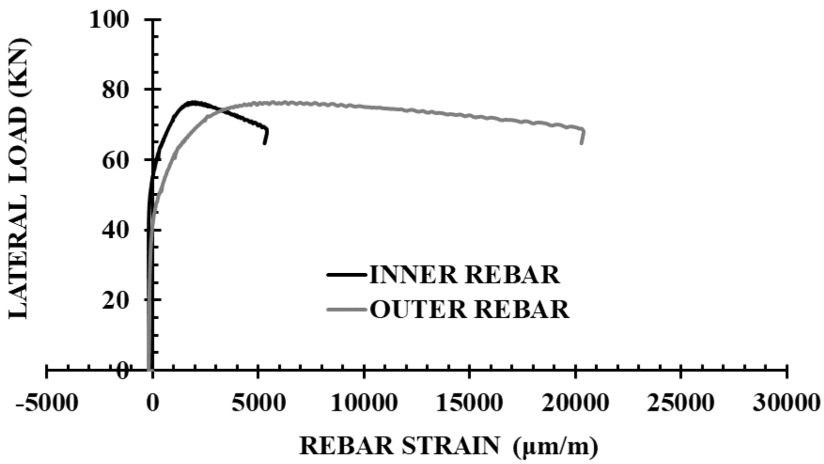

B) - Middle

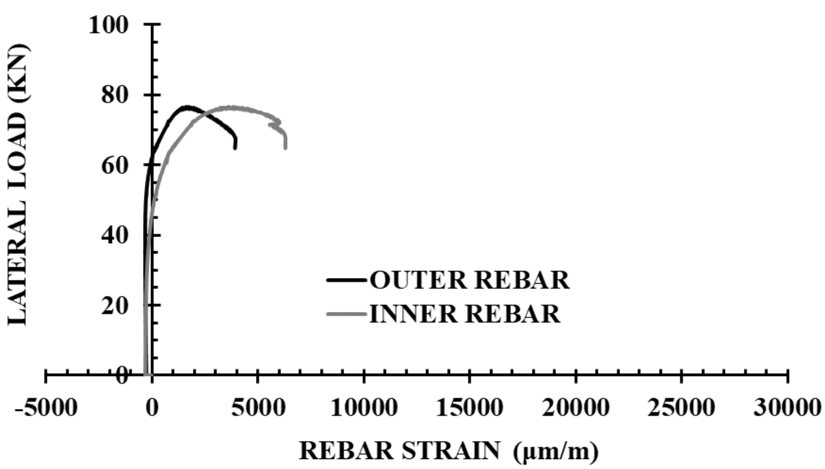

C) - Bottom

Figure 3.31 – Wall 2 (*Boundary Rebar*) Strain Plots

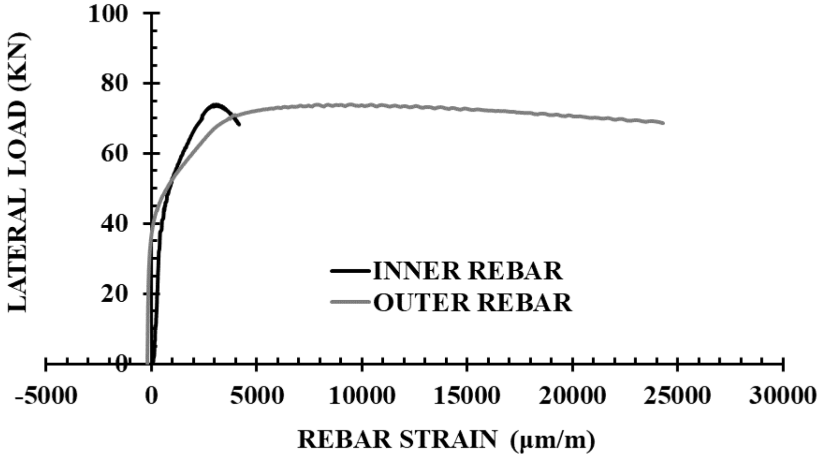

A) - Top

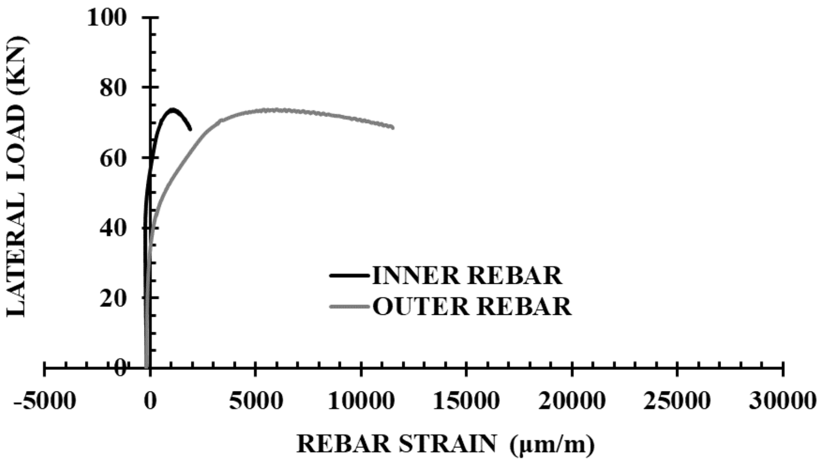

A) - Middle

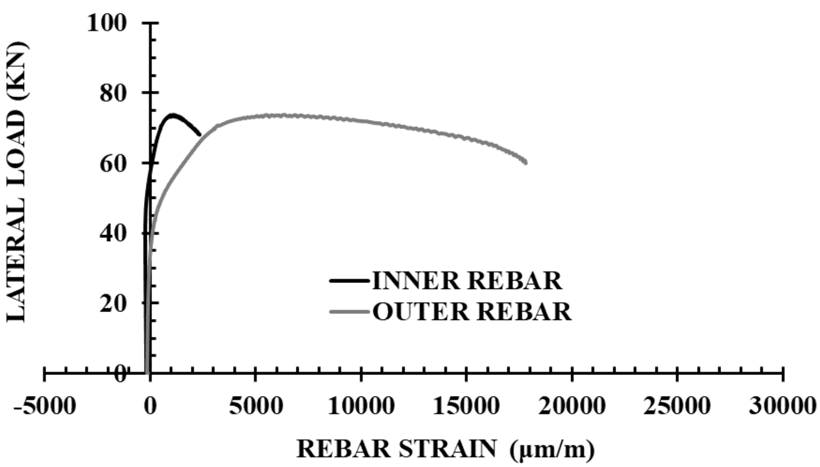

B) - Bottom

Figure 3.32 – Wall 3 (*Cage – 350 kN Axial*) Strain Plots

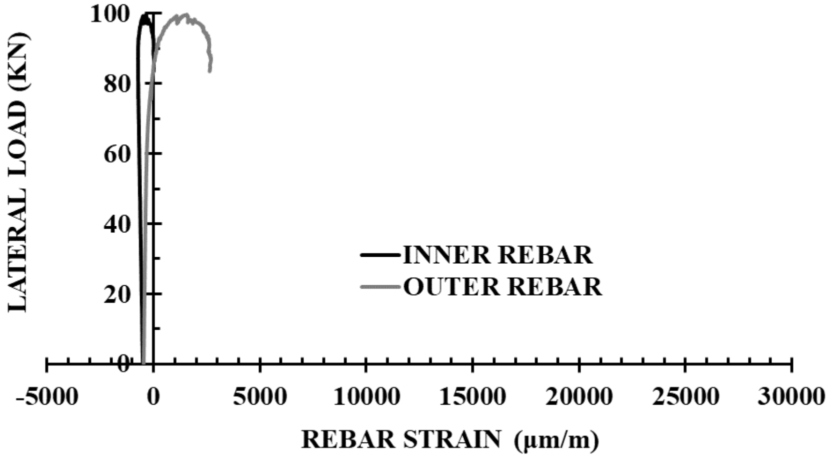

A) - Top

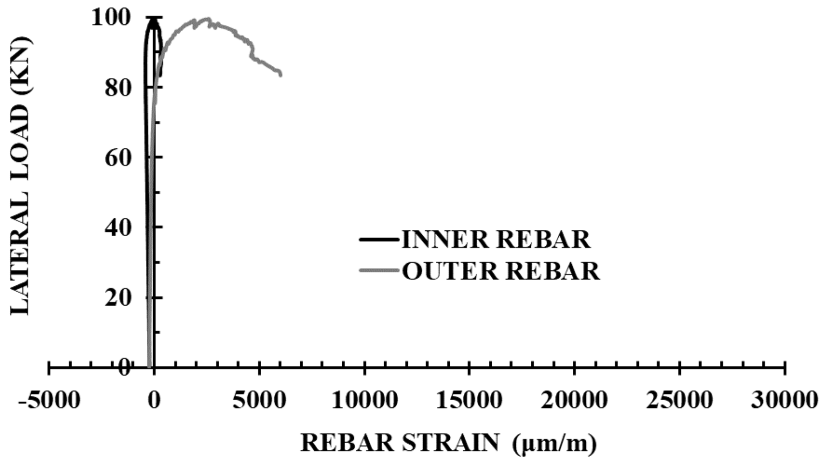

B) - Middle

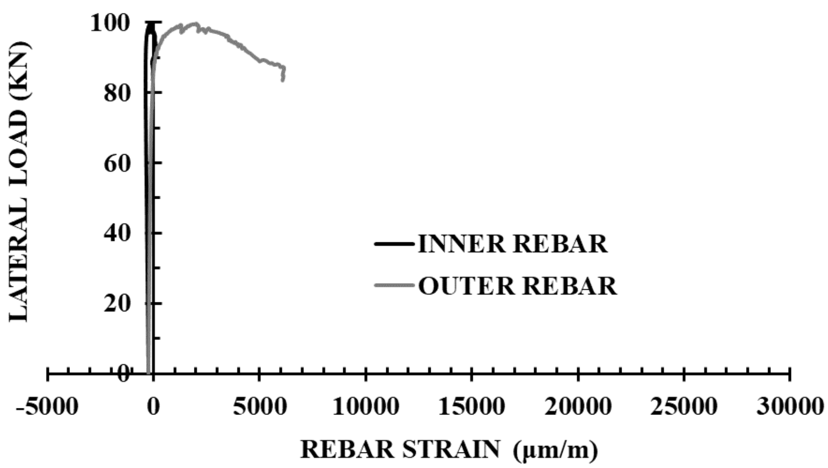

C) - Bottom

Figure 3.33 – Wall 4 (*Cage – 680 kN Axial*) Strain Plots

Figure 3.30 shows that the strain in the central reinforcing layer of wall 1 does not turn tensile until approximately 50 kN lateral load. This is approximately 14 kN prior to ultimate load. Figure 3.31 and Figure 3.32 show that the rebar on both the inner and outer face of wall 2 and wall 3 is in tension at lateral load well before ultimate. The outer layer rebar strain turns tensile at approximately 45 kN lateral load and the inner layer at 60 kN. Figure 3.33 shows that in wall 4, the strain in the outer layer of rebar turns tensile at approximately 90 kN lateral load. The inner rebar layer approaches zero strain at ultimate.

The gradual progression of the neutral axis toward the inner face of the wall, as described previously, is visually depicted by the strain profiles in Figure 3.34, 3.35, 3.36 and Figure 3.37. For wall 1, only discrete points are shown since strain reading were taken only on the central rebar. For wall 2 and 3, strain profiles at OOP loads below 50 are not shown since they would appear to lie on the x-axis. For wall 4, strain profiles at three levels of lateral load approaching failure are shown. Selection of an appropriate level of axial load for wall 4 was done with elastic stiffness of the wall in mind. The axial load of 680 kN represents an ideal load to retain compressive stress in the inner rebar layer throughout the duration of the test. It was desired that only immediately prior to failure the neutral axis would approach the inner layer of rebar.

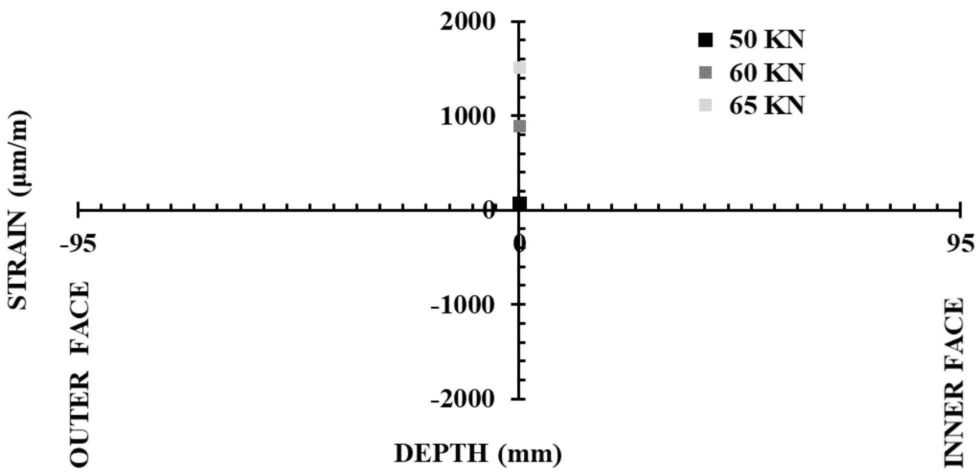

Figure 3.34 - Wall 1 (*Conventional*) Strain Profiles

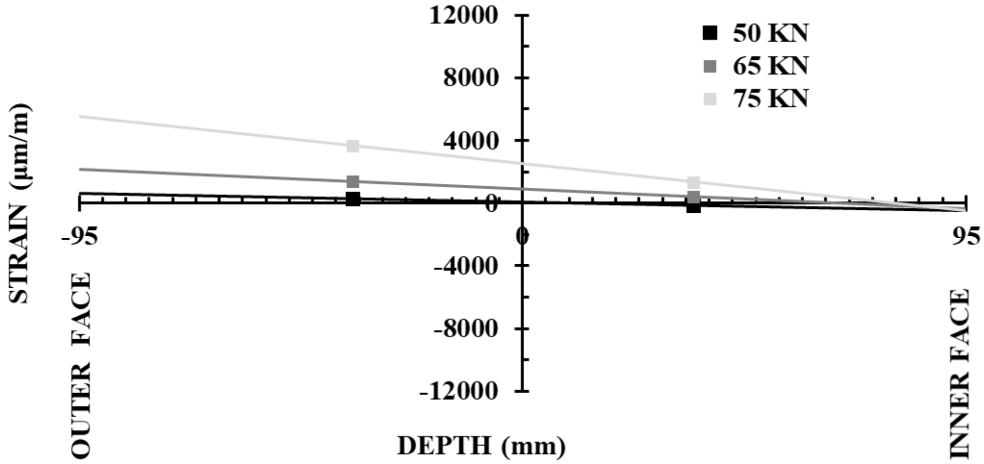

Figure 3.35 - Wall 2 (*Boundary Rebar*) Strain Profiles

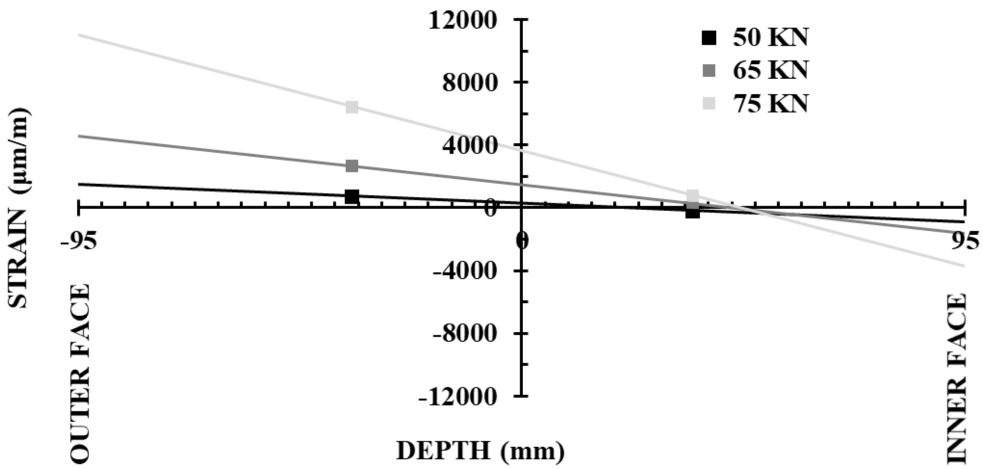

Figure 3.36 – Wall 3 (*Cage – 350 kN Axial*) Strain Profiles

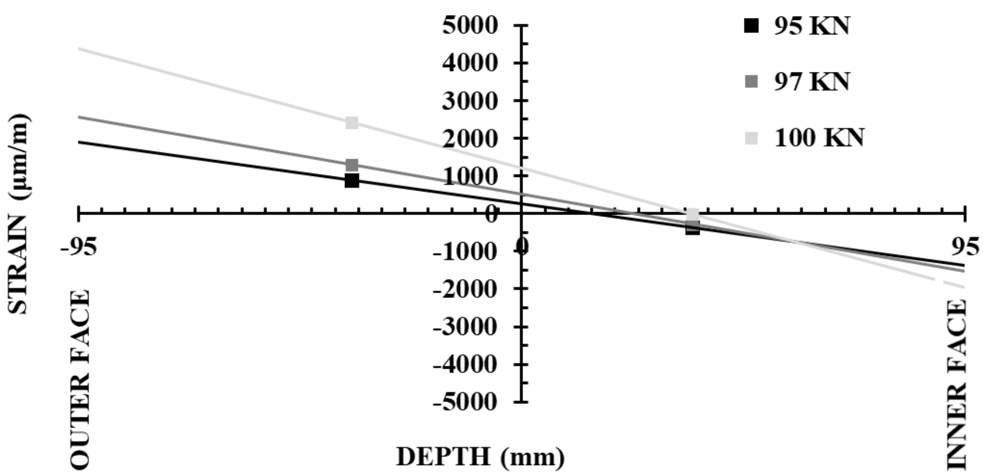

Figure 3.37 – Wall 4 (*Cage – 680 kN Axial*) Strain Profiles

Although it is not possible to construct strain profiles for wall 1 in Figure 3.34 due to a lack of simultaneous strain readings, it can reasonably be assumed that the neutral axis progresses toward the inner face of the wall, as described earlier, based on the increasing tensile rebar strain.

The development of tensile strain in both the inner and outer rebar layers, as is the case for wall 2 and wall 3, does not promote optimal OOP stiffness. This has been demonstrated by the results of the eccentric prism tests in chapter 1. It was shown in chapter 1 that for prisms tested at an eccentricity of t/3 (63.3 mm), cage reinforced specimens are 21.4% stiffer than conventionally reinforced specimens with identical reinforcing ratios. Likewise, at an eccentricity of 5t/12, cage reinforced prisms are 12% stiffer in comparison to conventionally reinforced prisms.

This discrepancy in prism stiffness enhancement at two loading eccentricities is best explained by an analysis of the rebar strains at failure. The average compressive strain in the inner rebar layer for prisms tested at t/6, t/3, and 5t/12 is 0.0012 mm/mm, 0.0008 mm/mm, and 0.000369 mm/mm, respectively. Larger eccentricates cause higher moments, which result in reduced axial capacity. The reduced axial load, combined with a higher bending moment, results in a shift of the neutral axis toward the inner face of the prisms. The proximity of the neutral axis to the inner rebar layer is directly proportional to the amount of compressive strain it develops. Figure 3.38 shows that the compressive strain in the inner rebar layer increases as the loading eccentricity decreases. Therefore, it can be concluded that the level of axial load is directly correlated with the degree of expected stiffness enhancement.

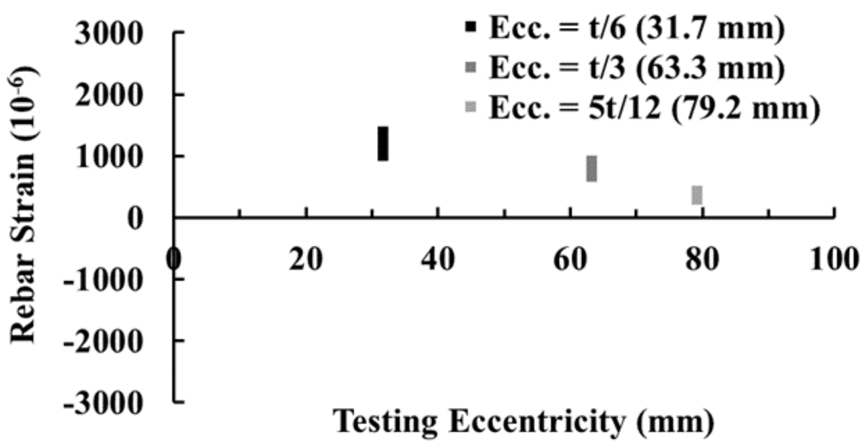

Figure 3.38 – Prism Concave Side Rebar Strain

It is likely that the same phenomenon is present in wall 2 and 3. The 350 kN axial load used for wall 2 and 3, was not high enough to promote compressive strain in the inner layer of reinforcing steel. All the potential stiffness enhancement offered by the two-rebar layer configuration was not realized. In order to do so, the distance between the rebar layers needs to be increased. For future research, investigation must be conducted to develop innovative blocks that allow placement of the cage with a larger distance between rebar layers, either by reducing the faceshell thickness or designing innovative shapes.

As seen in Figure 3.37, the strain in the inner rebar layer of wall 4 is virtually zero at ultimate load. This indicates that the axial load of 680 kN allowed for engagement of the inner layer steel rebar in compression at any level of lateral load up until failure. This will necessarily result in an increase in stiffness due to the relative difference in the steel and masonry compressive strength and modulus of elasticity

Figure 3.39 depicts the strain profiles in a masonry wall with identical properties and construction as wall 2, 3 and 4 at three levels of axial load. The sole difference is that the block width is now 390 mm instead of 190 mm; leaving 273 mm between the rebar layers

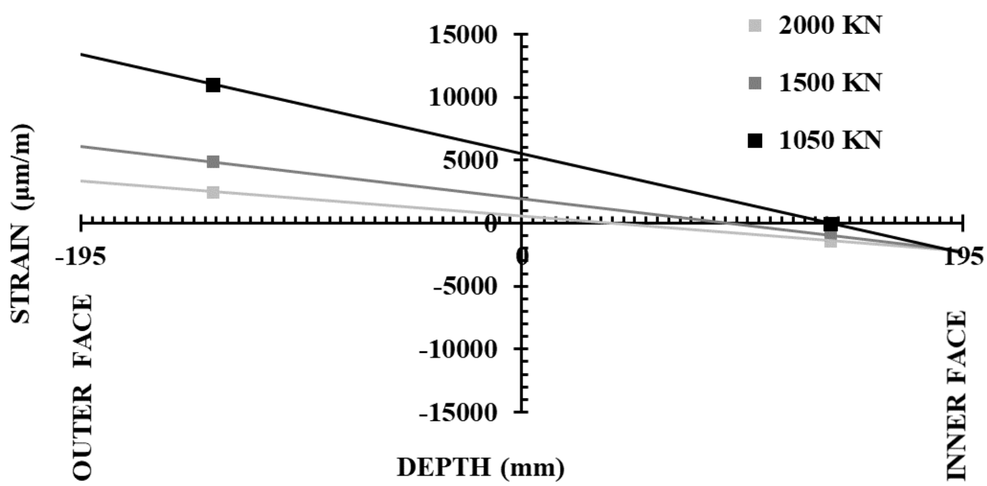

Figure 3.39 – 390 mm Block Strain Profiles

Based on findings of the prism and wall tests, it may be concluded that if the neutral axis at failure is located somewhere between the two layers, at least some stiffness enhancement can be expected. An axial load of 1050 kN represents the lower limit required to retain compressive strain in the inner layer, while 2000 kN represents the upper limit for the axial load if a degree of ductility is desired in the outer layer. An intermediate axial load of 1500 kN would likely be ideal for testing this design configuration.

3.5.4 Effective Flexural Rigidity, EI_{eff}

Table 3.5 provides the peak OOP load, and the corresponding primary moment, total moment, and inner and outer rebar layer strains for wall 2, 3 and 4. Wall 1 is not included since strain readings were taken only on the central rebar layer. Using the provided strain values and a rebar layer spacing of 73 mm, the section curvature was determined at the wall mid-height - the location of maximum moment. EI_{eff} is calculated as the ratio of total moment to curvature.

The S304 prescribed values of EI_{eff} are also provided using the equation given in Section 1.1.4. For the S304 equation, the kern eccentricity (e_k) was determined to be 42.8 mm, the cracked moment of inertia (I_{cr}) was calculated as 29.4 x 10^6 mm^4, the uncracked moment of inertia (I_o) was calculated as 585 x 10^6 mm^4, and the masonry modules of elasticity (E_m) was taken as 850f'm = 22.4 x 10^3 MPa; with an upper limit of 20 x 10^3 MPa

Table 3.5 – EI_{eff} Data

Wall	Peak OOP Load (kN)	Primary Moment at Peak Load (kN-m)	Total Moment at Peak Load (kN-m)	Inner Rebar Layer Strain (μmm/mm)	Outer Rebar Layer Strain (μmm/mm)	Curvature (μrad)	EI_{eff} (10^8 N-mm^2)	S304 EI_{eff} (10^8 N-mm^2)
2	76.6	38.3	50.5	1989	6265	58.6	8618	11084
3	73.9	36.9	48.1	1074	9454	114.8	4189	12182
4	99.6	49.8	63.4	27	2573	34.9	18166	20934

The difference in the empirically established values of EI_{eff} for wall 2 and 3 is likely due to the positioning of the rebar within the grouted cells as explained in Section 3.5.2. Slight deviations in rebar positioning affect the rebar strain and ultimately the curvature and the value of $EI_{eff.}$ The higher empirical value of EI_{eff} in wall 4 is explained by the larger ultimate moment and the lower curvature as a result of the higher axial load. The data in Table 3.5 indicates that S304 overestimates the effective flexural rigidity for all three walls at ultimate. The overestimation is less pronounced for wall 4, which has a higher axial load.

3.5.5 P-M Response

A mechanics-based section analysis model was used to generate moment-curvature (M-C) diagrams representative of the four wall specimens (Fig. 3.40). The model does not account for possible core confinement effects imparted by the reinforcing cage; therefore, the MC response for wall 2 and 3 is identical because there is no other distinguishing characteristic. Based on the M-C curves, it is expected that all four walls will have varying degrees of ductility prior to collapse. Table 3.6 contains the predicted curvatures at yield moment and at ultimate moment for each of the four walls.

Table 3.6 – M-C Data

Wall	Yield Moment (kN-m)	Yield Moment Curvature (µrad)	Ultimate Moment (kN-m)	Ultimate Moment Curvature (µrad)
1 - *Conventional*	38.3	25.9	46.2	93.5
2 - *Boundary Rebar*	45.6	34.6	50.8	104.8
3 - *Cage - 350 kN Axial*	45.6	34.6	50.8	104.8
4 - *Cage - 680 kN Axial*	69.7	38.94	71.3	63.5

The predicted ductility for wall 1, 2, 3, and 4 is 3.60, 3.03, 3.03, and 1.63, respectively. As expected, due to the higher axial load, the ductility for wall 4 is significantly lower.

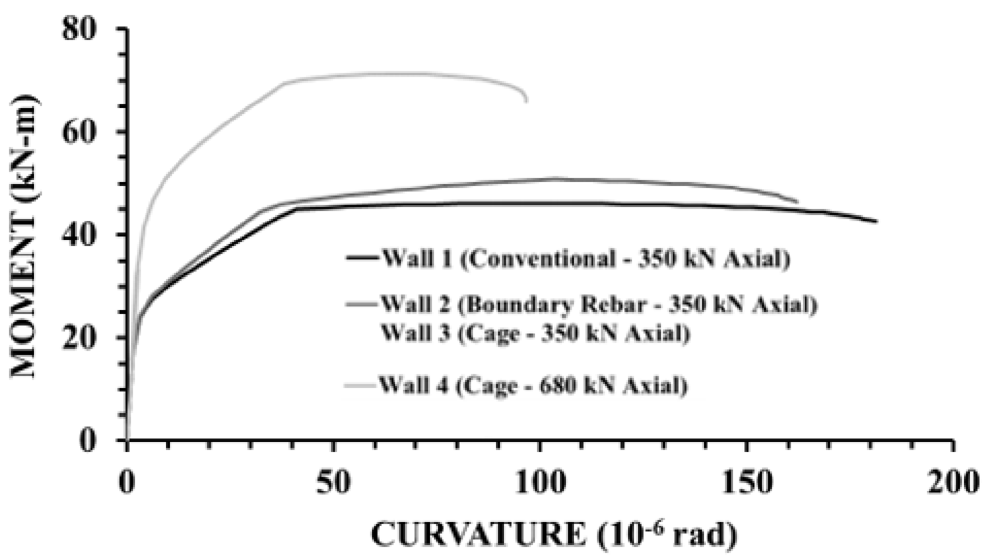

Figure 3.40 – M-C Diagrams

The mechanics-based model was also used to produce the P-M interaction diagrams in Figure 3.43, 3.44, 3.45, and 3.46. The discretization of a typical wall section, as for modeling, is shown in Figure 3.41.

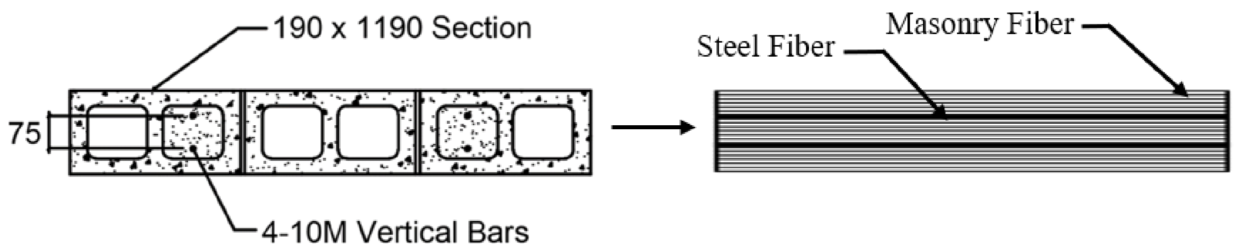

Figure 3.41 – Fiber Section Wall Model

For these theoretical models, the wall section was divided into 100 masonry fibers in the OOP direction. Each layer of reinforcing steel was modeled as a single fiber of equivalent area with the same width as the masonry section. Recall that a plane section compatibility analysis has only first-order analysis capabilities without accounting for second-order effects introduced by variables such as wall height or elastic/inelastic deformations. Due to the inherent restrictions present in this type of this analysis, the model does not account for the possibility of other failure mechanisms, such as compression buckling and member instability. It is assumed that failure will occur at the section level due to material failure such as steel yielding or masonry crushing. Based on the empirical observations of the failure mechanisms presented in the previous sections, this assumption appears to be correct.

Table 3.7 contains the first order moment, caused by OOP load, and the second-order moment, caused by axial load in combination with lateral deflection, for each wall specimen. The peak moment capacity of wall 2 and wall 3 differs by only 1.8% and is not statistically significant to warrant an explanation. The peak moment capacity of wall 1 is lower than both wall 2 and wall 3 despite having 34% stronger rebar. As explained earlier, this increased rebar strength is not able to overcome the disadvantage that wall 1 has in a smaller moment arm and smaller moment of inertia. Wall 4 has highest OOP stiffness and strength.

Table 3.7 – P-M Data

Wall	Axial Load (kN)	Peak Lateral Load (kN)	Peak Mid-Span Deflection (mm)	Peak First-Order Moment (kN-m)	Peak Second-Order Moment (kN-m)	Peak Total Moment (kN-m)
1 - *Conventional*	350	67.7	38.9	39.5	13.6	53.1
2 - *Boundary Rebar*	350	76.6	34.7	43.3	12.1	55.4
3 - *Cage - 350 kN Axial*	350	73.9	32.1	43.2	11.2	54.4
4 - *Cage - 680 kN Axial*	680	99.6	19.8	56.8	13.5	70.3

The contribution of the second-order moment to the total moment is 26%, 22%, 21%, and 19% for wall 1, 2, 3, and 4, respectively. Based on the discussion in the previous section, this trend appears to be reasonable since the second-order moment is directly related to OOP stiffness. It was demonstrated previously that wall 1 has the lowest stiffness of the four walls, wall 4 has the highest stiffness, and wall 2 and 3 have nearly identical stiffness.

Figure 3.42 shows the mid-span moment vs. lateral deflection for all four walls. A cursory assessment of the graph indicates that the three walls tested at 350 kN axial load have similar moment capacities. As expected, wall 4 has much higher moment capacity and OOP stiffness, but less ductility, due to the higher axial load.

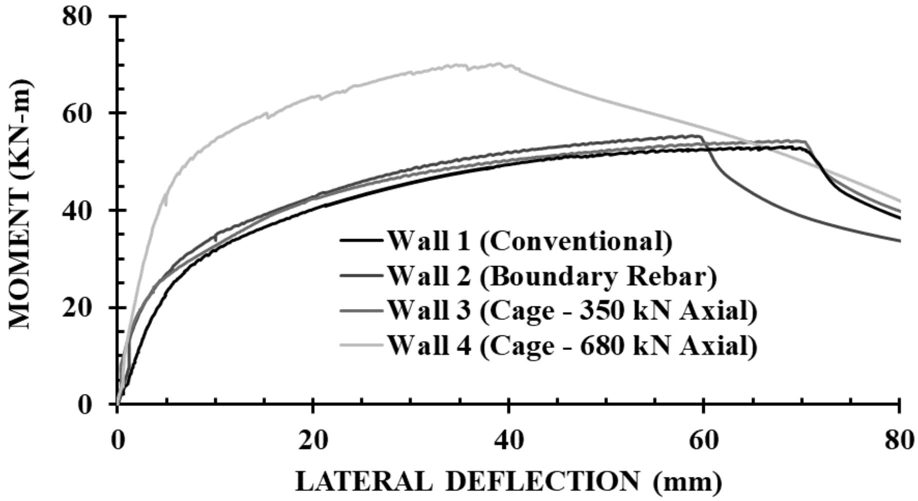

Figure 3.42 – Moment-Deflection Diagrams

The P-M data points from Table 3.7 are superimposed on theoretical P-M interaction diagrams developed for the wall sections in Figure 3.43 and Figure 3.44. No distinction is made between the P-M interaction diagram for wall 2, 3, and 4 because the model does not have the capacity to account for the core confining effects provided by a pre-tied rebar cage. These interaction diagrams were developed using the actual masonry and rebar material properties provided earlier.

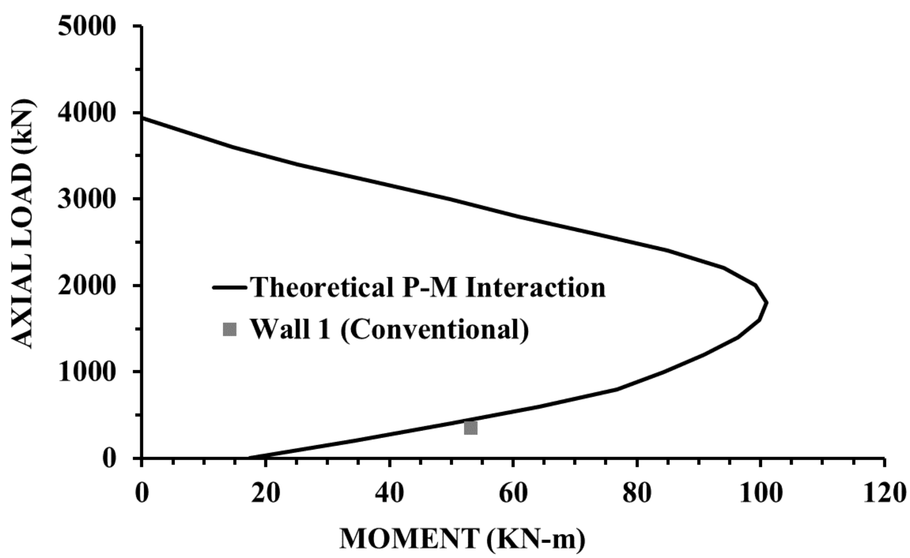

Figure 3.43 – Wall 1 P-M Interaction

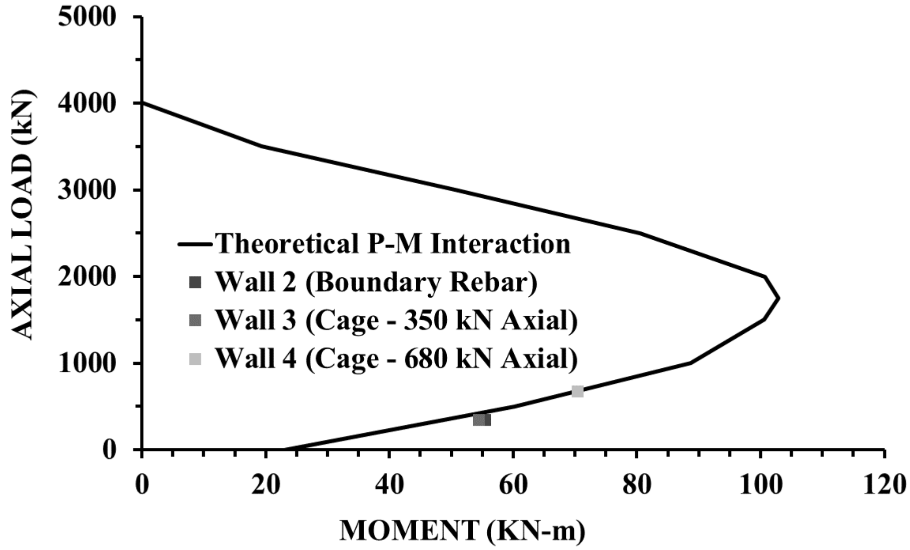

Figure 3.44 – Wall 2, 3 & 4 P-M Interaction

Based on the limited sample size, the mechanics-based model appears to predict the P-M response of all wall types with excellent precision at the two levels of axial load utilized. The accuracy of the model could be further verified by testing walls at axial loads within the range of pure bending and pure axial load.

Figure 3.45 contains superimposed graphs of the P-M interaction diagrams developed for wall 1 and for walls 2, 3, and 4 using the actual material properties. The response is similar, although there is a range of axial load, from 0.25 PMax to 0.5 PMax, in which walls 2/3/4 possess slightly higher moment capacity than wall 1.

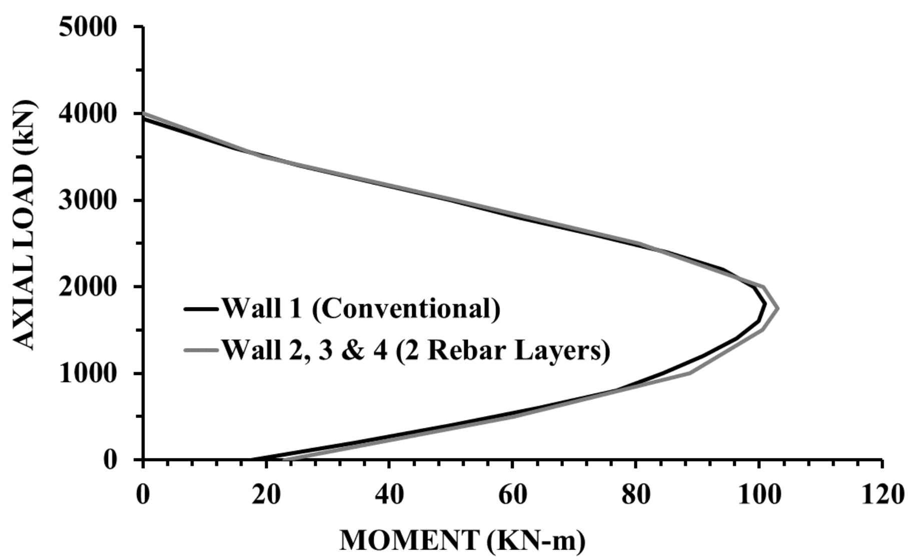

Figure 3.45 – P-M Response Comparison

An additional P-M comparison is shown in Figure 3.46. A P-M interaction diagram was developed for wall 1 using the same material properties as used for wall 2, 3 and 4. The results are virtually identical to those in Figure 3.45. This leads to the conclusion that the moment arm of the reinforcing, and the moment of inertia of the section have a greater effect on moment capacity than material properties such as rebar yield strength.

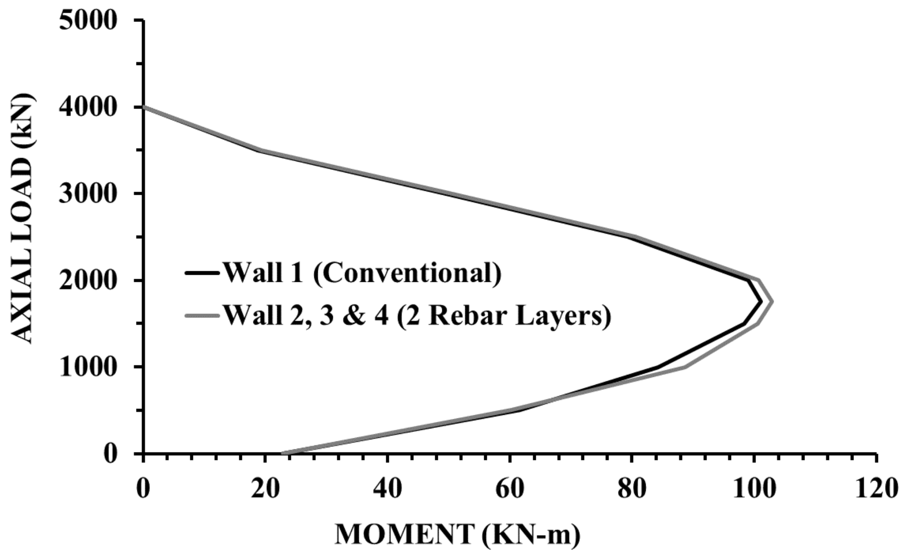

Figure 3.46 – P-M Response Comparison (Identical Materials)

CHAPTER 4: SUMMARY AND CONCLUSIONS

4.1 SUMMARY

Chapter 2 contains the results obtained from a series of masonry prisms tested under concentric and eccentric axial load. A total of 20 prisms were tested concentrically, and 19 prisms were tested eccentrically. Of the concentrically tested prisms, five were unreinforced and 15 had cage-reinforcing. Of the eccentrically tested prisms, 15 had cage reinforcing and four had central rebar. For the concentrically loaded prisms, the variable was the transverse tie spacing while for the eccentrically loaded prisms the manipulated variable was the degree of load eccentricity.

Under concentric axial load, the cage reinforced prisms demonstrated satisfactory structural performance, in terms of core integrity. Transverse tie spacings for compression members closer than the minimum code prescription were demonstrated to have no impact on the axial capacity of concentrically loaded prisms. P-M interaction plane-section compatibility analyses show that prisms with reinforcing cages have greater moment capacities for comparable levels of axial load for a wide range of reinforcing steel areas. Under eccentric load, cage reinforced prisms were demonstrated to have higher moment capacities and greater stiffness in contrast to conventionally reinforced prisms. It was discovered that the level of axial load in the cage reinforced prisms is directly related to the degree of stiffness enhancement due to the engagement of the concave side rebar in compression.

Chapter 3 contains the results obtained from a series of four masonry walls tested under simultaneous axial and OOP load. Three walls were subjected to an axial load of 350 kN and the fourth wall to 680 kN. Three different reinforcing configurations were utilised: wall 1 had conventional central reinforcing, wall 2 had two layers of un-tied reinforcing, and wall 3 and 4 had pre-tied cage reinforcing.

Wall 2 and 3 had almost identical flexural capacity and OOP stiffness. The slight variation within these two walls is likely explained by construction imperfections. Although wall 1 had significantly higher rebar strength, its flexural capacity and OOP stiffness was lower than that of wall 2 and 3 due to its lower rebar moment arm and moment of inertia. Wall 4 demonstrated greater flexural strength and OOP stiffness than the other three walls due to its higher axial load. Wall 4 was the only specimen that fully realized the stiffness enhancement potential of the two-rebar layer configuration due to engagement of the inner rebar later in compression until immediately prior to ultimate load; a characteristic which was demonstrated to be responsible for increasing the OOP stiffness in chapter 1. A mechanics-based section analysis model was shown to be capable of precisely predicting the flexural capacity of the four specimens at both 350 kN and 680 kN axial load. The model predicts that when identical materials properties are utilized, the flexural capacity of a cage reinforced wall will be slightly higher than that of a conventionally reinforced wall over an axial load range of 0.25 PMax to 0.5 PMax

4.2 CONCLUSIONS

Insights gained from this research program relate to experiment design, wall and prism specimen design, and to the mechanisms through which certain desirable characteristics, such as OOP stiffness and flexural strength, are enhanced.

- The techniques and materials proposed for construction of the innovative masonry assemblage are viable. The sliding blocks and pre-tied cages did not cause construction delays or any other impositions beyond those of normal construction tasks.

- Rebar buckling was not observed in any of the concentrically or eccentrically tested cage-reinforced prisms. The code stipulation for maximum transverse tie spacing appears to be valid.

- Cage-reinforced prisms have greater flexural strength than prisms with untied, centrally-located, rebar with equivalent reinforcing ratios over the range of axial load from 0 to PMax.

- For prisms tested at t/3 (63.3 mm) and 5t/12 (79.2 mm), cage-reinforced prisms have 21.4% and 12.1% greater stiffness than conventionally-reinforced prisms, respectively. A comparison could not be made for t/6 (31.7 mm) since the conventionally-reinforced prism intended to be tested at that eccentricity had a significant construction defect and was discarded.

- The primary mechanism by which stiffness is enhanced in a cage reinforced prism or wall is inducing a compressive force in one of the rebar layers. The relative difference in the compressive strength and modulus of elasticity between masonry grout and steel rebar is responsible for a quantifiable stiffness enhancement when the rebar is in compression.

- The effects of cage reinforcing on OOP stiffness were not as noticeable as anticipated for the wall tests. The axial loads were not high enough to engage the inner rebar layer in compression outside of the elastic range. The axial load utilized for walls 1, 2, and 3 was 0.06Aef'm. For typical exterior load-bearing walls, the factored axial UDL would be within the range of 50 kN/m to 500 kN/m. For f'm = 26.3 MPa, this translates to 0.01Aef'm and 0.1Aef'm. Therefore, in specific situations, with relatively high axial load levels, it can be expected that the OOP wall stiffness would be enhanced by the utilization of cage reinforcing.

- The wall slenderness ratio of 12.6, in combination with the two chosen reinforcing configurations, resulted in significant second-order moments. The contribution of the second-order moment to the total moment was 26%, 22%, 21%, and 19% for wall 1, 2, 3, and 4, respectively. In Section 1.3 it was stated that second-order effects in the wall tests were expected to be observable and quantifiable. It can be concluded that the specific parameters selected for the wall specimens were conducive for the development of second-order effects.

- The moment arm (distance between the rebar layers) in wall 2, 3, and 4 was not optimal for development of compressive forces in the inner rebar layer. A larger moment arm would facilitate positioning of the neutral axis between the rebar layers as suggested in the next section.

- Although there is no significant difference between the flexural strength and OOP stiffness of the cage-reinforced wall and the boundary rebar wall at 350 kN axial load, the pre-tied cage aids in positioning of the reinforcing bars during construction. Also, pre-tied cages can be constructed by a supplier and delivered to a construction site, which offers potential labour and time savings.

- Previous empirical research indicates that CSA S304 underestimates the value of EI_{eff} for RM walls at peak OOP load. However, for walls 2, 3 and 4 S304 actually overestimates EI_{eff}. In this case, using the code prescribed values of EIeff to calculate the flexural capacity would not result in design inefficiencies.

4.3 RECOMENDATIONS FOR FUTURE WORK

Future research on the topic of OOP loaded slender masonry wall should be conducted with the following considerations in mind.

- Future investigations must be conducted to develop innovative blocks that allow placement of the cage with a larger distance between rebar layers, either by reducing the faceshell thickness or designing innovative shapes. This would increase the rebar moment arm and facilitate development of compression in the inner rebar layer.

- The height of the wall specimens should be sufficient to achieve a slenderness ratio where second-order effects are prominent. Using 190 mm thick blocks, and a minimum wall height of 2 400 mm, second-order moments of approximately 25% (of the total moment) can be achieved.

- Models built to simulate OOP loaded cage-reinforced walls would benefit from a clear definition of the cage's confining effects on the grouted core. The mechanics-based model used in this research program did not include this effect. It is possible that confining effects were responsible for at least a portion of the enhanced stiffness experienced by the wall and prism specimens. However, the complexity involved in quantifying these effects in a model was beyond the scope of this research.

- Code-related wall design parameters, such as, end fixity conditions should be explored

- The four-point bending setup used in this research program could be upgraded to uniform loading by implementation of an airbag system. This would allow for uniform pressure to be exerted on a wall - representative of wind loading. Furthermore, air bag OOP loading would allow for realization of asymmetric deflection profiles which would necessarily occur because of nonuniform support conditions.

REFERENCES

[1] Canadian Standards Association (2004). "Design of Masonry Structures." *CSA S304.1-04.* Rexdale, ON, Canada

[2] The Masonry Society (2016). "Building Code Requirements and Specifications for Masonry Structures." *TMS 402/602-16.* Longmont, CO, U.S.A

[3] Yokel, F.Y. (1971). "Stability and Load Capacity of Members with no Tensile Strength." *Journal of the Structural Division,* Proceedings of the ASCE, Vol.97, No. ST7, July 1971, Proc. Paper 8253, 1913-1926.

[4] Cranston, W.B and Roberts, J.J. (1976). "The Structural Behaviour of Concrete Masonry Reinforced and Unreinforced." *The Structural Engineer.*, 54(11)

[5] Hatzinikolas, M.A, Longworth, J. and Warwaruk, J. (1976). *Concrete Masonry Walls*, University of Alberta, Edmonton, AB, Canada

[6] Western States Clay Products Association (1984). "Design of Reinforced Masonry Tall Slender Walls." San Francisco, California, USA

[7] ACI-SEASC Task Committee on Slender Walls, "Test Report on Slender Walls," American Concrete Institute and the Structural Engineers Association of Southern California, February 1980 - September 1982, Los Angeles.

[8] Hamid. Ahmad A., Abboud. Bechara E., Farah. Muris W., Hatem. Michel K., Harris, Harry G., "Response of Reinforced Block Masonry Walls to Out-of-Plane Static Loads," Drexel University, September 1989, Philadelphia.

[9] Tumialan, J. G. and Nanni, A. (2002). "Strengthening of Masonry Walls with FRP Bars." *Composites Fabricator Magazine*.

[10] Korany, Yasser. and Drysdale, Robert. (2006). "Rehabilitation of Masonry Walls Using Unobtrusive FRP Techniques for Enhanced Out-of-Plane Seismic Resistance." *Journal of Composites for Construction.*, 10(3), 213-222.

[11] Mierzejewski, Wojciech. (2010). "Out-of-Plane Bending of Masonry Walls with Near-Surface-Mounted and Externally-Bonded Corrosion-Resistant Reinforcement,", Queen's University, Kingston, ON, Canada

[12] Drysdale, R.G., Sallam S.E.A. and Karaluk, E (1976). "Design of Masonry Walls and Columns for Combined Axial Load and Bending Moment.", *First Canadian Masonry Conference.*, 394-408, Calgary, AB, Canada

[13] Suwalski, P.D. and Drysdale, R.G. "Influence of Slenderness on the Capacity of Concrete Block Walls."

[14] Liu, Y. and Dawe, J. (2001). "Experimental Determination of Masonry Beam Column Behaviour." *Canadian Journal of Civil Engineering.*, 28(5), 794-803.

[15] Maksoud, A.A., and Drysdale, R.G. 1993. "Rational moment magnification factor for slender unreinforced masonry walls." In Proceedings of the 6th North American Masonry Conference, Vol. 1, pp. 443–454.

[16] Liu, Y. and Dawe, J. (2003). "Analytical Modeling of Masonry Load-bearing Walls." *Canadian Journal of Civil Engineering.*, 36(3), 795-806.

[17] Liu, Y. and Hu, K. (2007). "Experimental Study of Reinforced Masonry Walls Subjected to Combined Axial and Out-of-Plane Bending." *Canadian Journal of Civil Engineering.*, 34(6), 1486-1494.

[18] M*ü*ller, Anna Louisa, Isfeld, Andrea C., Hagel, Mark, and Shrive, Nigel G. (2017). "Review and Analysis of Capacity of Slender Concrete Masonry Walls." *13th Canadian Masonry Symposium Halifax, Canada.*

[19] Isfeld, Andrea C., M*ü*ller, Anna Louisa, Hagel, Mark, and Shrive, Nigel G. (2018). "Analysis of Safety of Slender Concrete Masonry Walls in Relation to CSA S304-14."

[20] A.C. Isfeld, M. Hagel, A.L. M*ü*ller, and N.G. Shrive. (2018). "Out of Plane Behaviour of Concrete Block Masonry Wall with Different Base Support Conditions." *10th Australasian Masonry Conference Sydney, Australia.*

[21] Banting, B. R. and El-Dakhakhni, W. W. (2014). "Seismic Performance Quantification of Reinforced Masonry Structural Walls with Boundary Elements." J. *Struct. Eng.*, 140(5), 1477-1491.

[22] Cyrier, Willis Bradford. (2012). *Performance of Concrete Masonry Shear Walls with Integral Confined Concrete Boundary Elements*, Washington State University, Pullman, WA, USA

[23] Banting, Bennett Ralph. (2013). *Seismic Performance Quantification of Concrete Block Masonry Structural Walls with Confined Boundary Elements and Development of the Normal Strain-Adjusted Shear Strength Expression (NSSSE)*, McMaster University, Hamilton, ON, Canada

[24] Drysdale, Robert G. and Hamid, Ahmad A. (1983). "Capacity of Concrete Block Masonry Prisms Under Eccentric Compressive Loading." *ACI Journal.*, 102-108